

REPORT DOCUMENTATION PAGE			Form Approved OMB No. 0704-0188	
Public reporting burden for this collection of information is estimated to average 1 hour per response, including the time for reviewing instructions, searching existing data sources, gathering and maintaining the data needed, and completing and reviewing the collection of information. Send comments regarding this burden estimate or any other aspect of this collection of information, including suggestions for reducing this burden, to Washington Headquarters Services, Directorate for Information Operations and Reports, 1215 Jefferson Davis Highway, Suite 1204, Arlington, VA 22202-4302, and to the Office of Management and Budget, Paperwork Reduction Project (0704-0188), Washington, DC 20503.				
1. AGENCY USE ONLY (Leave blank)		2. REPORT DATE 31 Jan. 03		3. REPORT TYPE AND DATES COVERED THESIS
4. TITLE AND SUBTITLE GAS-SOLID ABSORPTION CHARACTERISTICS OF SUPRMOLECULAR COMPOUNDS USING A HERMETICALLY CONTROLLED ATMOSPHERE AUTOMATED ABSORPTION BALANCE (H-CAAAB)			5. FUNDING NUMBERS	
6. AUTHOR(S) CAPT WARRENSFORD DANIEL E JR				
7. PERFORMING ORGANIZATION NAME(S) AND ADDRESS(ES) UNIVERSITY OF SOUTH FLORIDA			8. PERFORMING ORGANIZATION REPORT NUMBER CI02-850	
9. SPONSORING/MONITORING AGENCY NAME(S) AND ADDRESS(ES) THE DEPARTMENT OF THE AIR FORCE AFIT/CIA, BLDG 125 2950 P STREET WPAFB OH 45433			10. SPONSORING/MONITORING AGENCY REPORT NUMBER	
11. SUPPLEMENTARY NOTES				
12a. DISTRIBUTION AVAILABILITY STATEMENT Unlimited distribution In Accordance With AFI 35-205/AFIT Sup 1			12b. DISTRIBUTION CODE	
13. ABSTRACT (Maximum 200 words)				
<div style="display: flex; justify-content: space-between; align-items: center;"> <div style="text-align: center;"> DISTRIBUTION STATEMENT A Approved for Public Release Distribution Unlimited </div> <div style="font-size: 2em; font-weight: bold;">20030221 176</div> </div>				
14. SUBJECT TERMS			15. NUMBER OF PAGES 98	
			16. PRICE CODE	
17. SECURITY CLASSIFICATION OF REPORT	18. SECURITY CLASSIFICATION OF THIS PAGE	19. SECURITY CLASSIFICATION OF ABSTRACT	20. LIMITATION OF ABSTRACT	

Author: Daniel E. Warrensford Jr.

Rank: O-3E/Capt

Branch: United States Air Force

Thesis Title: GAS-SOLID ABSORPTION CHARACTERISTICS OF
SUPRAMOLECULAR COMPOUNDS USING A HERMETICALLY CONTROLLED
ATMOSPHERE AUTOMATED ABSORPTION BALANCE (H-CAAAB)

Year: 2002

Pages: 98 total

Degree Awarded: Master of Science in Chemistry

Name of Institution: University of South Florida, Tampa, Florida

ABSTRACT

Rigid supramolecular structures recently discovered present new options for those wishing to develop gravimetric humidity sensors. Although humidity sensors are an established technology, there is room to grow in this field. This thesis backgrounds the current state of the art in humidity sensing materials, but will concentrate on gravimetric humidity sensors. It details the benefits and drawbacks of current materials in use. Limitations of current sensing materials are explored. The advantages of using rigid porous supramolecular structures are explained. Using a Hermetically Controlled Atmosphere Automated Absorption Balance, this work studied the absorption characteristics of some of the more promising supramolecular materials that have recently been developed in the Zaworotko research group.

Bibliography

1. M. Kondo, T. Yoshitomi, K. Seki, H. Matsuzaka, S. Kitigawa, *Angew. Chem. Int. Ed.*, **1997**, 36, 1725 – 1727.
2. IUPAC *Pure. Appl. Chem.*, **1985**, 57, 603 – 619.
3. H. Li, M. Eddaoudi, T. L. Groy, O.M. Yaghi, *J. Am. Chem. Soc.*, **1998**, 120, 8571 – 8572.
4. M. Eddaoudi, H. Li, O.M. Yaghi, *J. Am. Chem. Soc.*, **2000**, 122, 1391 – 1397.
5. Y. Sakai, Y. Sadaoka, M. Matsuguchi, *Sens. Actuators B*, **1996**, 35-36, 85 – 90.
6. Z.M. Rittersma, *Sens. Actuators A*, **2002**, 96, 196 – 210.
7. R. Buchhold, A. Nakladal, G. Gerlach, P. Neumann, *Sens. Actuators B*, **1998**, 53, 1 – 7.
8. A. Glück, W. Halder, G. Lindner, H. Müller, P. Weindler, *Sens. Actuators B*, **1994**, 18/19, 554 – 557.
9. J. E. Huheey, E. A. Keiter, R. L. Keiter, *Inorganic Chemistry; Principles of Structure and reactivity*, Harper Collins, New York, NY, **1993**.
10. S. Chatterjee, S. Basu, D. Chattopadhyay, K. K. Mistry, K. Sengupta, *Rev. Sci. Inst.*, **2001**, 72, 2792 – 2795.
11. L.J. Barbour, K. Achleitner, J.R. Greene, *Thermochim. Acta*, **1992**, 205, 171 – 177.
12. R. Feynman, *Eng. Sci.*, **1960**, 22 – 36.
13. B. Moulton, M.J. Zaworotko, *Chem. Rev.*, **2001**, 101, 1629 – 1658.
14. J. Lu, A. Mondal, B. Moulton, M.J. Zaworotko, *Angew. Chem. Int. Ed.*, **2001**, 40, 2113 – 2116.

15. S. Budavari, *Merck Index Eleventh Edition*, Merck, Rahway, NJ, **1989**.
16. S. S. -Y. Chui, S. M. -F. Lo, J. P. H. Charmant, A. G. Orpen, I. D. Williams, *Science*, **1999**, 283, 1148 – 1150.
17. B. Moulton, J. Lu, R. Hajndl, S. Hariharan, M.J. Zaworotko, *Angew. Chem. Int. Ed.*, **2002**, 41, 2821 – 2824.
18. E. Rather, D. E. Warrensford, B. Moulton, M.J. Zaworotko, Unpublished Results, **2002**.
19. L. J. Barbour, *Clathration by diol hosts: thermodynamics and structure*, University of Cape Town, South Africa, **1994**.
20. L.J. Barbour, K. Achleitner, J.R. Greene, *Thermochim. Acta*, **1992**, 205, 171 – 177.
21. H. Abourahma, A.W. Coleman, B. Moulton, B. Rather, P. Shahgaldian, M.J. Zaworotko, *Chem. Commun.*, **2001**, 2380 – 2381.
22. B. Moulton, J. Lu, A. Mondal, M.J. Zaworotko, *Chem. Commun.*, **2001**, 863 – 864.
23. M.J. Zaworotko, *Chem. Commun.*, **2001**, 1 – 9.

Office of Graduate Studies
University of South Florida
Tampa, Florida


CERTIFICATE OF APPROVAL

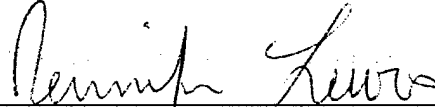
This is to certify that the thesis of

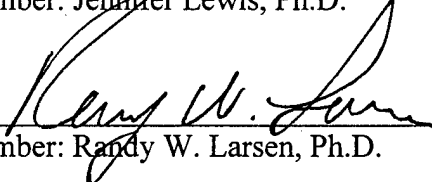
DANIEL E. WARRENSFORD JR.

in the graduate degree program of
Chemistry
was approved on November 18, 2002
for the Master of Science degree.


Examining Committee:


Major Professor: Michael J. Zaworotko, Ph.D.


Member: Jennifer Lewis, Ph.D.


Member: Randy W. Larsen, Ph.D.

Committee Verification:


Program Director

GAS-SOLID ABSORPTION CHARACTERISTICS OF SUPRAMOLECULAR
COMPOUNDS USING A HERMETICALLY CONTROLLED ATMOSPHERE
AUTOMATED ABSORPTION BALANCE (H-CAAAB)

by

DANIEL E. WARRENSFORD JR.

A thesis submitted in partial fulfillment
of the requirements for the degree of
Master of Science
Department of Chemistry
College of Arts and Sciences
University of South Florida

Date of Approval:
November 18, 2002

Major Professor: Michael J. Zaworotko, Ph.D.

© Copyright by Daniel E. Warrensford Jr. 2002
All rights reserved

Acknowledgments

Great thanks goes to Dr. Michael J. Zaworotko, for his support, ideas, and the opportunity to be a member of his outstanding research group. The work being done in our group is what has inspired me to want more and more knowledge of chemistry. Forward thinking in the field encourages innovation, and gives inspiration. Others that need mention are Dr. Rosa Bailey Walsh, Brian Moulton, Heba Abourahma, Scott Fleischman, and Leslie Morales. I thank them for their guidance, help, encouragement and their company at lunch.

Table of Contents

List of Figures	ii
List of Tables	iii
List of Abbreviations	iv
Abstract	v
Chapter 1 Introduction	1
Chapter 2 Results	8
Molecular Sieve Standard	8
2-D Kagomé Structure	9
3-D Zinc Cubic Structure	9
3-D Copper Octahedral Structures	10
Chapter 3 Discussion	11
2-D Kagomé Structure	13
3-D Zinc Cubic Structure	15
3-D Copper Octahedral Structures	17
Chapter 4 Experimental	19
Materials and Instruments	19
H-CAAAB Procedures/Check List	20
Sample Preparation	21
Apparatus Preparation	22
Desorption Experiment Run	23
Absorption Experiment Run	23
Chapter 5 Conclusions and Future Directions	24
Conclusions	24
Future Directions	25
References	27
Appendix A: H-CAAAB Profiles	29
Appendix B: TGA Thermograms	66
Appendix C: X-ray Powder Diffraction Patterns	77

List of Figures

Figure 1	Example of Cantilever Gravimetric Humidity Sensor	3
Figure 2	Schematic of H-CAAAB System	6
Figure 3	Illustrations of the Secondary Building Unit and the "Square" SBU Schematic Representation in Green, $L_2M_2(RCO_2)_4$	12
Figure 4	Face on Schematic Illustration of a Kagomé Lattice	14
Figure 5	Edge on Schematic Illustration of a Kagomé Lattice	15
Figure 6	Space Filling Model of a Kagomé Structure	15
Figure 7	Schematic Illustration of a Zinc Cubic Structure	16
Figure 8	Space Filling Model 3-D Zinc Cubic Structure	16
Figure 9	Space Filling Model of Copper Octahedral 1 Structure	17
Figure 10	Space Filling Model of Copper Octahedral 2 Structure	18
Figure 11	Space Filling Model of Copper Octahedral 3 Structure	18

List of Tables

Table 1	Representative Techniques, Outputs and Materials Used for Humidity Sensing	4
Table 2	Materials for Humidity Study	7
Table 3	Percentage Weight Loss and Weight Gain for 4 Å Molecular Sieves	8
Table 4	Percentage Weight Loss and Weight Gain for Kagomé Structure	9
Table 5	Percentage Weight Loss and Weight Gain for Zinc Cubic Structure	9
Table 6	Percentage Weight Loss and Weight Gain for Copper Octahedral Structure	10

List of Abbreviations

BDC = Benzene di-carboxylate

TMA = Triamezic Acid

PS = Porous Silicon

TGA = Thermogravimetric analysis

QCM = Quartz Crystal Microbalance

XPD = X-ray powder diffraction

H-CAAAB = Hermetically Controlled Atmosphere Automated Absorption Balance

nSBU = Nanoscale Secondary Building Unit

SBU = Secondary Building Unit

Py = Pyridine

BiPy = 4,4'-Bipyridine

BiPyEt = 4,4' Bipyridine Ethane

PVDF = polyvinyl-difluorene

MOF = Metal Organic Framework

GAS-SOLID ABSORPTION CHARACTERISTICS OF SUPRAMOLECULAR
COMPOUNDS USING A HERMETICALLY CONTROLLED ATMOSPHERE
AUTOMATED ABSORPTION BALANCE (H-CAAAB)

by

DANIEL E. WARRENSFORD JR.

An Abstract

of a thesis submitted in partial fulfillment
of the requirements for the degree of
Master of Science
Department of Chemistry
College of Arts and Sciences
University of South Florida

Date of Approval:
November 18, 2002

Major Professor: Michael J. Zaworotko, Ph.D.

Rigid supramolecular structures recently discovered present new options for those wishing to develop gravimetric humidity sensors. Although humidity sensors are an established technology, there is room to grow in this field. This thesis backgrounds the current state of the art in humidity sensing materials, but will concentrate on gravimetric humidity sensors. It details the benefits and drawbacks of current materials in use. Limitations of current sensing materials are explored. The advantages of using rigid porous supramolecular structures are explained. Using a Hermetically Controlled Atmosphere Automated Absorption Balance, this work studied the absorption characteristics of some of the more promising supramolecular materials that have recently been developed in the Zaworotko research group.

Abstract Approved: _____



Major Professor: Michael J. Zaworotko, Ph.D.
Professor, Department of Chemistry

Date Approved: _____

11/18/02

Chapter 1

Introduction

Our group's research direction in the area of metal organic polymers has led to the discovery of some very interesting and novel structures. The main objectives for this work were to 1) Ascertain whether the novel materials could absorb water in quantities sufficient to make them a viable sensing material for gravimetric humidity sensing and 2) Determine if these materials could stand the rigors of repeated cycling. The structures of interest for this work are those that appear to have the physical property of permanent porosity. Permanent porosity is defined here as retaining porosity after all guest molecules are removed from the structure. Permanent porosity is stipulated because many of the materials that our group (and other groups in this field) works with have porosity only while hosting a guest within the pores. In this case, of conditional porosity, upon removal of the guest the structures will collapse in on themselves. Why is porosity of so much interest one may ask? With porosity goes the possibility to reversibly absorb water and thus the possibility to serve as a suitable material for humidity sensing applications. Professor Susumu Kitagawa's group first researched the ability of coordination polymers with permanent microporosity to absorb small molecules, in their 1997 *Angewandte Chemie* paper. Up to this point, gas isotherm measurements had confirmed microporosity in zeolites, used in molecular sieves, but these studies had not been accomplished on metal organic polymers. Kitagawa's group

measured the absorption characteristics of anhydrous $\{[\text{Co}_2(4,4'\text{-bipy})_3(\text{NO}_3)_4](\text{H}_2\text{O})_x\}_n$, obtained by drying under vacuum, with CH_4 , N_2 , and O_2 [1]. The resulting isotherms showed a rapid uptake of gases from 0 – 5 atm, indicating a type I isotherm according to IUPAC classification [2], that is, absorption of the gases into the cavities of the structure. The research group of Professor Omar Yaghi also demonstrated microporosity in metal organic polymers, which they now refer to as metal organic frameworks (MOF's) [3]. In this paper, Yaghi's group clearly demonstrated the ability to create metal organic polymers with permanent porosity and confirmed this with gas isotherm measurements [3]. In addition, Yaghi's group has presented a metal organic polymer with the highest known percent of free volume for any known substance, his MOF-5. Using N_2 absorption, MOF-5 was shown to have a pore volume of $0.61 \text{ cm}^3/\text{cm}^3$, which is greater than any pore volume calculated for zeolites [4]. By using metal organic polymers such as the ones being studied in the Zaworotko group, we can create new and useful novel porous materials by design, making materials that absorb water by size exclusion, such as molecular sieves, and/or by their hygroscopic nature.

There are a great many different types of humidity sensing devices, they work on different principals and utilize a variety of materials. A few of the currently known types of humidity sensors are capacitive, resistive, hygrometric, gravimetric, and optical types. The first two types, capacitive and resistive humidity sensors, rely on reading differences in various electrical signals [5]. If a humidity sensor measures dielectric changes in thin films during water vapor absorption, then it would be classified as a capacitive type humidity sensor. The abilities of capacitive humidity sensors are influenced by the hygroscopic material and the electrode geometry [6]. Resistive humidity sensors are

devices that act as a transducer of air humidity into an impedance change that can be measured by a current, a voltage or a resistance. Resistive type humidity detectors rely upon three main groups of materials: ceramics, polymers and electrolytes [6]. Hygrometric humidity sensors utilize the mechanical influences of humidity as a means to produce a transducer. An example of which would be the piezoresistive device described by Gerlach et al. This device consists of a silicon/polysilicon membrane (the piezoresistive layer) with a hygroscopic polyimide layer on top. As the air humidity increases, the polyimide swells due to the uptake of water molecules from ambient humid air. This swelling in turn activates the piezoresistors [6,7]. Gravimetric humidity sensors, as the name suggests, rely upon a definite mass change caused by the sorption of water molecules. Figure 1 is an example of a cantilever resonator proposed by Glück et. al.

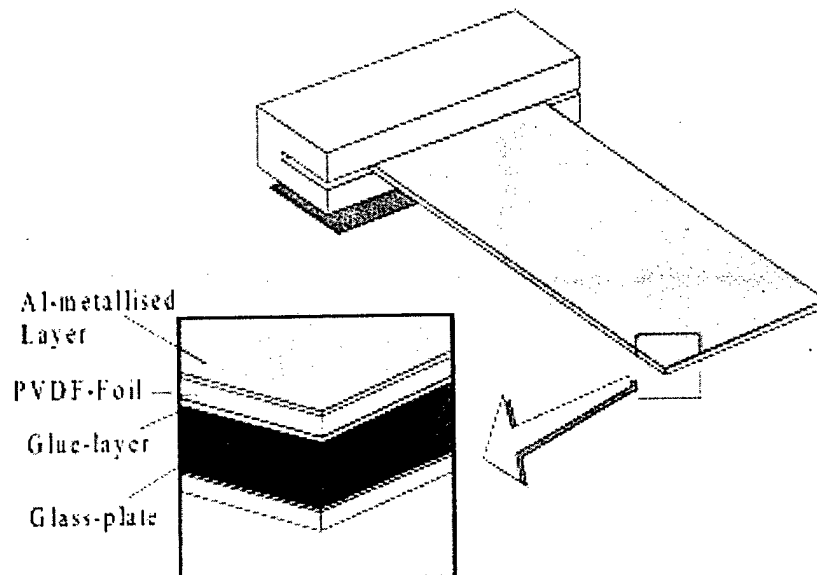


Figure 1. Example of Cantilever Gravimetric Humidity Sensor [8].

This sensor works by applying an electrical signal across electrodes in a layer of piezoelectric polymer called polyvinyl-difluorene, (PVDF) [8]. The PVDF layer expands

or contracts sending the cantilever into vibration. The weight change that follows the absorption or desorption of water vapor will change the frequency of the vibration, providing a measurable output of humidity. The most widely known gravimetric humidity sensor is the quartz crystal microbalance (QCM) [6]. QCMs work by measuring the frequency of resonance of thin plates of piezoelectric quartz. By coating these thin plates of piezoelectric quartz with a hygroscopic layer (usually a zeolite) and providing a reference non-coated device, the humidity can be measured. Optical humidity sensors take advantage of the absorption wavelength of water. They operate by passing light through a gas, they then observe the absorption of certain wavelengths providing information about the composition of the gas [6].

The unifying theme for all of these different humidity sensors is that they all rely upon the manipulation of some form of matter to act as a transducer, converting a physical property, moisture uptake, into some measurable information. Some of these materials are listed in Table 1. Of particular interest for the purposes of this thesis are the materials and techniques associated with the material property of porosity.

Technique	Output	Material
Capacitive	Capacitance, Voltage, current, frequency	Polyimide
Resistive	Resistance, voltage, current	Ceramics, polymers, electrolytes
Hygrometric	Voltage	Polysilicon, polyimide,
Gravimetric	Frequency	Al, polyimide, polymers, metal oxides, zeolites
Optical	Light intensity, transmission	p-type PS

Table 1. Representative Techniques, Outputs and Materials Used for Humidity Sensing [6].

Some porous materials can be very similar in chemical composition to materials that are not porous, but differ significantly in morphology. Although they may have a similar chemical composition to non-porous materials, the morphology of porous materials gives them the added benefit of greater surface area with which to utilize their chemical structure. Instead of having just the surface area of two dimensions (low disordered porosity), they can contain a third dimension. Zeolites are probably the best-known porous absorbent materials used. They are aluminosilicate framework minerals with the general formula $M_{x/n}^{n+} [Al_xSi_yO_{2x+2y}]^{x-} \cdot zH_2O$. There are both natural and synthetic zeolites, but both are characterized by open structures that allow the exchange of cations and water molecules [9].

Several materials synthesized in the Zaworotko group at the University of South Florida have indicated that they possess porosity properties that could be taken advantage of for application to gravimetric humidity sensors. Gravimetric humidity sensors need materials with controllable porosity, pore size distribution, and pore shape in order to optimize the detection of humidity [10]. Our materials may be altered to provide this control over the attributes that are important to those devising better humidity sensors. Using a Hermetically Controlled Atmosphere Automated Absorption Balance (H-CAAAB) (Figure 2.), Thermogravimetric Analysis, and Single crystal and X-ray powder diffraction, this research determined if novel materials produced by our group would be useful in humidity sensing applications.

done by design either to increase their hydrophobicity or their hydrophilic nature. A list of the different materials that will be the focus of this paper is given in Table 2.

Structure Type	Dimensions	Molecular Formula
Kagomé	2-D	$[(\text{Cu}_2(\text{Py})_2(\text{BDC})_2)_3]_n$
Zinc Cubic	3-D	$\{[\text{L}_2\text{Zn}_2(\text{TMA})_{1.333}]_{12}\}_n$ L=H ₂ O or Py
Copper Octahedral 1	3-D	$\{\text{Cu}_2(\text{Glutarate})_2(\text{BiPy}) \cdot 3\text{H}_2\text{O}\}$
Copper Octahedral 2	3-D	$\{\text{Cu}_2(\text{Glutarate})_2(\text{BiPyEt}) \cdot 3\text{H}_2\text{O}\}$
Copper Octahedral 3	3-D	$\{\text{Cu}_2(\text{Adipate})_2(\text{BiPyEt}) \cdot 3\text{H}_2\text{O}\}$

Table 2. Materials for Humidity Study.

Chapter 2

Results

Sets of three H-CAAAB profiles were generated during this research. Although not all results were reproduced exactly, this was expected to some extent. In experiments preliminary to this research, it was noted that the crystalline nature of the samples would degrade. This will of course increase the surface area available, and in turn alter the absorption characteristics of the material. In addition, it is thought that the Kagomé and Zinc Cubic materials become able to absorb more water as the axially coordinated Pyridines within the structure are displaced. The results that have been generated are quantitative, but it should be understood, that for the purposes of this research it is the qualitative results that may have more impact.

Molecular Sieve Standard

	Profile 1	Profile 2	Profile 3
% Weight Loss	7.6	12.0	13.9
% Weight Gain	8.2	9.2	10.9

Table 3. Percentage Weight Loss and Weight Gain for 4 Å Molecular Sieves.

4 Å molecular sieves were used as a standard to gauge the effectiveness of the H-CAAAB at detecting a weight change for a given sample. Our own metal-organic polymers mimic the zeolitic physical properties of the molecular sieves. The actual percentage weight loss and gain for three profiles of molecular sieves in saturated humidity are show in Table 3. It is reported by Acros Organics that these molecular

sieves are capable of absorbing approximately 21 percent of their weight in an environment of 50% relative humidity. The discrepancy between the reported absorption percentage and that observed could be explained by the crushing of the 4 to 8 mesh sieves to obtain the 63 – 125 μm particle size used in our experiments. The percent weight loss and gain profiles can be found in Appendix A.

Kagomé Structure

	Profile 1	Profile 2	Profile 3
% Weight Loss	29	15	18
% Weight Gain	9	5.8	11

Table 4. Percentage Weight Loss and Weight Gain for Kagomé Structure.

The Kagomé structure, first synthesized in our group, is of particular interest for sorption studies. In addition to having a porous structure, it also has non-ferromagnetic properties that are of interest. Upon desorption the Kagomé structure will change color from a light blue/teal color to a very deep, almost sapphire color. When the material was removed from the H-CAAAB after an absorption experiment an odor of Pyridine could be detected. Table 4 lists percentage weight losses and gains for three profiles. The percent weight loss and gain profiles can be found in Appendix A.

Zinc Cubic Structure

	Profile 1	Profile 2	Profile 3
% Weight Loss	6	10	33
% Weight Gain	3.2	7.4	13.8

Table 5. Percentage Weight Loss and Weight Gain for Zinc Cubic Structure.

The most successful compound, in terms of absorbance and ability to be recycled successfully, tested thus far is the Zinc cubic structure. This compound has demonstrated that it readily absorbs and desorbs water. Similar to results obtained with the Kagomé

structure, the smell of Pyridine could be detected after absorption experiments with the Zinc Cubic structure. Table 5 lists the respective percent weight loss and weight gain of the material when placed under vacuum and exposed to a 100 % humidity atmosphere. The percent weight loss and gain profiles can be found in Appendix A.

Copper Octahedral Structures

	% Weight	Profile 1	Profile 2	Profile 3
Cu Octahedral One	Loss	45.7	7	11.9
	Gain	2.8	N/A	N/A
	Additional Loss	N/A	4.1	5.8
Cu Octahedral Two	Loss	5.1	--	2.4
	Gain	2.1	0.7	1.2
	Additional Loss	N/A	N/A	N/A
Cu Octahedral Three	Loss	24.8	12.1	29.8
	Gain	12.0	N/A	1.5
	Additional Loss	N/A	2.4	N/A

Table 6. Percentage Weight Loss and Weight Gain for Copper Octahedral Structure.

The three novel Copper Octahedral structures developed by our group are also capable of sorption and desorption. However, none of the Copper Octahedral structures are as adept at absorption as the Kagomé and Zinc Cubic materials. The initial desorption profile for Copper Octahedral One seems exaggerated due to the material still having quite a bit of solvent in the sample. While the Kagomé and Zinc Cubic structures had a net increase in weight during absorption experiments the Copper Octahedral structures would on average present a net decrease in weight. No change in color was observed to indicate a change in the chromophore. Table 6 lists the respective percent weight loss and weight gain of the materials when placed under vacuum or exposed to saturated humidity atmospheres. The percent weight loss and gain profiles can be found in Appendix A.

Chapter 3

Discussion

Discussion

Why bother to investigate the water absorption properties of our materials when there is already a vast and varied field of materials that accomplish the same general goal? In our group we like to quote Richard Feynman, "What would the properties of materials be if we could really arrange the atoms the way we want them?" [12]. Our group finds itself at the cusp of an expanding field in chemistry, Crystal engineering within supramolecular chemistry. One must know that there is a difference between crystal engineering and the precise practice of crystal structure prediction. Crystal engineering is more closely associated with network prediction and typically deals with new phases of matter created with very well characterized molecules [13]. Our group is now wading into the deep end of this field of study and more often than not, we will get a structure that was not predicted before we went into the synthesis. However, once this structure has been thoroughly characterized and the synthesis well known and reproducible, we can consider the alteration of variables to create a similar but different structure. Examples of alterations could include, changing the substituents on the molecules forming the structure or altering the solvent system. Any other of a number of variables can be slightly modified to bring about the desired results. All of the structures that are addressed in this thesis are formed using the $L_2M_2(RCO_2)_4$ secondary building

unit (SBU) (Figure 3). Only the metal atoms (copper color), the ligand (gray)

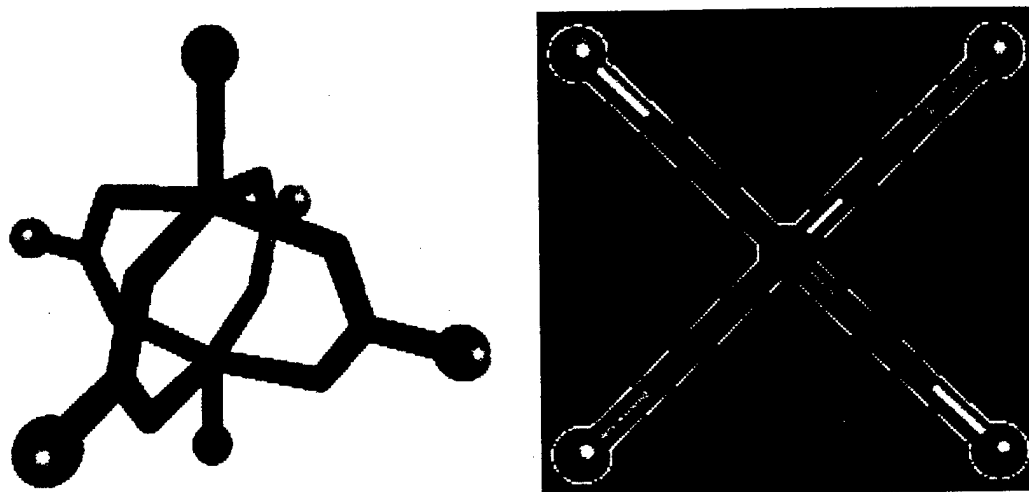


Figure 3. Illustrations of the Secondary Building Unit and the “Square” SBU Schematic Representation in Green, $L_2M_2(RCO_2)_4$ [14].

attached to the carboxylate moiety (gray and red), the axial ligand (violet), the solvent, and guest are changed. The square SBU schematic representation of the SBU is used to illustrate the basic schematic of all the different structures that are formed using the same SBU. The square SBU schematic is formed by turning the SBU and looking down the axial site. Structural schematics are formed by linking these square SBU schematics at the four vertices of the square.

The structures synthesized by our group with SBU's are very similar in morphology to naturally occurring zeolites in that they have cavities formed by cages, tunnels, or layers. We believe the main difference that separates these materials from zeolites is the method of water absorption. Natural zeolites absorb water by clathration, that is, the geometry of the cavities determines what will be absorbed. They do not absorb via chemical similarity with the absorbate [15]. Our metal organic polymers can utilize both clathration and chemical similarity with the absorbate to absorb. Our

materials can form stable two and three-dimensional structures with the SBU in Figure 3 and have the axial sites (shown in blue) available to reversibly absorb water molecules. Yaghi and Williams have shown that these types of metal organic polymers can have coordinatively unsaturated (open axial positions) on the SBU when desorbed of it's axial ligand, ready to coordinate with another ligands or guests [4,16]. We believe that it is possible that the axially bound pyridines in our Kagomé and Zinc Cubic structures can be desorbed under conditions of vacuum and heat to provide such coordinatively unsaturated axial positions, we will discuss possible ways to prove this in the "Future Directions" section.

This research was entered into knowing that the materials selected for study may not be ideal for the task of absorption due to the hydrophobicity of the equatorial ligands used. However, if any promise was shown in their ability to absorb water we knew that the knowledge of the concepts of supramolecular chemistry and crystal engineering might be called upon to enhance their capabilities. For example, the size of the equatorially coordinated ligands could be changed to affect the metrics of the structure or a more hydrophilic substituent could be strategically placed to alter the hydrophobicity of the structure one way or the other.

2-D Kagomé Structures

The Kagomé structure, synthesized and characterized by the Zaworotko group, depicted in schematic in Figure 4, has a crystal structure that is described as an arrangement of bowl-shaped triangular nSBUs, which come together to form a nanoscale Kagomé lattice. This material has interesting physical properties of anti-ferromagnetism, along with its porous structure, that could be taken advantage of further down the road.

The points of the lattice are Cu₂ dimers that are bridged by bdc ligands [17]. This arrangement creates large hexagonal cavities in each layer that are the key feature for this research. The bowl-shaped nSBU drives the structure to it's most stable packing wherein the bowls are eclipsed. This in turn causes the hexagonal cavities within each layer to become eclipsed and form hexagonal channels with the same dimensions as the cavities,

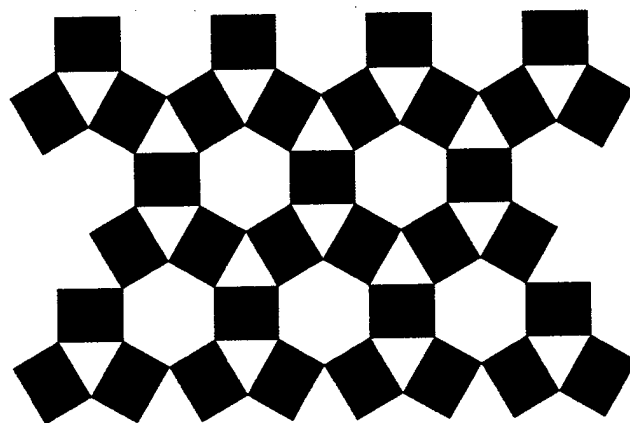


Figure 4. Face on Schematic Illustration of a Kagomé Lattice [17].

a 0.91 nm effective diameter. As can be seen in Figure 5, the Kagomé sheets are undulating because of the curvature imposed by the bdc moiety. Each sheet has a height of 1.24 nm, with each layer overlapping the next by approximately 20% [17]. Of special note for the Kagomé structure, is that it has to be handled differently from the more stable cubic structures. Excessive desorption of the axially bound pyridine could cause overlap of adjacent layers to increase and possibly cause the occlusion of the open axial positions and carboxylate oxygens that can absorb water between the sheets. As noted in the results section, a color change is observed as desorption of the Kagomé material takes place, indicating a change in the environment of the materials chromophore. This could be a physical indication of the increased overlap of the adjacent layers.



Figure 5. Edge on Schematic Illustration of a Kagomé Lattice [17].

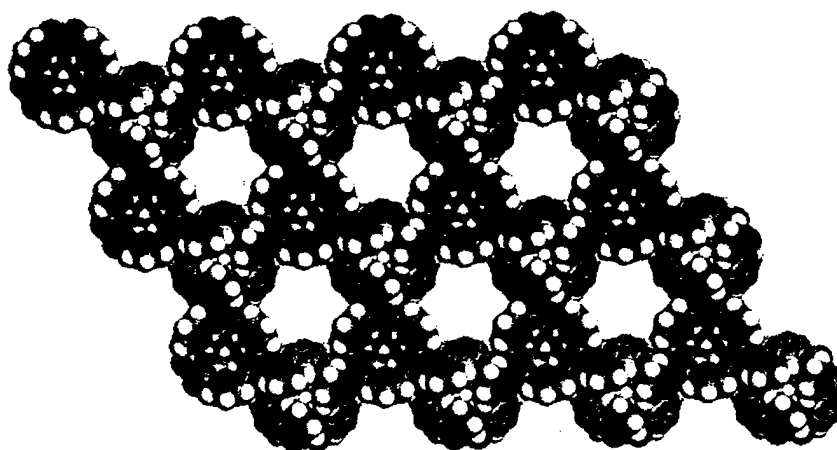


Figure 6. Space Filling Model of a Kagomé Lattice [17].

Zinc Cubic Structures

Of all the materials studied during this work, the Zinc Cubic structure was best able to absorb water. Its structure is very robust and has a very low density due to the faceted polyhedra that compose the structure, shown in schematic in Figure 7. There are 12 axial sites available within the spherical cavities, diameter 11.816 Å, that are linked by square channels with an effective channel size of 8.355 Å [14]. The Zinc Cubic structure performed as was expected and desorbed and absorbed water in a range from 3 percent by weight to 13 percent by weight. As shown in Table 5, the Zinc Cubic structure becomes more effective at absorbing moisture as it is cycled. The limit of this trend was not reached in our experiments. The TGA results showed a loss of solvent and guest of

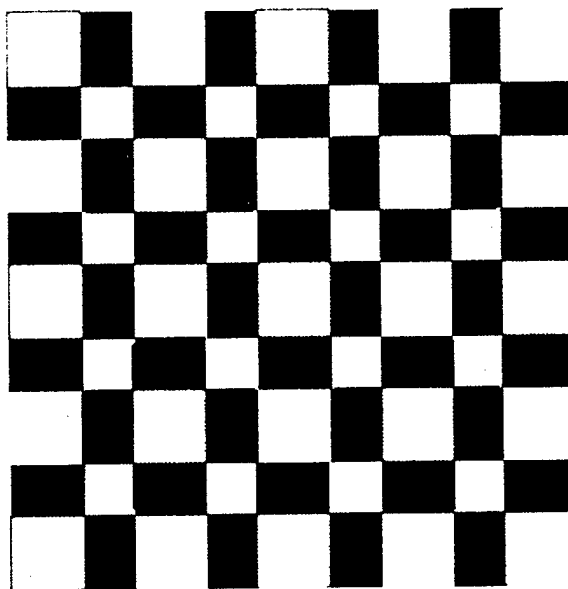


Figure 7. Schematic Illustration of a Zinc Cubic Structure [14].

about 20 percent by weight prior to decomposition. An odor of Pyridine coming from the H-CAAAB after absorption experiments, indicates that this phenomena is caused by axially bound pyridine ligands (shown in blue in Figure 8) being slowly displaced by water as cycling continues. It is safe to assume that the increasing absorption trend will

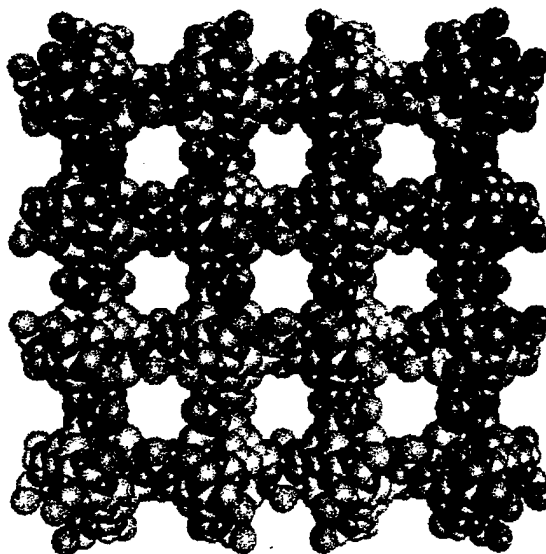


Figure 8. Space Filling Model of Zinc Cubic Structure.

continue until all of the pyridine is displaced by water. The complete displacement of the pyridine ligand could probably be hastened by increasing the temperature at which the sample is desorbed. After the desorption of all the axially bound pyridine, the channels and cavities of the Zinc Cubic structure should become quite hydrophilic.

Copper Octahedral Structures

The desorption and absorption characteristics of the three Copper Octahedral structures (Figures 9,10,11) were very interesting, but these materials would not be suitable for humidity sensing. Somewhat standard looking desorption profiles were obtained with the H-CAAAB, but sorption isotherms were difficult to interpret. As can be seen in Appendix A, after more than one cycle in the H-CAAAB the Copper Octahedral structures begin to lose weight upon desorption and absorption runs. This phenomenon is explained by degradation of the structure under vacuum. As the system

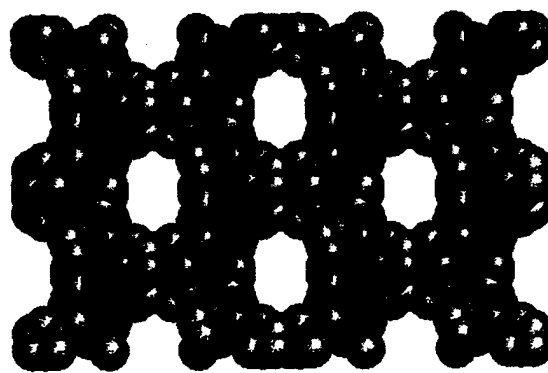


Figure 9. Space Filling Model of Copper Octahedral 1 Structure [18].

goes to 100 percent humidity, the material would then lose weight. This has not been confirmed, but is recommended for future work. What is intriguing is that these compounds all being synthesized in water and all having single crystal x-ray diffraction patterns showing disordered water in the structures channels one would conclude that

they should absorb water [18]. These materials may be more limited than the Kagomé and Zinc Cubic structures in moisture absorption due to the absence of an available

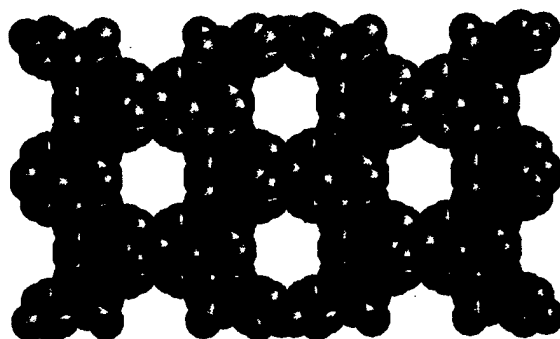


Figure 10. Space Filling Model of Copper Octahedral 2 Structure [18].

axial coordinating site. Otherwise, the hydrophobicity of the pores, 5.45 Å by 6.58 Å for Copper Octahedral 1, 6.95 Å by 7.62 Å for Copper Octahedral 2, and 6.08 Å by 7.44 Å for Copper Octahedral 3, are is similar. Also likely, is that these materials have too slight response to humidity and that the error in measurement is just too great. This problem will be addressed in the “Future Directions” section of the thesis.

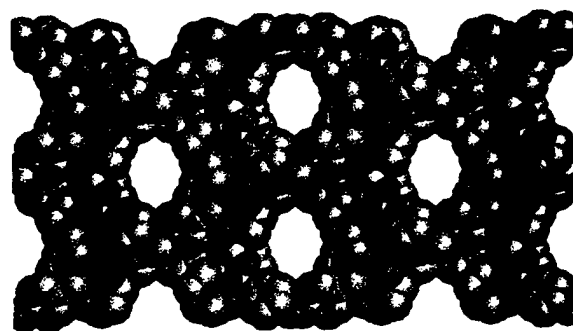


Figure 11. Space Filling Model of Copper Octahedral 3 Structure [18].

Chapter 4

Experimental

Materials and Instruments

All of the chemicals used in this work are commercially available and were purchased through Aldrich[®]. All reactions were carried out under standard atmosphere, temperature, and pressure. The materials studied were obtained using already published procedures [14,17,18]. Material identities were established using TGA and XPD. Thermogravimetric analysis was accomplished using a TA Instruments 2950 Hi-Resolution TGA. X-ray powder diffraction was accomplished using a Rigaku Miniflex Diffractometer using a Cu x-ray source operating at $K\alpha_1=1.540598$, 30kV, and 15mA. The powder diffraction patterns were obtained over a 2 theta scan range of 3 to 40 degrees in a continuous scan mode sampling at 0.020 degrees with a scan speed of 2.00 degrees per minute.

The Hermetically Controlled Atmosphere Automated Absorption Balance (Figure 2) was procured from the Department of Chemistry, University of Cape Town, South Africa. The H-CAAAB consists of a number of different components, instruments, and software. The center of the system is the specially designed reaction chamber that is connected to a vacuum pump [19]. Above the reaction chamber is an electromagnet suspended from a conventional bottom loading analytical balance (Ohaus Explorer E14130), which is in turn connected to a microcomputer running a special piece

of software called Balance.exe, developed by Dr. Leonard J. Barbour. The system operates by connecting a sample pan below a permanent magnet and suspending them both within the reaction chamber on an aluminum centering stage. This permanent magnet and thus the sample pan are then levitated by means of free magnetic suspension by the electromagnet suspended above the reaction chamber and connected below the balance. The electromagnet is controlled by a feedback control circuit, also designed and fabricated at the University of Cape Town [20]. The balance has a weighting range of 410 g with readability of 1 mg. The balance hang below suspension rod, electromagnet, permanent magnet, PTFE screen with hanger rod, and sample pan all together weight 79 g. This leaves an ample margin for a 200 – 1000 mg sample weight to be suspended in the system.

All H-CAAAB profiles were generated from the H-CAAAB data files being processed through a Microsoft® Excel 2000 spreadsheet.

H-CAAAB Procedures/Check List

Sample Preparation

Samples to be submitted for Absorption/Desorption testing should have any solvent molecules present in the sample removed. Vacuum, heat, or a combination of both can be used. The temperature needed to drive off solvent should be elucidated from results gained in TGA analysis. Care should be taken not to heat or vacuum too long. If the amount of sample available allows, the samples should be sieved to obtain an even particle size distribution of between 63 and 125 μm .

Apparatus Preparation

1. Clean Controlled Atmosphere Vessel including ground glass cap, glass cap should be as clean as possible to ensure good transmission of feedback light source.
2. Clean and dry sample pan.
3. Turn electromagnet power on. The power should be set to somewhere between 4 and 5 on the power dial.
4. Start the Balance program on the computer. Set the appropriate scale of the measurements to be taken, i.e. time and weight.
 - a. Remove the electromagnet and hook from bottom of balance if still attached from previous run.
 - b. Turn on the balance with the switch in the upper left of the screen and let it go through its self-calibration.
 - c. Calibrate if needed.
 - d. Hang the hook and electromagnet again and tare the balance.
5. Ensure ground glass mating points are sufficiently coated with high vacuum grease.
6. Set water bath to desired temperature, start the re-circulating pump, and allow approximately 15 minutes for the whole system to equilibrate to the desired temperature.
7. Place 200 – 1000 mg of sample into a cleaned and dried sample pan. Ensure that the sample is level in the pan.
8. Insert the hook through the aluminum support disk. Hang the sample pan on the hook with the hook opening facing up to ensure the pan won't be dropped when

inserting it into the vessel. Take care not to drop or bump the sample pan against the walls of the vessel when lowering the pan into position. Replace the ground glass cap afterwards.

9. Swing vessel into position under the electromagnet and lock into position with the knob on the back of the hinge.
10. After all movement of the sample pan has stopped, turn light source on. The vessel may need a slight soft tap to initiate suspension of the sample pan.
11. Once the sample pan has stopped moving or the balance is stable, tare the balance to zero and then shut off the magnet and remove the hanger and electromagnet from beneath the balance to obtain the true suspended weight of the system. Once the true suspended weight of the system is obtained, one can subtract the weight of everything except the sample to ensure the correct sample weight is recorded before beginning the experiment.

Desorption Experiment Run

1. Start the run on the Balance program and record a beginning base line for about 1 – 2 minutes.
2. While recording baseline, attach the vacuum hose to vessel. After the 1 – 2 minute baseline, slowly start bringing down the pressure to the desired level. A weight change may be evident immediately or may take a few minutes to be seen.
3. End the desorption run when the profile flattens out.
4. Save data at the end of the run.
5. Record the final true suspended weight in the same manner as in step 11 of the apparatus preparation.

Sorption Experiment Run

1. Measure out volume of solvent appropriate for the vapor pressure that needs to be established plus 1 mL extra. Be careful not to introduce excessive amounts of solvent, as this will cause excessive condensation on the vessel walls, which in turn will obstruct the path of the light beam and destabilize the electromagnetic suspension. In general, 5 mL is enough.
2. Start the run on the Balance program and record a beginning base line for about 1 – 2 minute.
3. When introducing the solvent into the system, slowly unscrew the stopcock of the introduction port until the movement of the solvent can be observed. Observe the solvent level carefully and be sure to stop the flow at the predetermined 1 mL level marking. (Failure to keep the 1 mL solvent reserve will rapidly introduce air into the system.)
4. Save data at the end of the run time.
5. Record the final true suspended weight in the same manner as in step 11 of the apparatus preparation.

Chapter 5

Conclusions and Future Directions

Conclusions

The main objectives of this research were accomplished. We were able to ascertain whether the porous metal organic polymer materials synthesized in our group would be candidates for humidity detection by gravimetric means. Most of the materials that we selected for desorption and sorption studies turned out to be good subjects for the experimental procedure that we chose. Positive H-CAAAB results were obtained for 4 Å molecular sieves (a known zeolite with strong absorption of small molecules such as water as it's main physical property) proving the ability of our instrument to provide valuable experimental results. Most of the materials that we used in our experiments provided absorption of water, in the 5 – 13 percent range, and possessed the valuable ability to be recycled through the desorption and absorption process. The material that performs the best is the Zinc Cubic structure due to it possessing a rigid 3-D framework structure and open metal sites that can coordinate with water molecules increasing the materials hygroscopic nature. The Copper Octahedral structures did not perform well in absorbing water, but provided useful information nonetheless. Perhaps the fact that the Kagomé and Zinc Cubic structures absorb water even though they have larger channels and cavities than the Cu Octahedral indicates that the open axial site on the SBU is

paramount in determining whether water will be absorbed, not the size of the channels or cavities.

Future Directions

Further mathematical studies should be completed to determine the nitrogen apparent Langmuir surface area. In addition, studies should determine the feasibility of deposition of the metal organic polymers on surfaces compatible with current real world gravimetric humidity sensing devices. Future synthesis efforts of the Zaworotko group could include altering the equatorially coordinated ligands to improve the overall hygroscopic nature of the materials tested. Since they do not have the advantage of an open axial metal site, as do the Kagomé and Zinc Cubic structures, the Copper Octahedral structures could benefit considerably from an alteration of the ligands used to ones more hygroscopic in nature. Studies to determine whether axially bound pyridine is actually present in Kagomé and Zinc cubic structures should be carried out. In addition, studies should be conducted to fully determine if water would be absorbed even if coordinatively unsaturated axial sites were unavailable. This could be accomplished by introducing a very strong field ligand, such as hydrogen cyanide, to the fully evacuated, anhydrous sample while it is in the H-CAAAB. The hydrogen cyanide should coordinate irreversibly to the axial sites. The sample could then be evacuated again and water absorption measurements taken to observe the results.

Improvements to the H-CAAAB could also be undertaken. An electronic pressure transducer connected to a microcomputer able to regulate the amount of vacuum exerted on the system would provide the ability to study desorption and absorption under a wider variety of atmospheric relative humidity conditions than is possible with the

current set up. In addition, a specially designed pressure manifold would be useful. This would negate the necessity of introducing liquid directly into the H-CAAAB vessel itself, which can cause certain problems if the system were to be subjected to periodic vacuum cycles caused by the aforementioned computerized control of the pressure within the vessel. An update of the current Balance program would be in order as well, incorporating controls for the pressure as well as the weight and time features already available.

References

1. M. Kondo, T. Yoshitomi, K. Seki, H. Matsuzaka, S. Kitigawa, *Angew. Chem. Int. Ed.*, **1997**, 36, 1725 – 1727.
2. IUPAC *Pure. Appl. Chem.*, **1985**, 57, 603 – 619.
3. H. Li, M. Eddaoudi, T. L. Groy, O.M. Yaghi, *J. Am. Chem. Soc.*, **1998**, 120, 8571 – 8572.
4. M. Eddaoudi, H. Li, O.M. Yaghi, *J. Am. Chem. Soc.*, **2000**, 122, 1391 – 1397.
5. Y. Sakai, Y. Sadaoka, M. Matsuguchi, *Sens. Actuators B*, **1996**, 35-36, 85 – 90.
6. Z.M. Rittersma, *Sens. Actuators A*, **2002**, 96, 196 – 210.
7. R. Buchhold, A. Nakladal, G. Gerlach, P. Neumann, *Sens. Actuators B*, **1998**, 53, 1 – 7.
8. A. Glück, W. Halder, G. Lindner, H. Müller, P. Weindler, *Sens. Actuators B*, **1994**, 18/19, 554 – 557.
9. J. E. Huheey, E. A. Keiter, R. L. Keiter, *Inorganic Chemistry; Principles of Structure and reactivity*, Harper Collins, New York, NY, **1993**.
10. S. Chatterjee, S. Basu, D. Chattopadhyay, K. K. Mistry, K. Sengupta, *Rev. Sci. Inst.*, **2001**, 72, 2792 – 2795.
11. L.J. Barbour, K. Achleitner, J.R. Greene, *Thermochim. Acta*, **1992**, 205, 171 – 177.
12. R. Feynman, *Eng. Sci.*, **1960**, 22 – 36.

13. B. Moulton, M.J. Zaworotko, *Chem. Rev.*, **2001**, 101, 1629 – 1658.
14. J. Lu, A. Mondal, B. Moulton, M.J. Zaworotko, *Angew. Chem. Int. Ed.*, **2001**, 40, 2113 – 2116.
15. S. Budavari, *Merck Index Eleventh Edition*, Merck, Rahway, NJ, **1989**.
16. S. S. -Y. Chui, S. M. -F. Lo, J. P. H. Charmant, A. G. Orpen, I. D. Williams, *Science*, **1999**, 283, 1148 – 1150.
17. B. Moulton, J. Lu, R. Hajndl, S. Hariharan, M.J. Zaworotko, *Angew. Chem. Int. Ed.*, **2002**, 41, 2821 – 2824.
18. E. Rather, D. E. Warrensford, B. Moulton, M.J. Zaworotko, Unpublished Results, **2002**.
19. L. J. Barbour, *Clathration by diol hosts: thermodynamics and structure*, University of Cape Town, South Africa, **1994**.
20. L.J. Barbour, K. Achleitner, J.R. Greene, *Thermochim. Acta*, **1992**, 205, 171 – 177.

Appendix A
H-CAAAB Profiles

Appendix A: TGA Thermograms

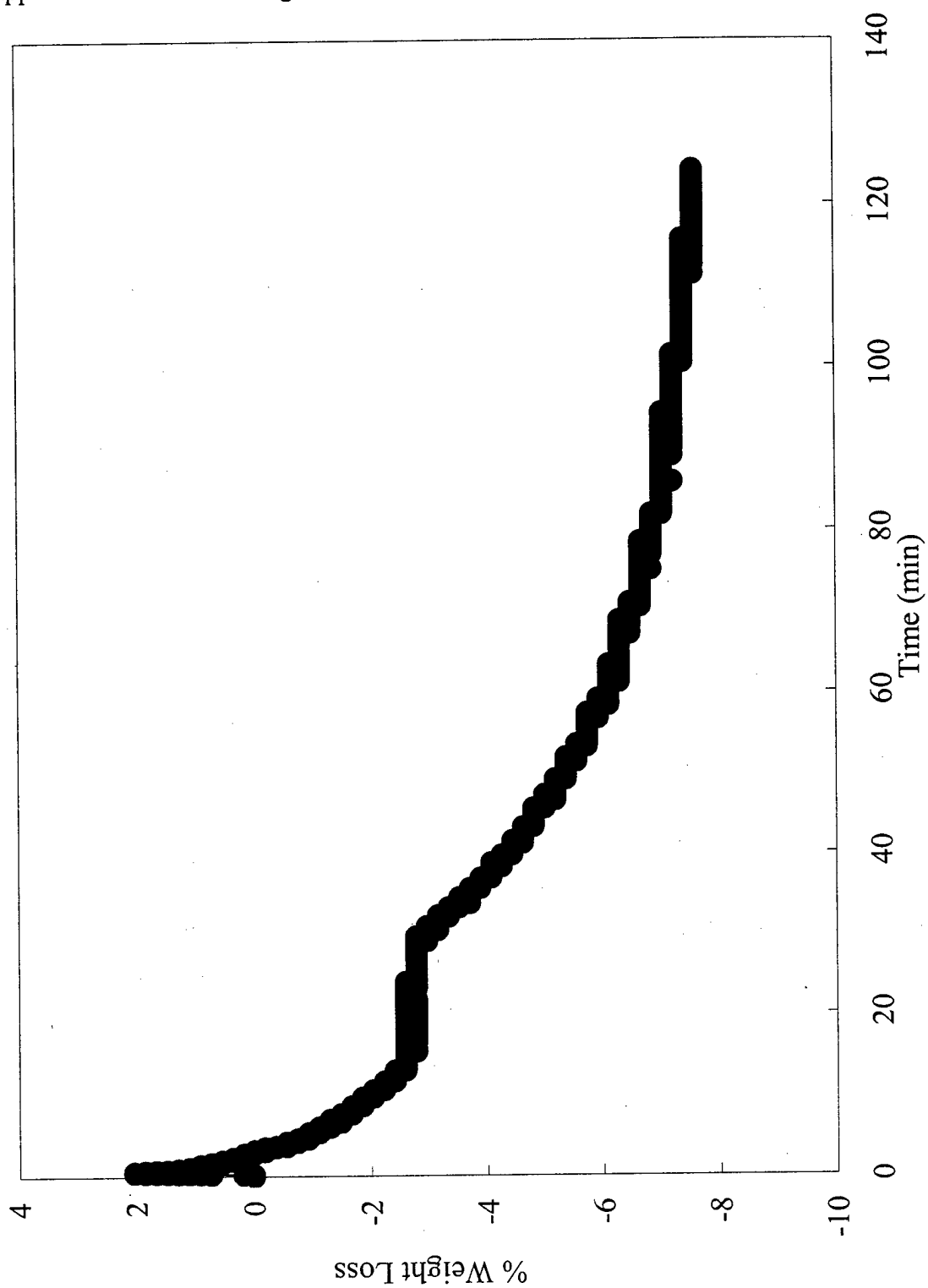


Figure A-1. 4 Å Molecular Sieves % Weight Loss vs Time, Profile 1

Appendix A: (Continued)

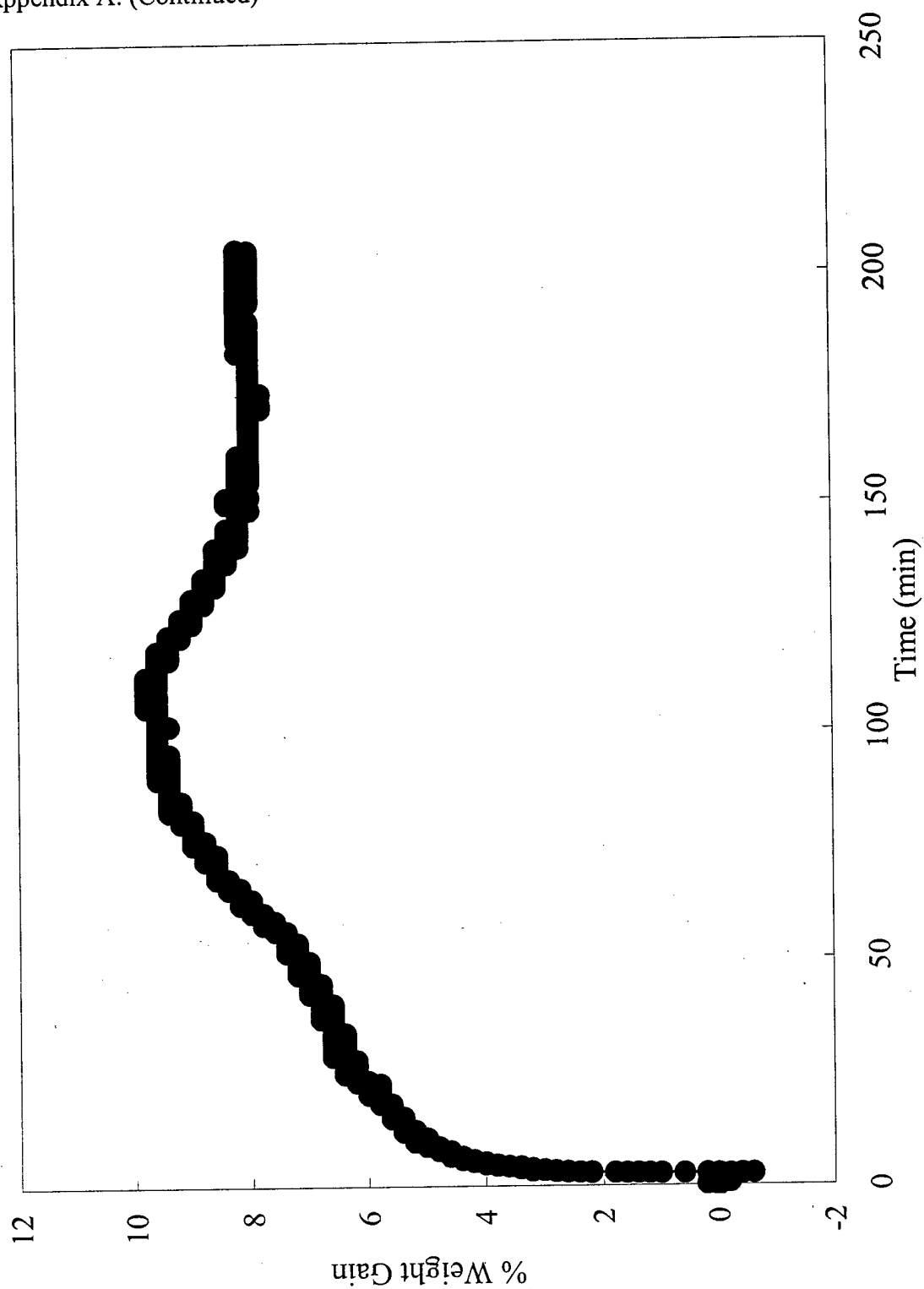


Figure A-2. 4 Å Molecular Sieves % Weight Gain vs Time, Profile 1

Appendix A: (Continued)

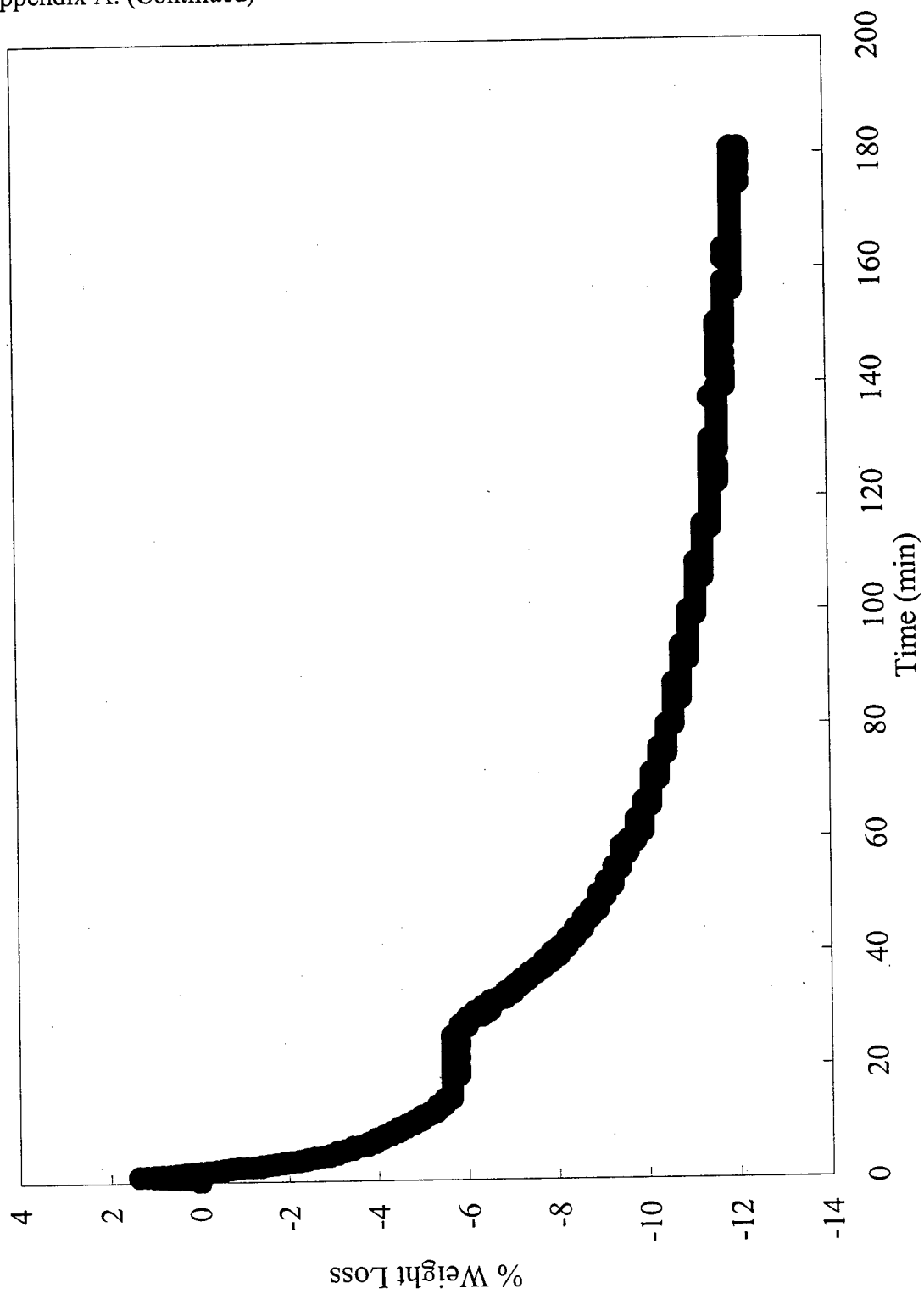


Figure A-3. 4 Å Molecular Sieves % Weight Loss vs Time, Profile 2

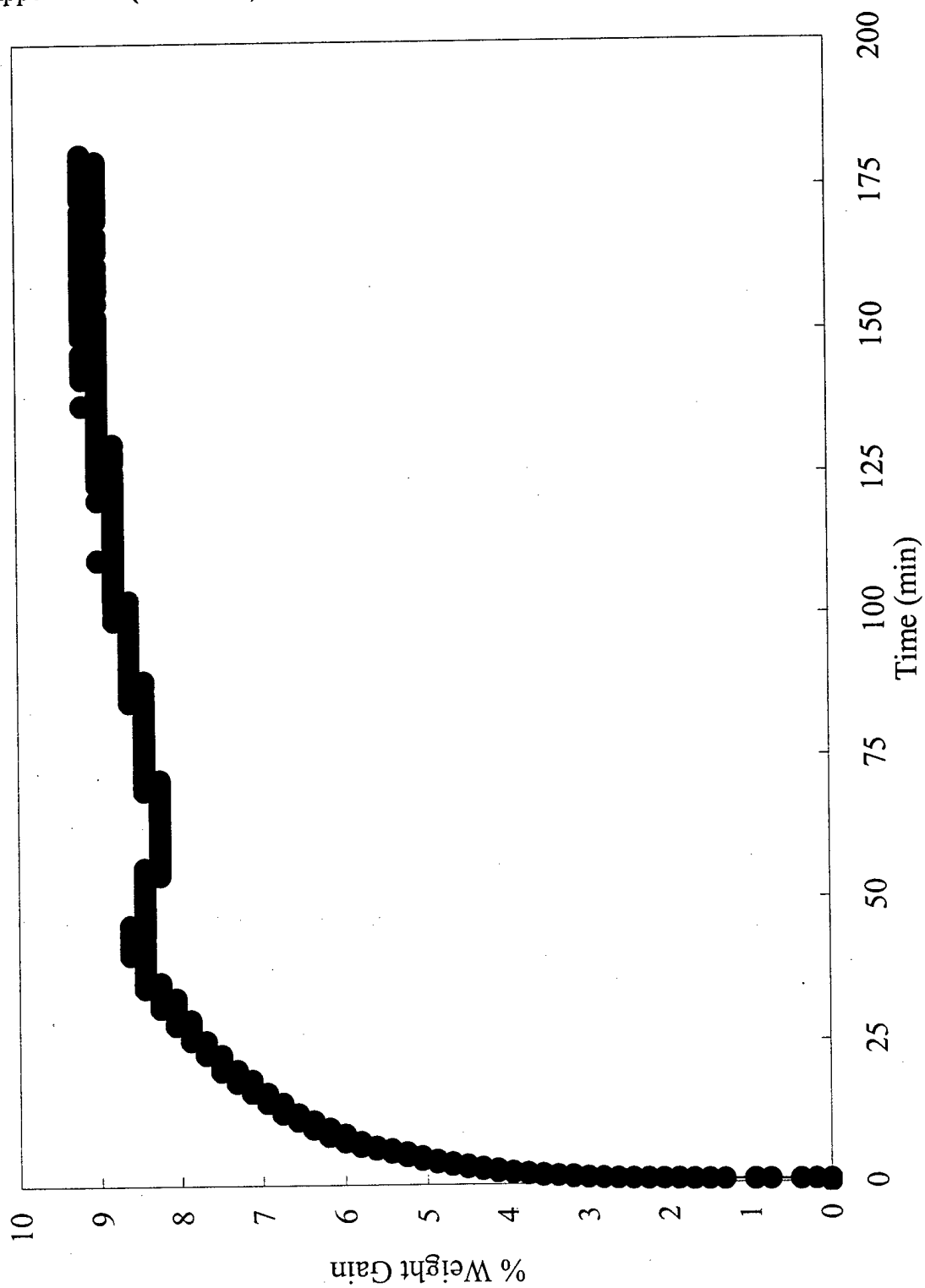


Figure A-4. 4 Å Molecular Sieves % Weight Gain vs Time, Profile 2

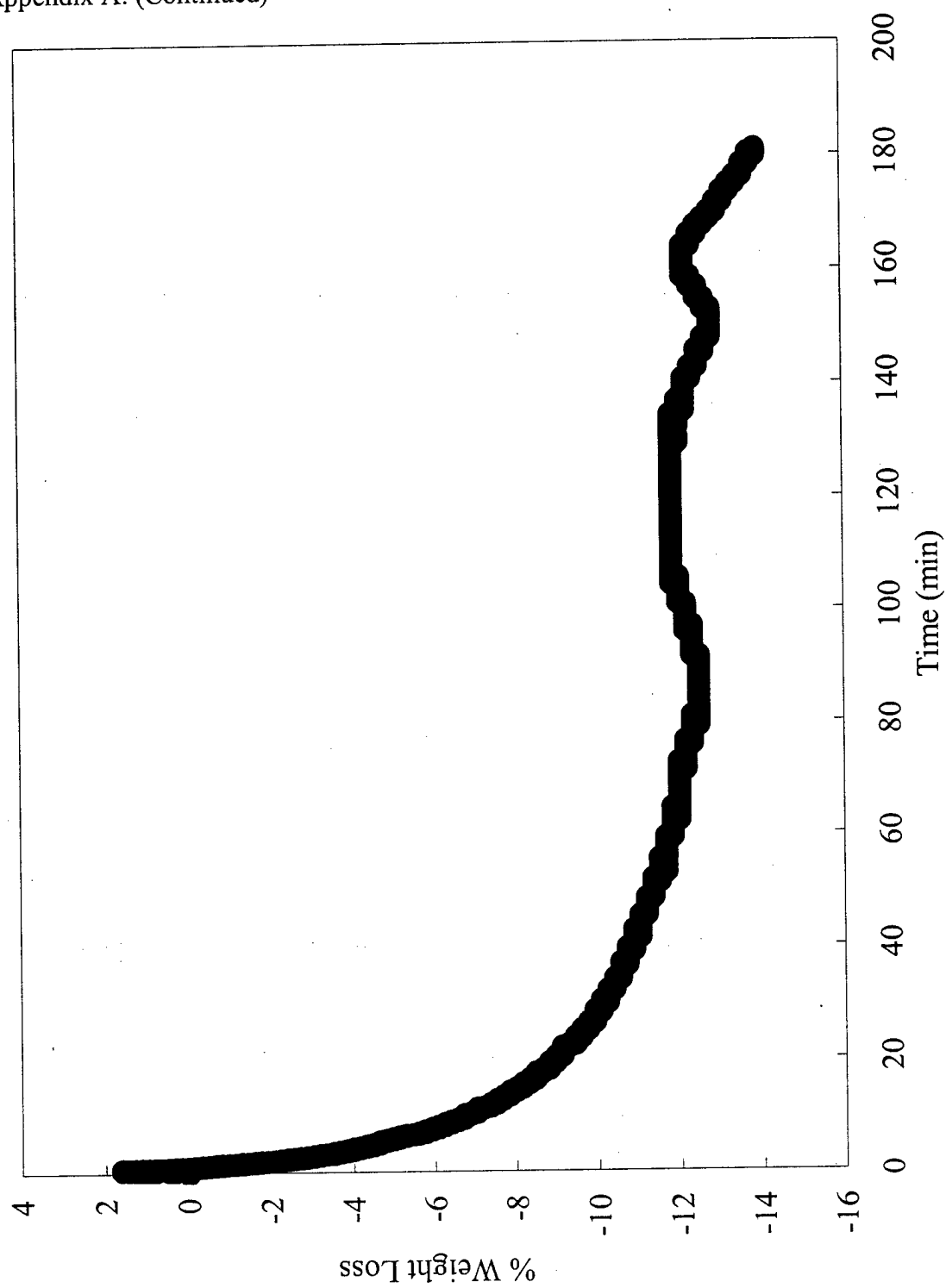


Figure A-5. 4 Å Molecular Sieves % Weight Loss vs Time, Profile 3

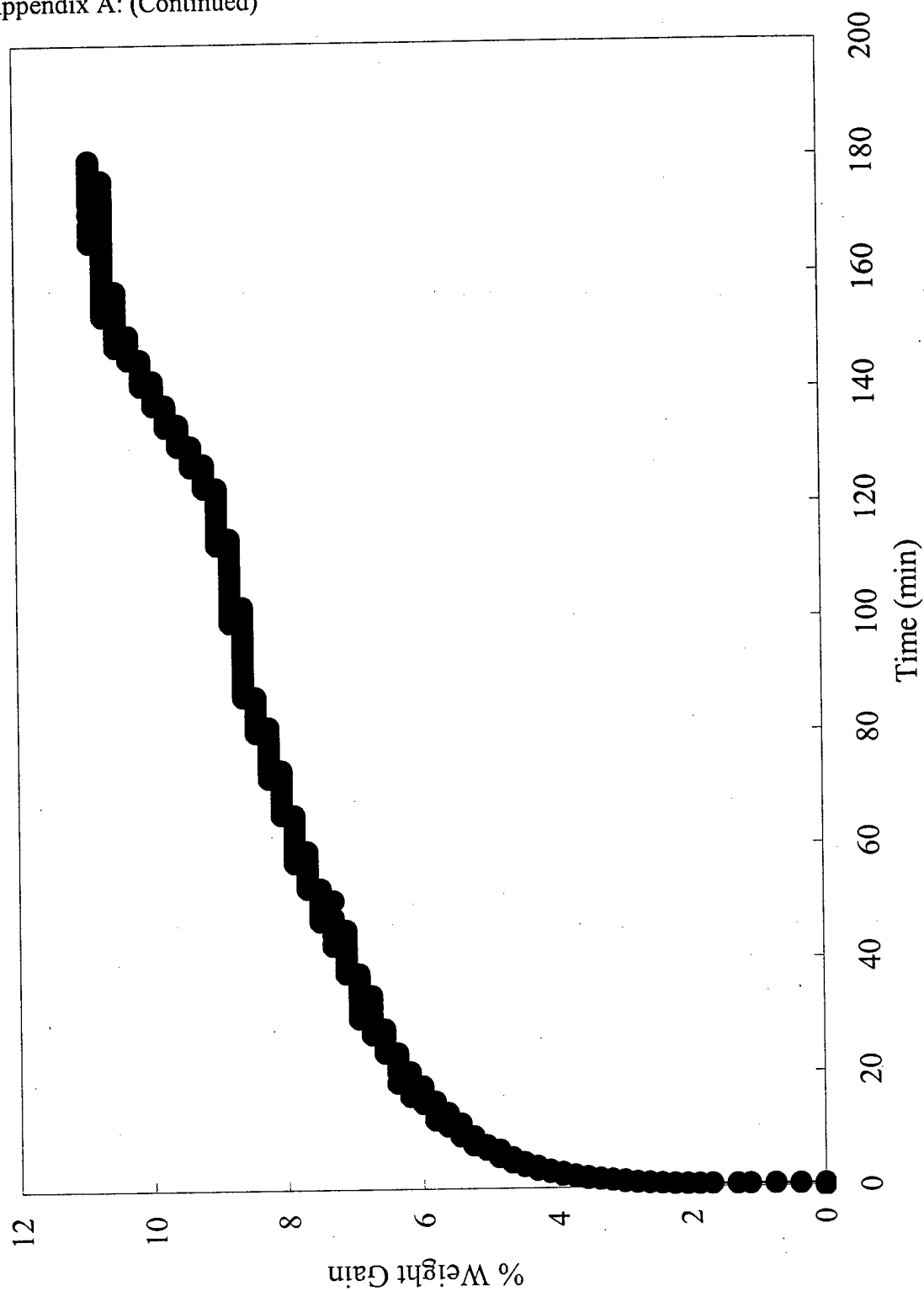


Figure A-6. 4 Å Molecular Sieves % Weight Gain vs Time, Profile 3

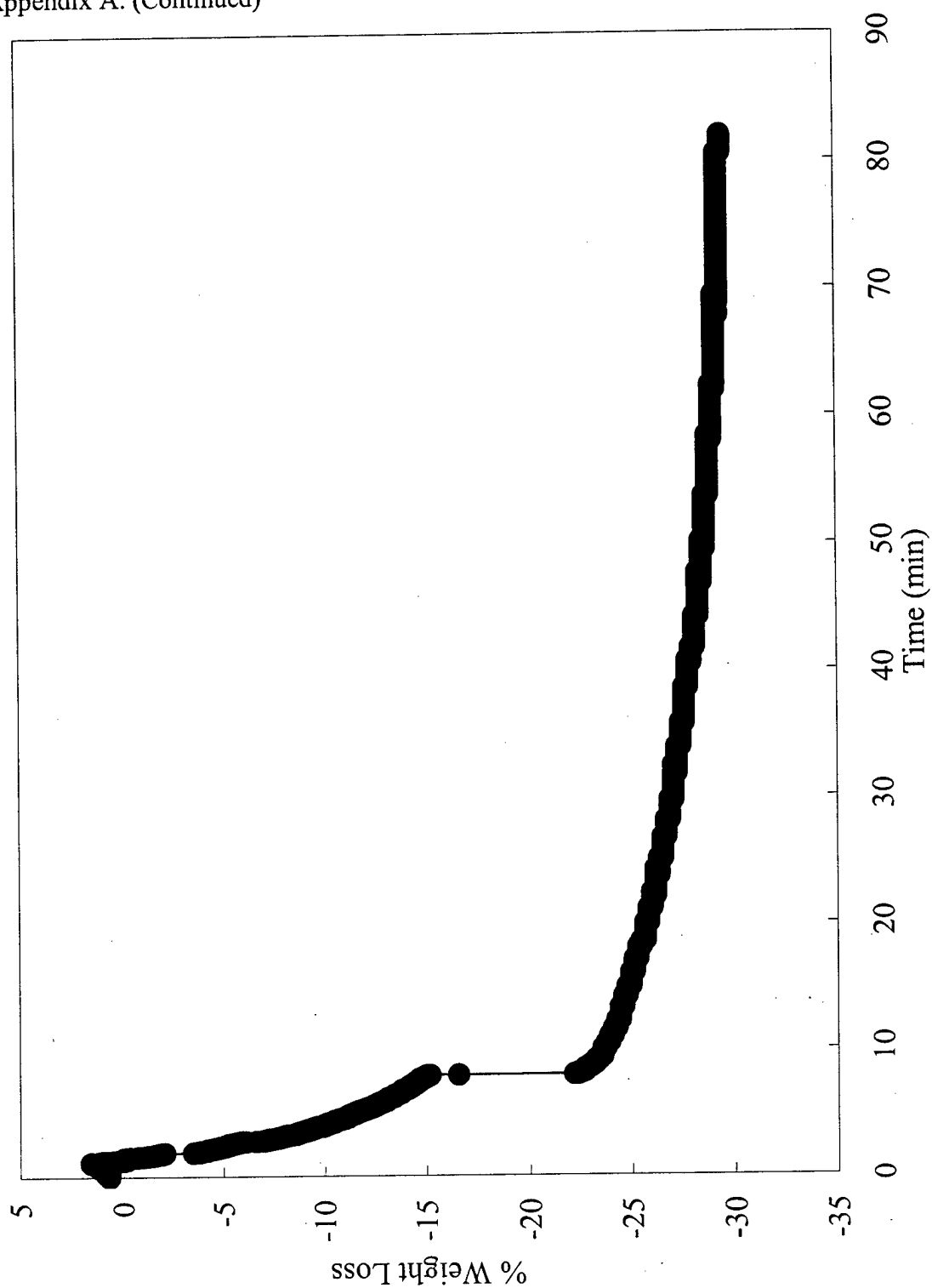


Figure A-7. Kagomé % Weight Loss vs Time, Profile 1

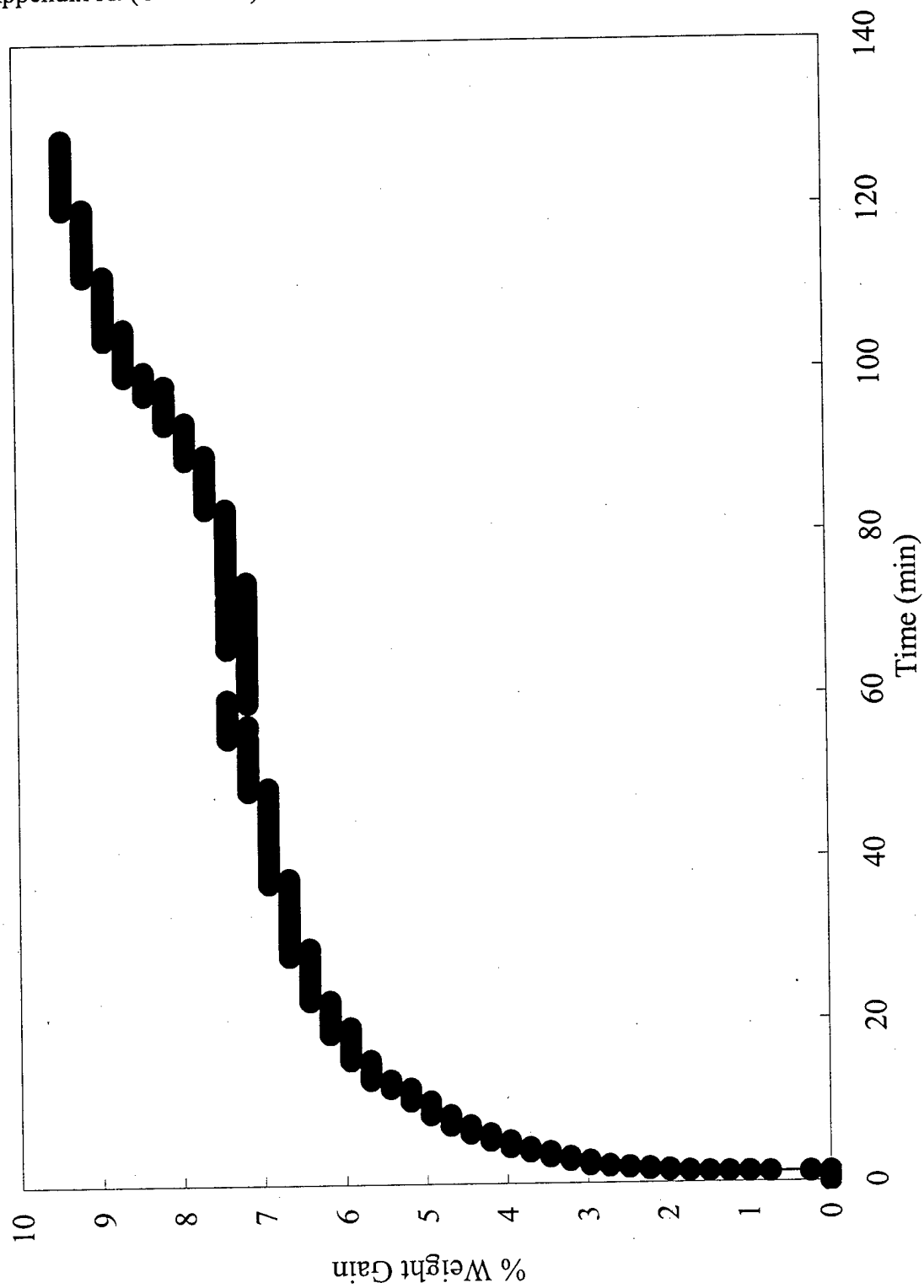


Figure A-8. Kagomé % Weight Gain vs Time, Profile 1

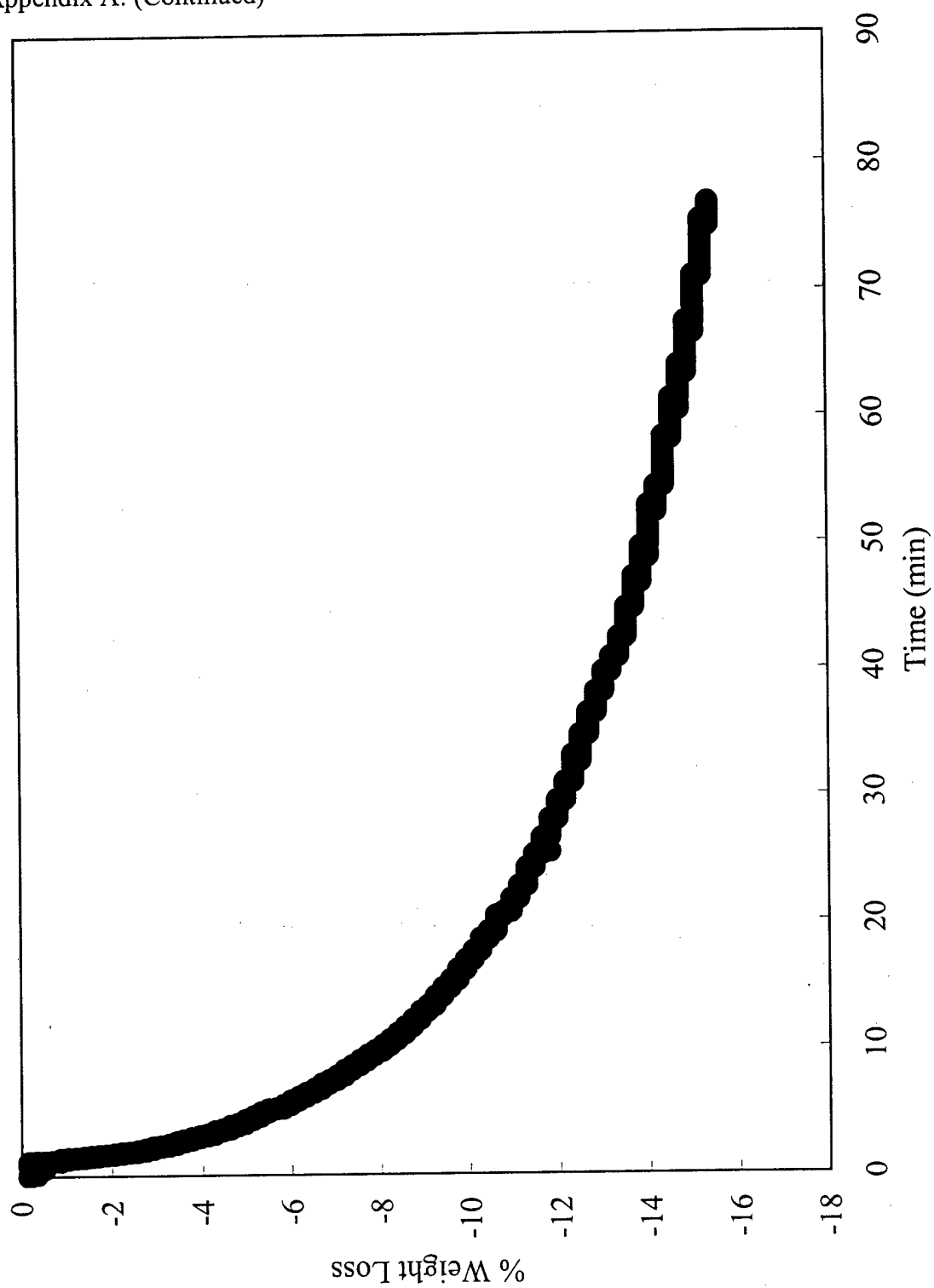


Figure A-9. Kagomé % Weight Loss vs Time, Profile 2

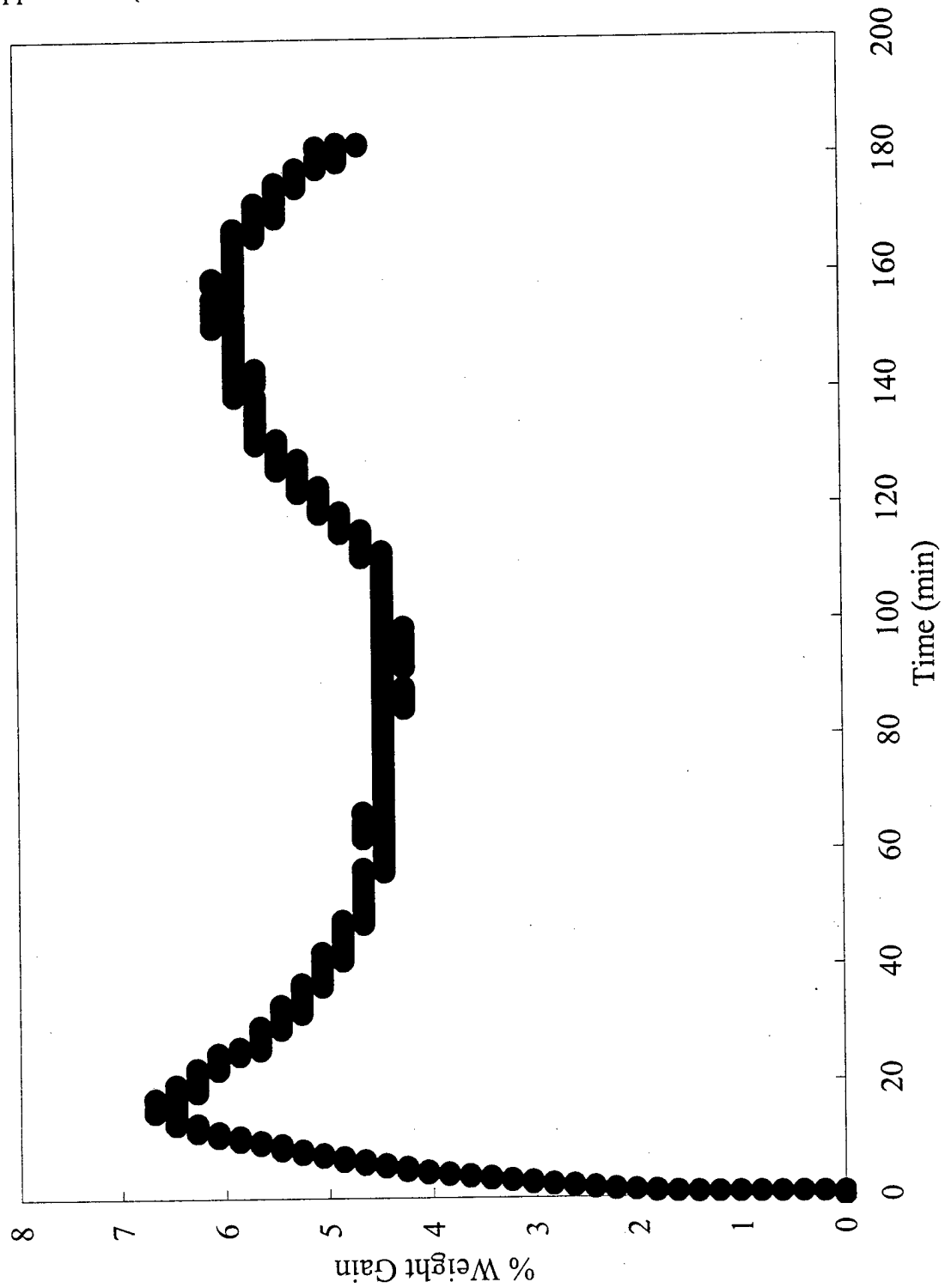


Figure A-10. Kagomé % Weight Gain vs Time, Profile 2

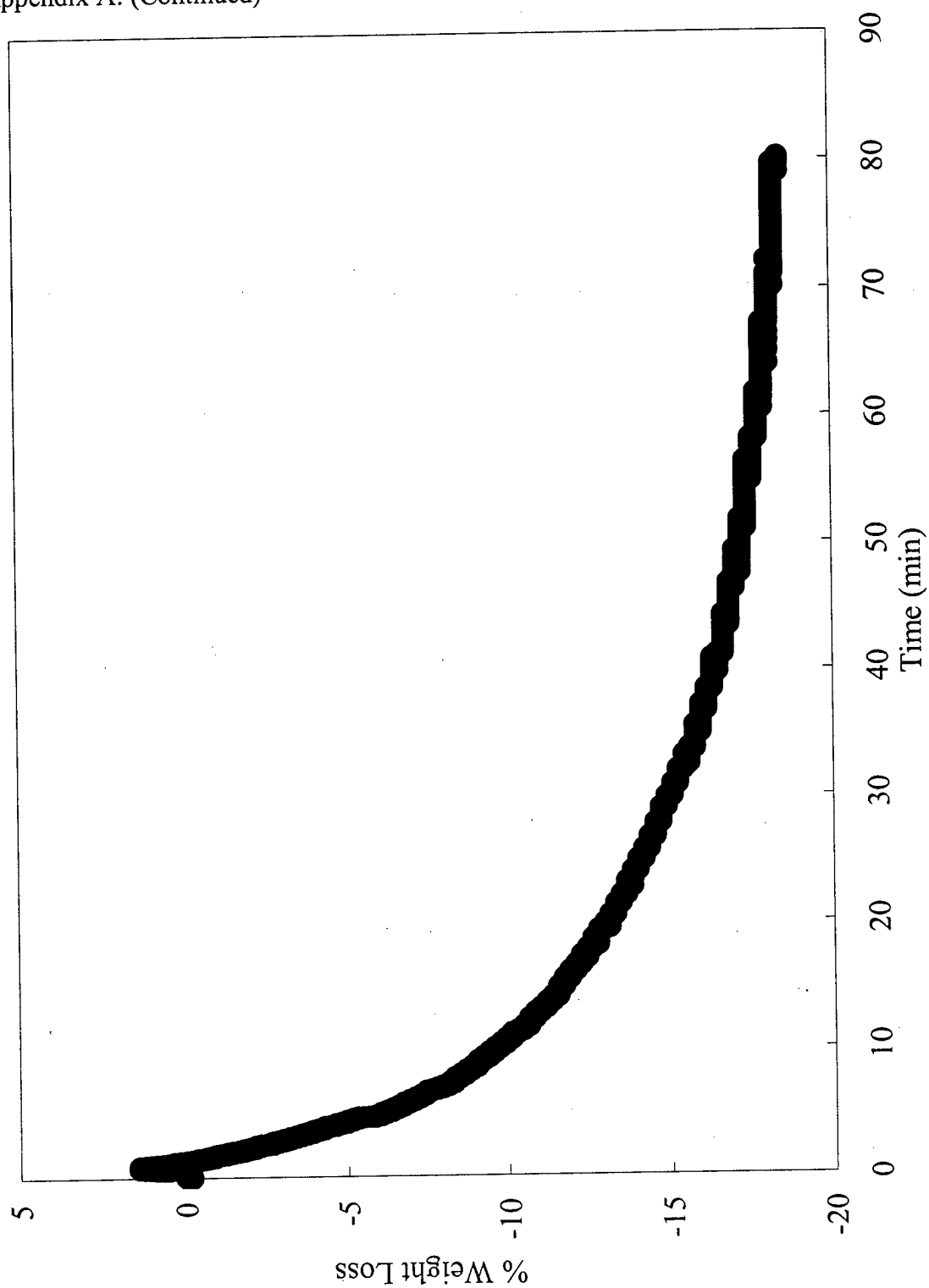


Figure A-11. Kagomé % Weight Loss vs Time, Profile 3

Appendix A: (Continued)

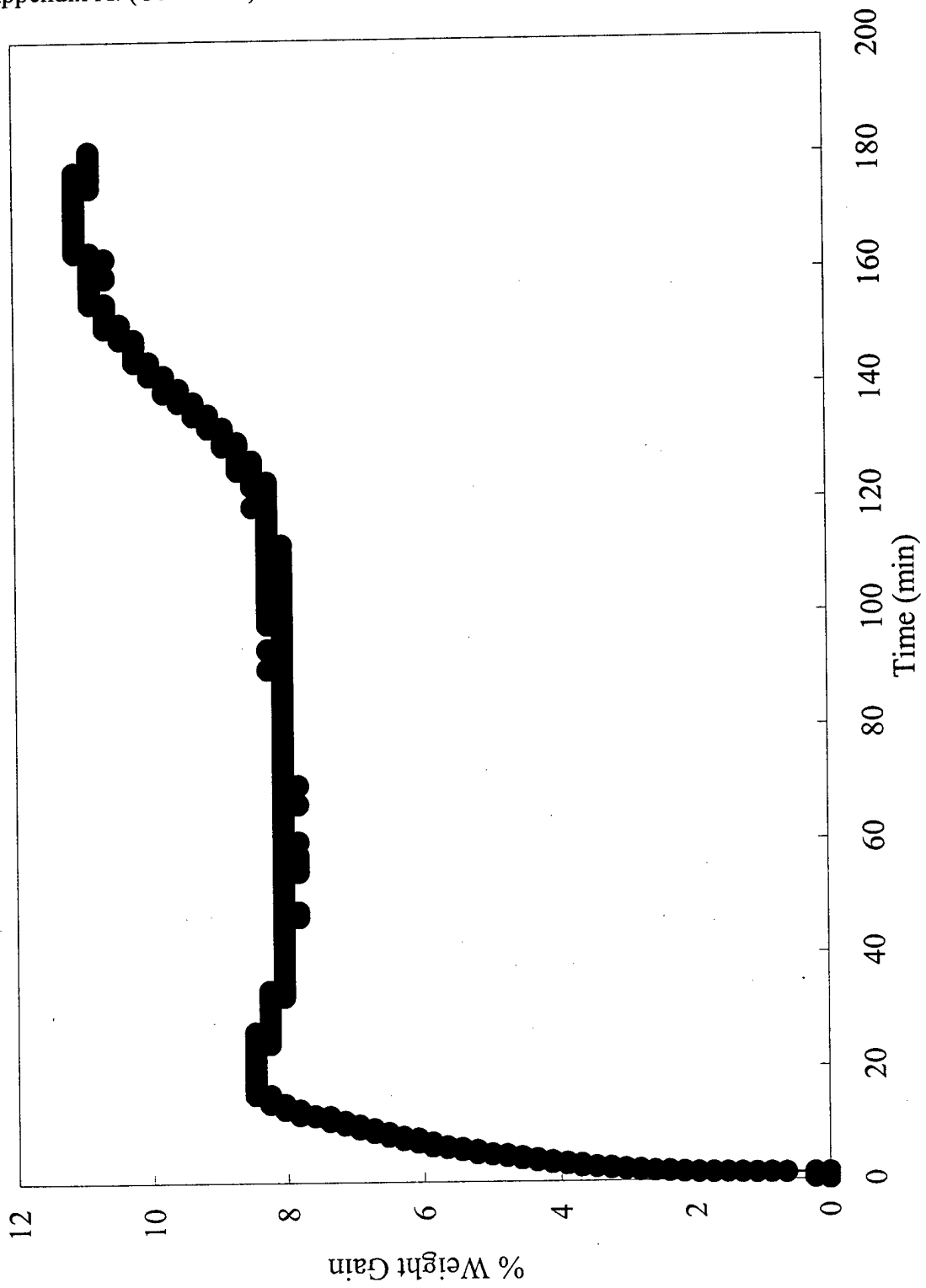


Figure A-12. Kagomé % Weight Gain vs Time, Profile 3

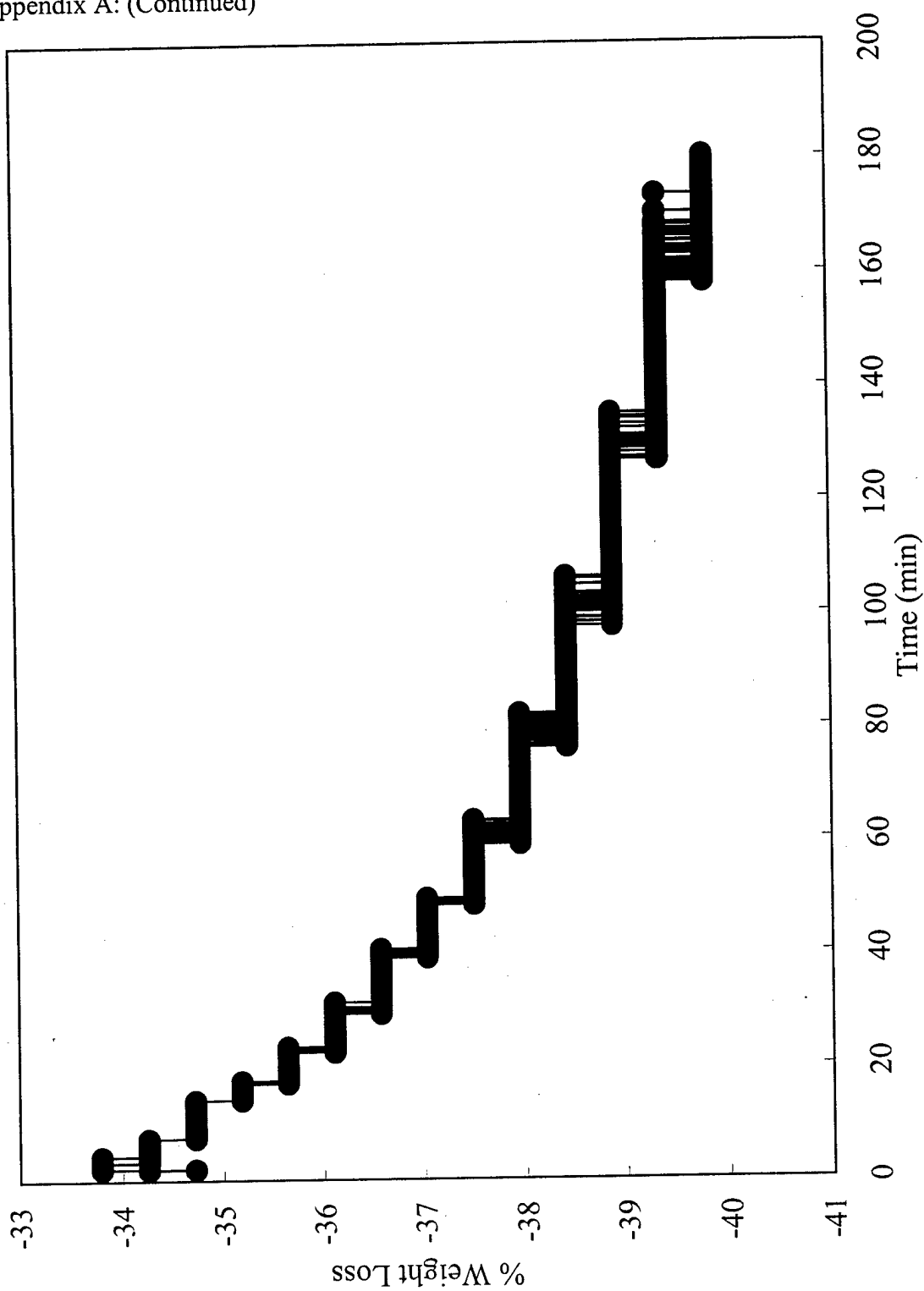


Figure A-13. Zinc Cubic % Weight Loss vs Time, Profile 1

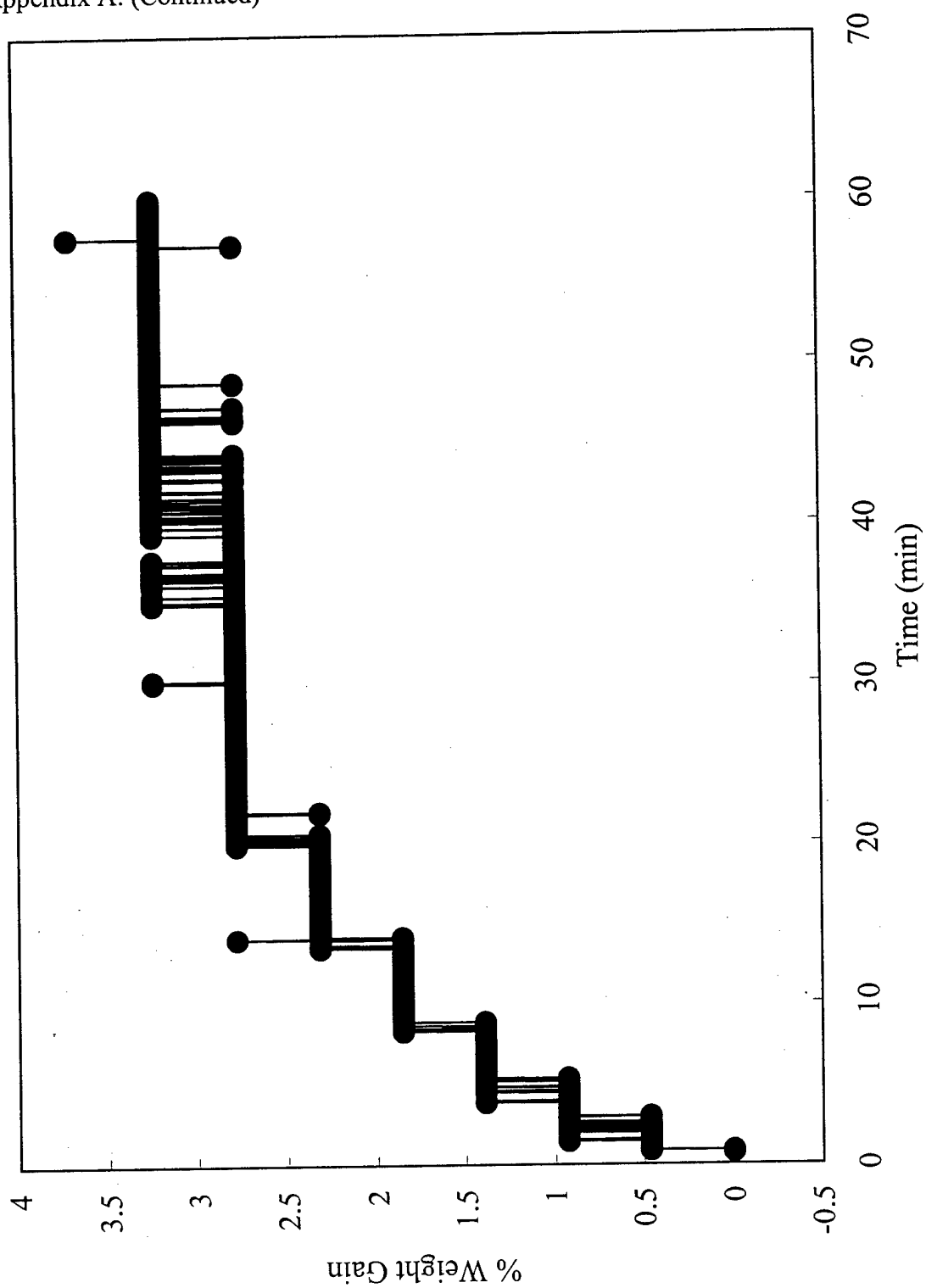


Figure A-14. Zinc Cubic % Weight Gain vs Time, Profile 1

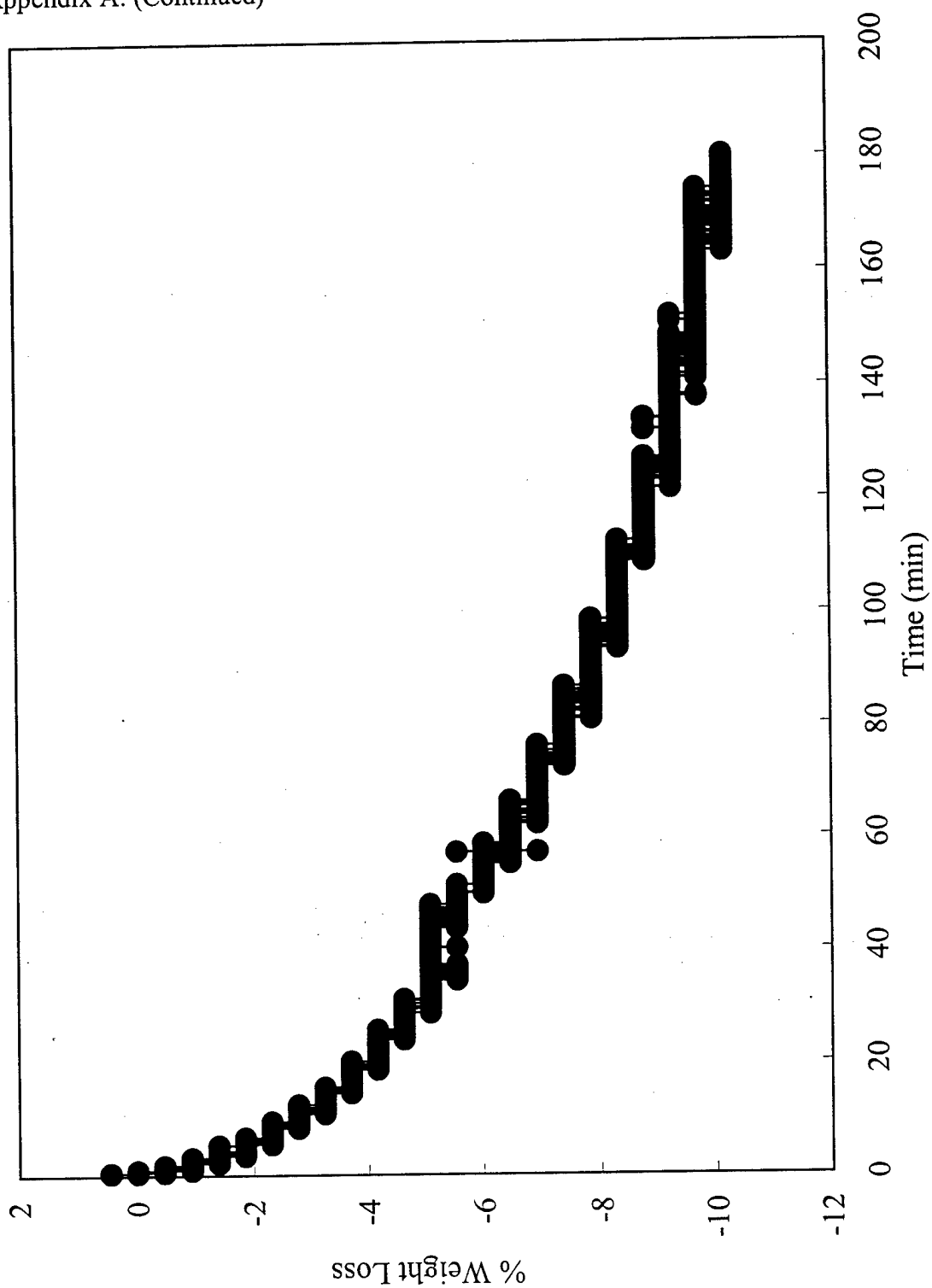


Figure A-15. Zinc Cubic % Weight Loss vs Time, Profile 2

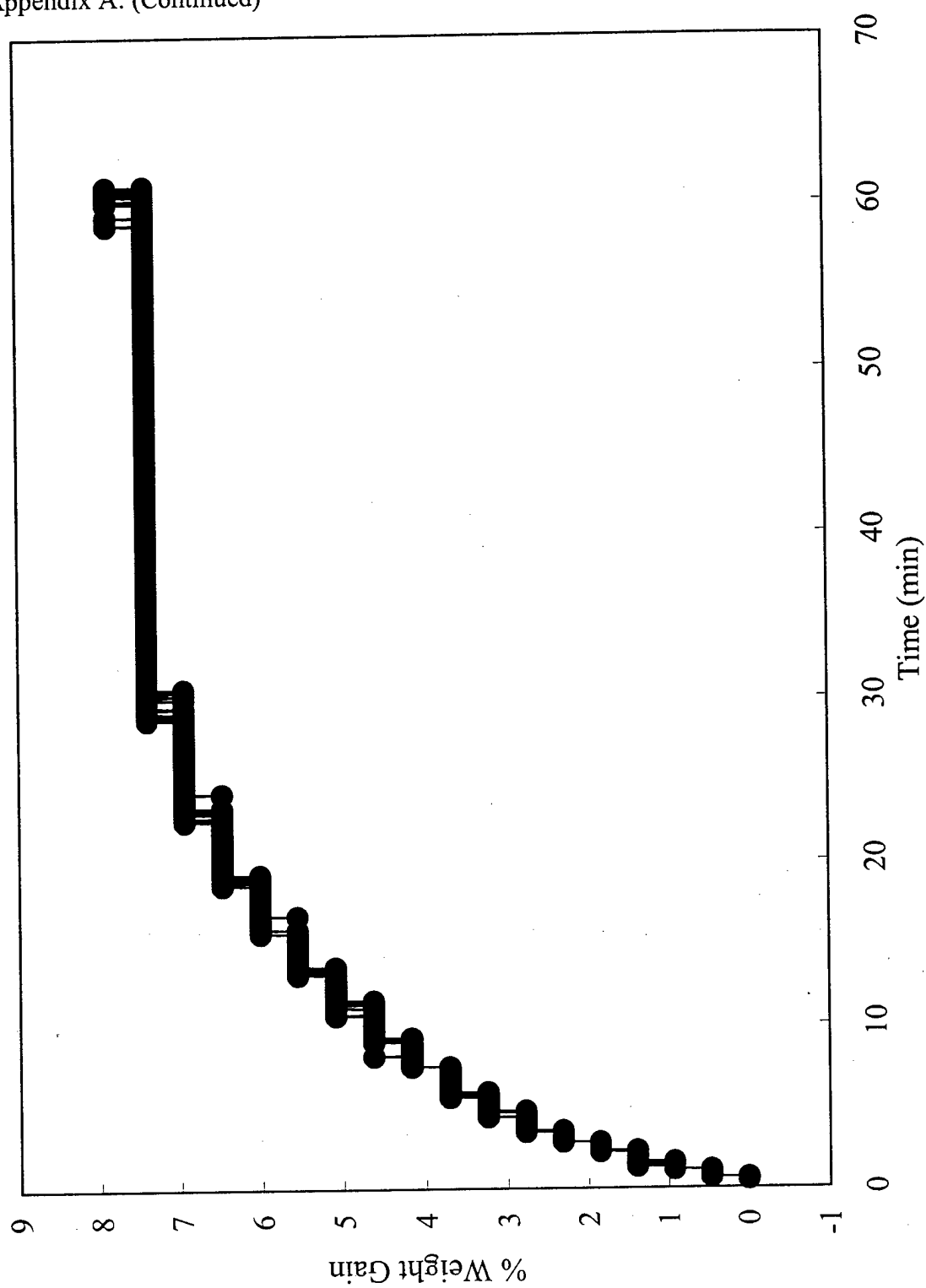


Figure A-16. Zinc Cubic % Weight Gain vs Time, Profile 2

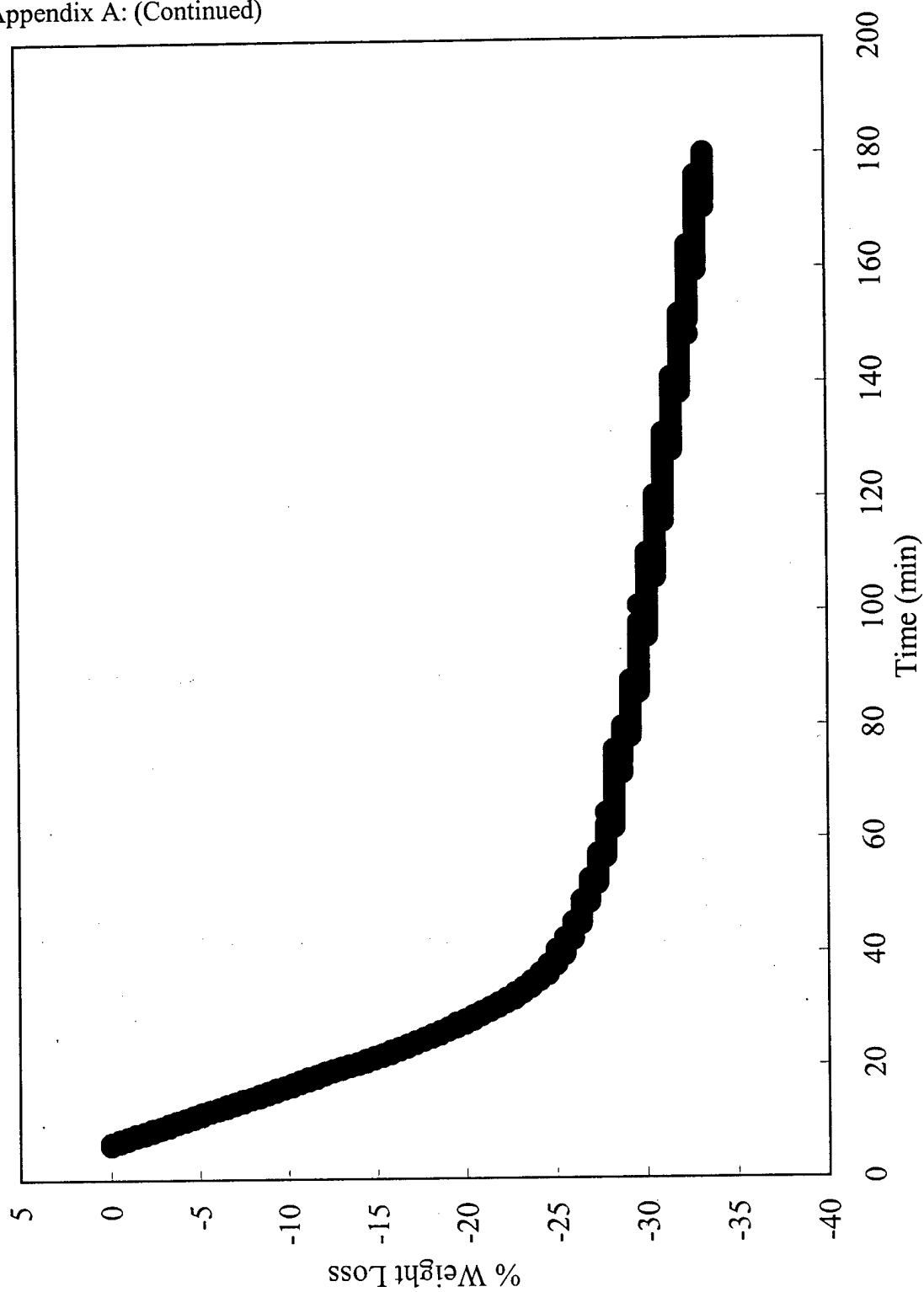


Figure A-17. Zinc Cubic % Weight Loss vs Time, Profile 3

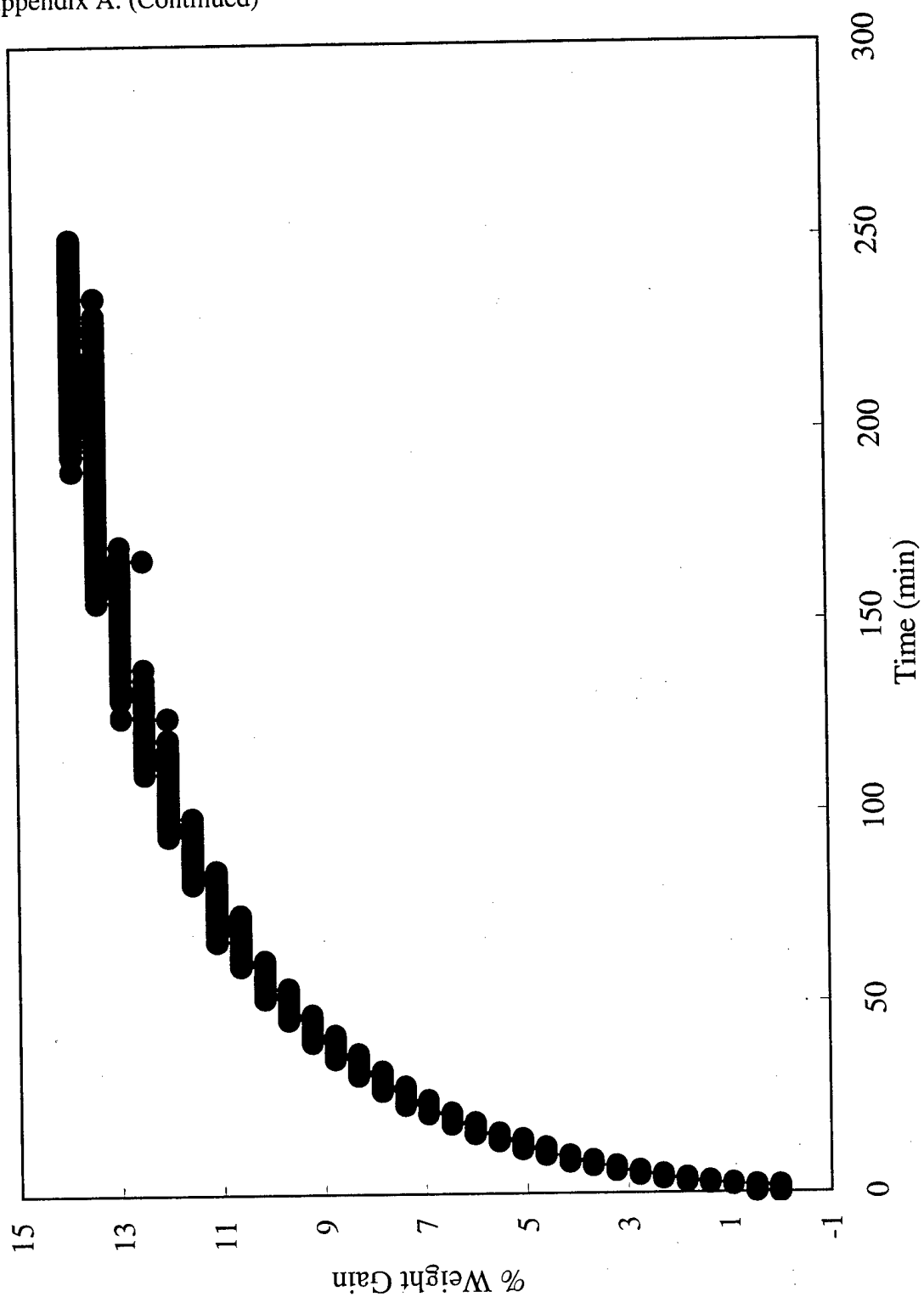


Figure A-18. Zinc Cubic % Weight Gain vs Time, Profile 3

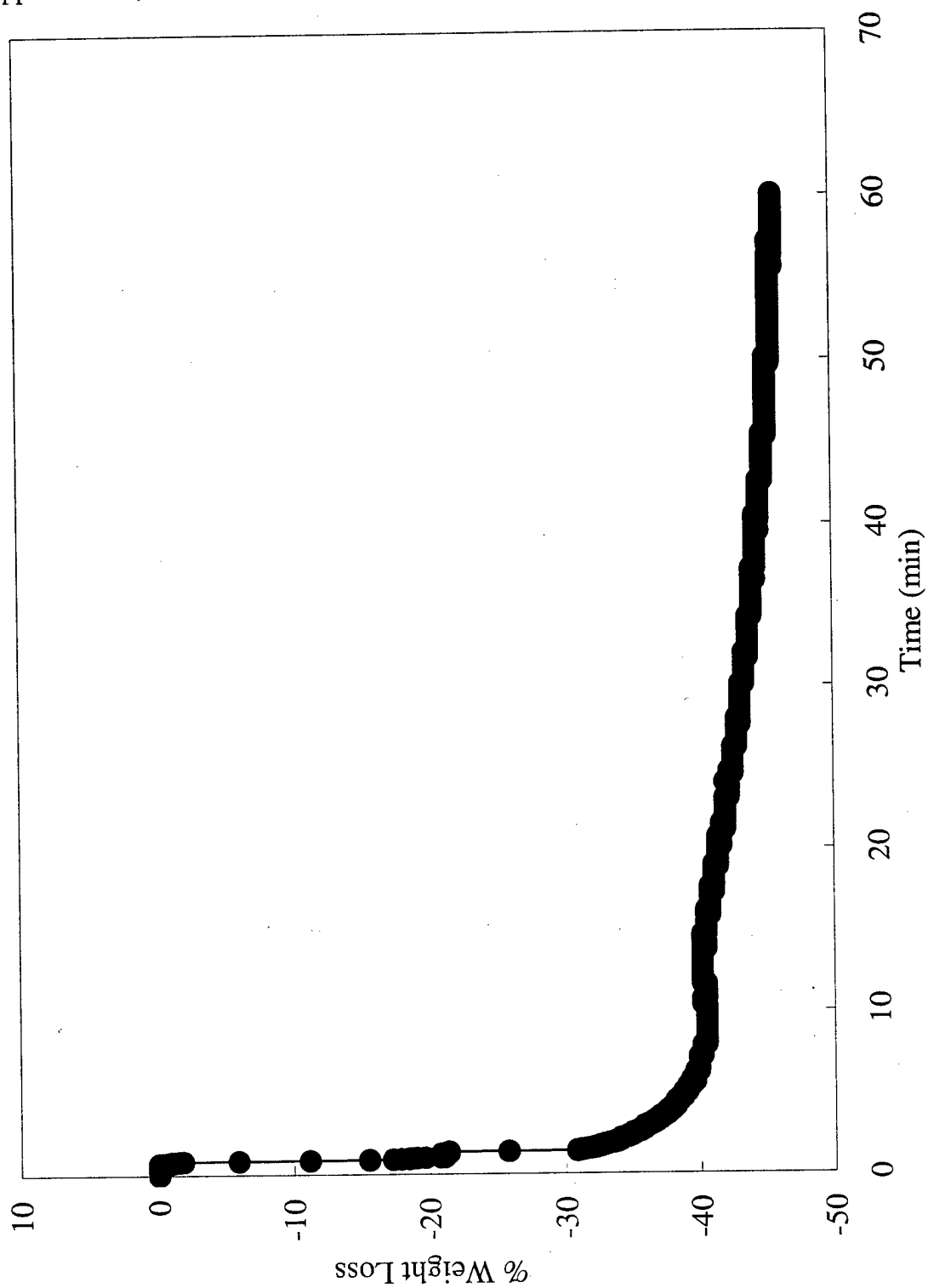


Figure A-19. Copper Octahedral 1, % Weight Loss vs Time, Profile 1

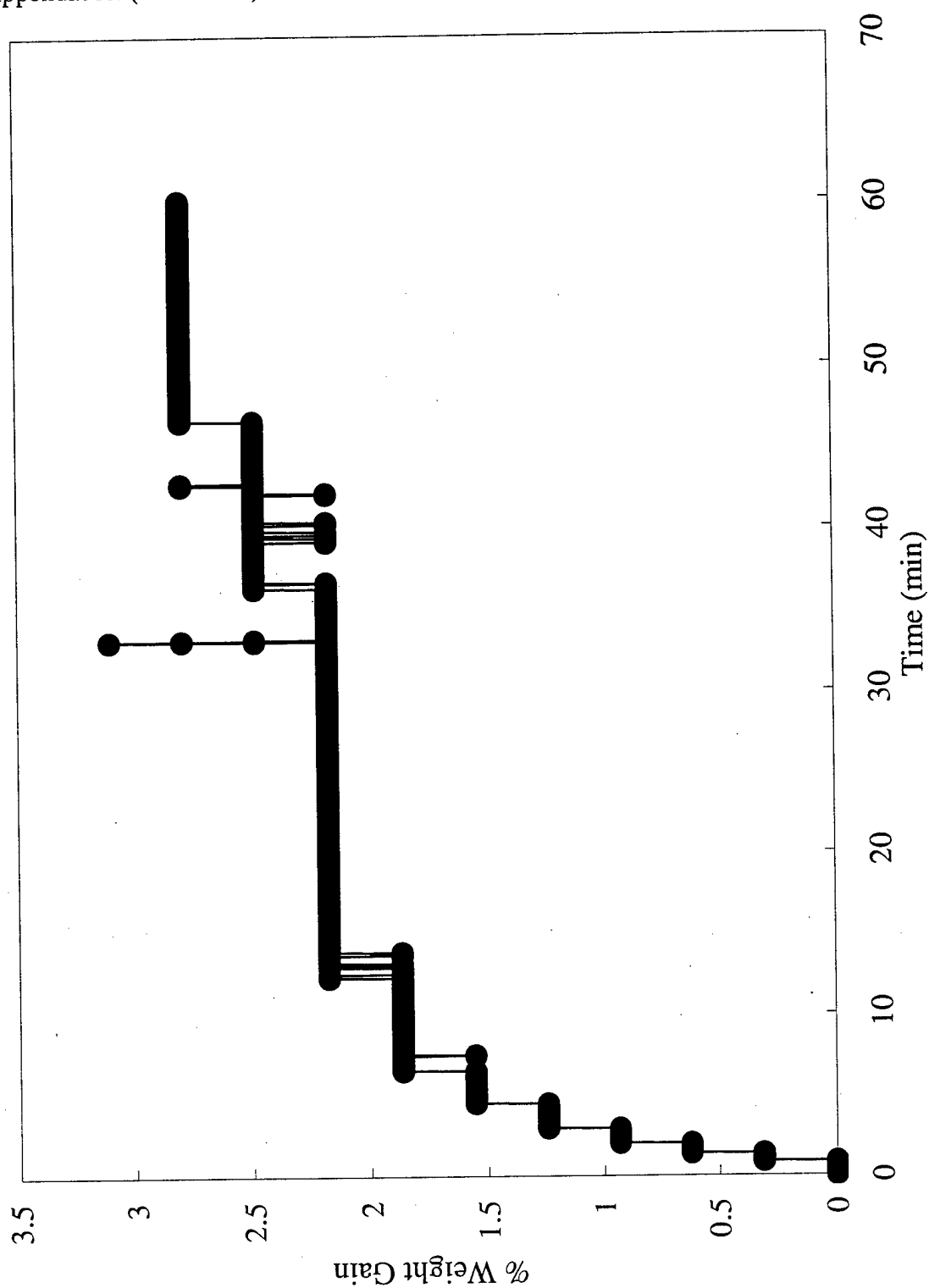


Figure A-20. Copper Octahedral 1, % Weight Gain vs Time, Profile 1

Appendix A: (Continued)

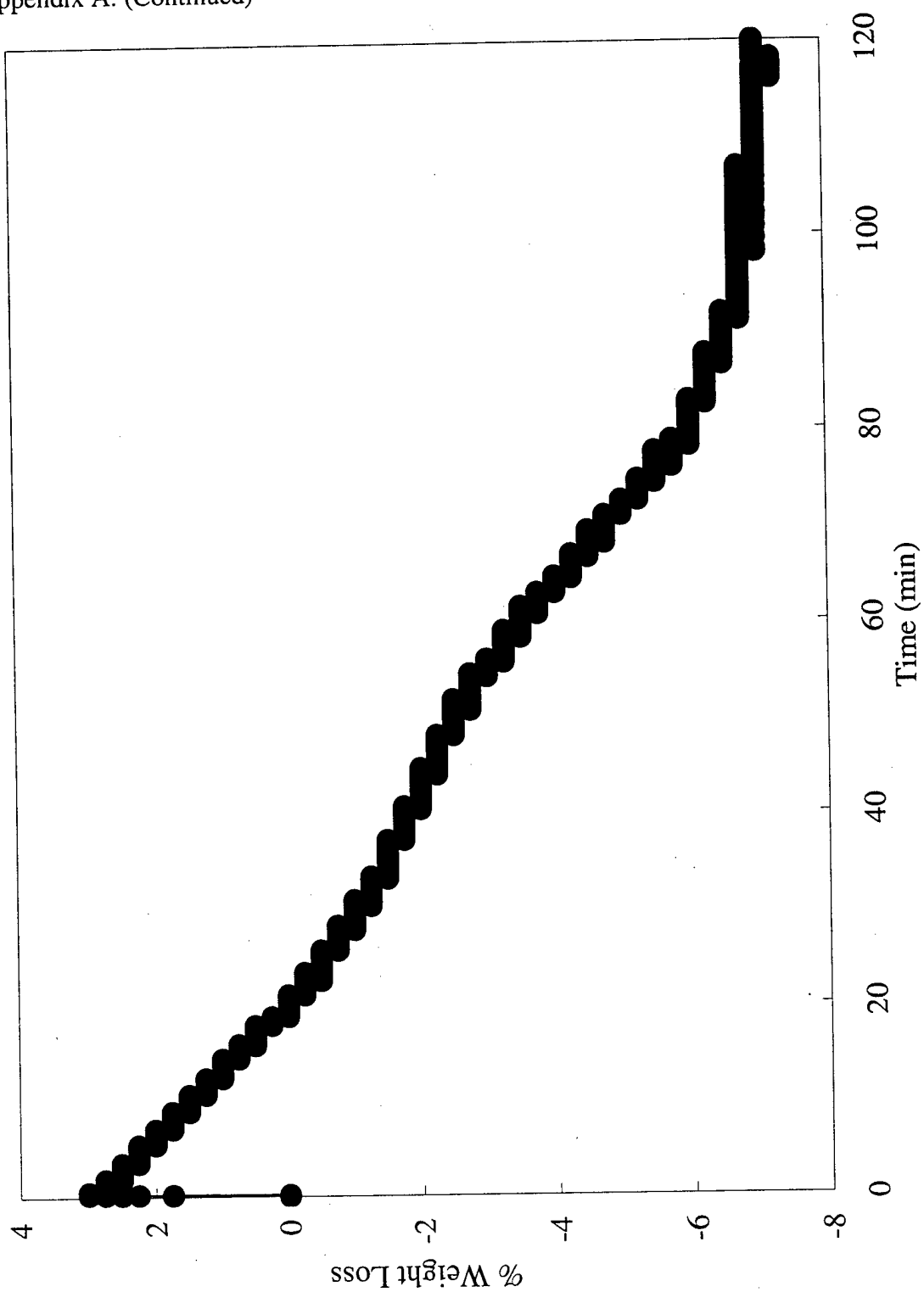


Figure A-21. Copper Octahedral 1, % Weight Loss vs Time, Profile 2

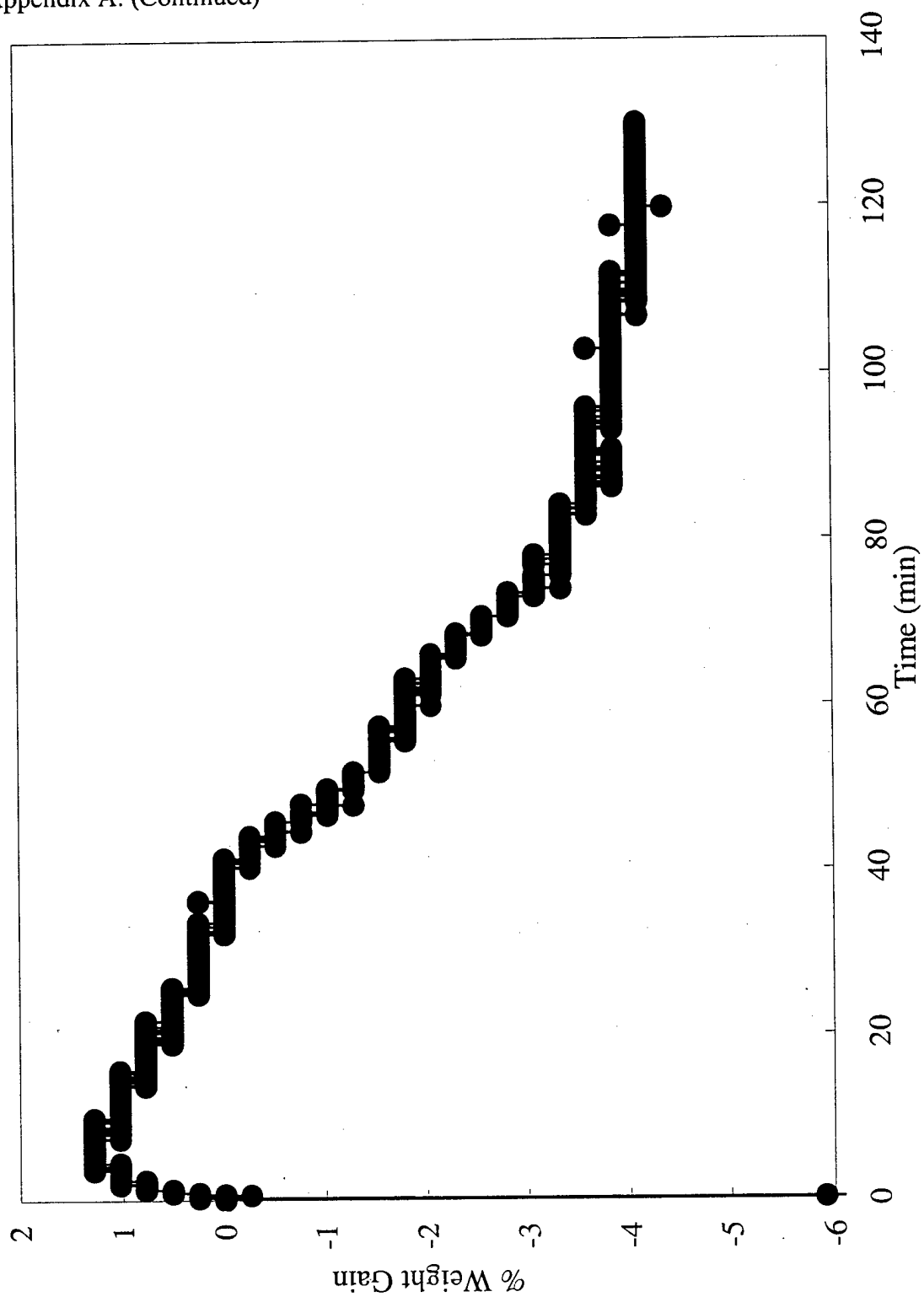


Figure A-22. Copper Octahedral 1, % Weight Gain vs Time, Profile 2

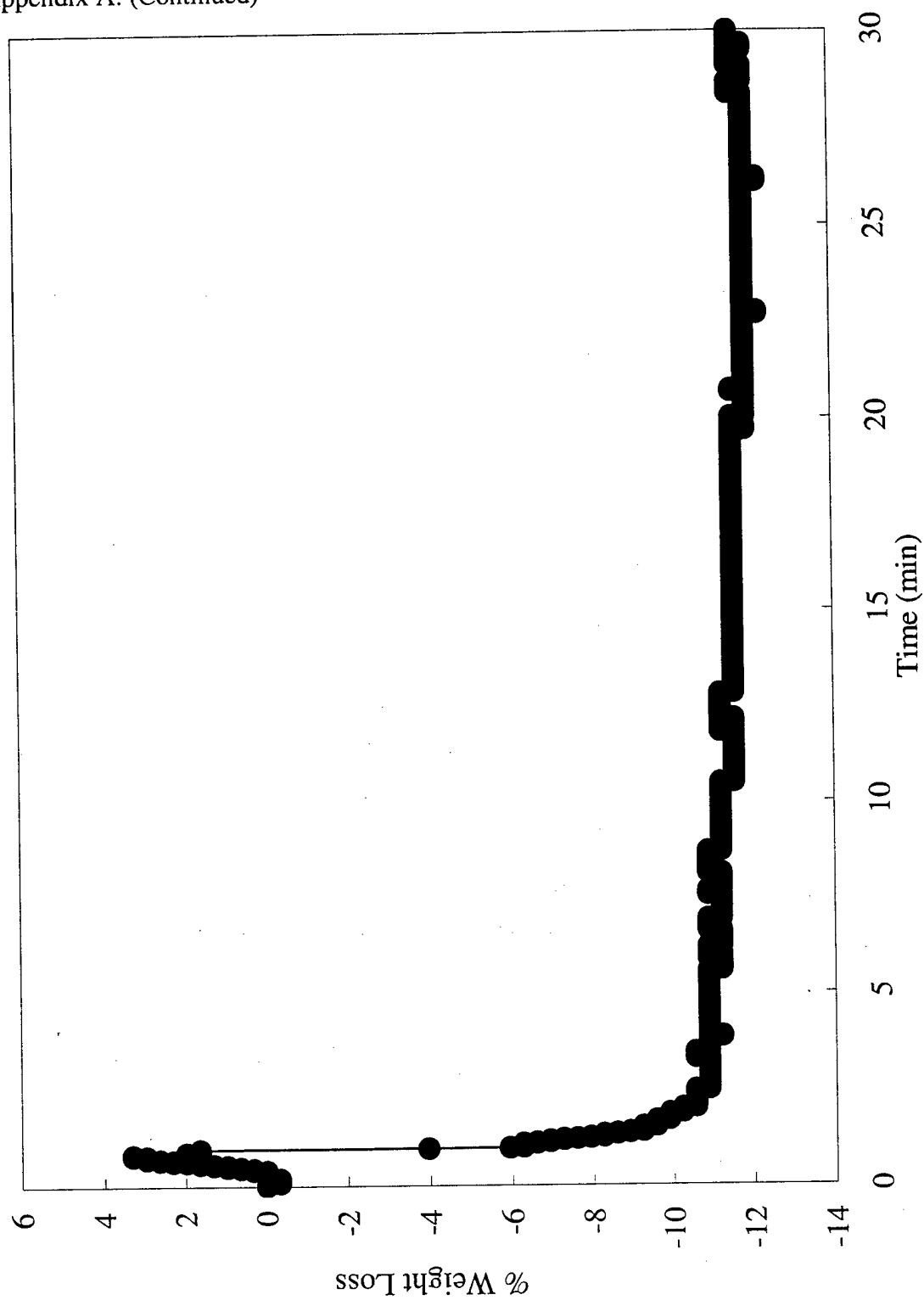


Figure A-23. Copper Octahedral 1, % Weight Loss vs Time, Profile 3

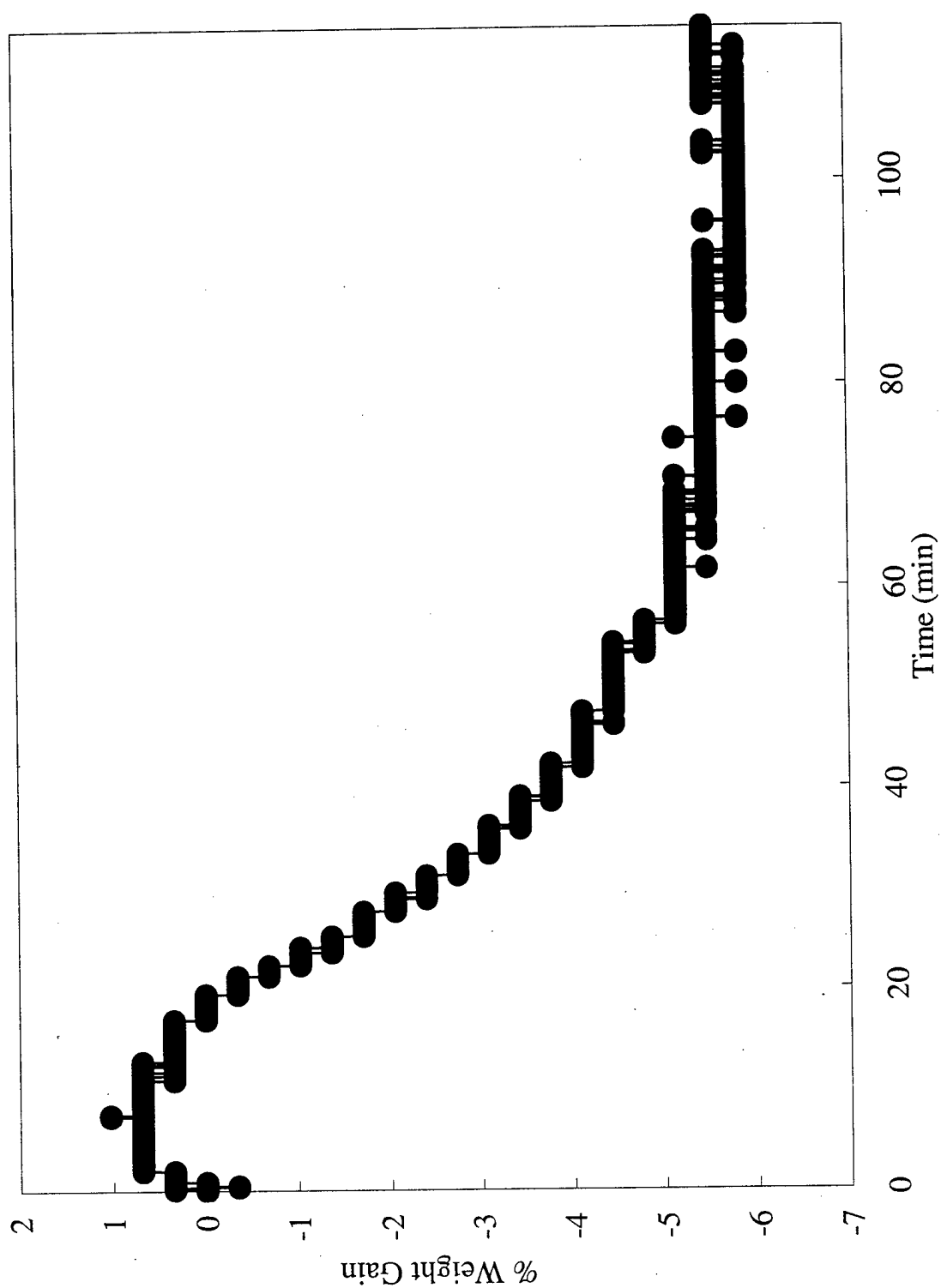


Figure A-24. Copper Octahedral 1, % Weight Gain vs Time, Profile 3

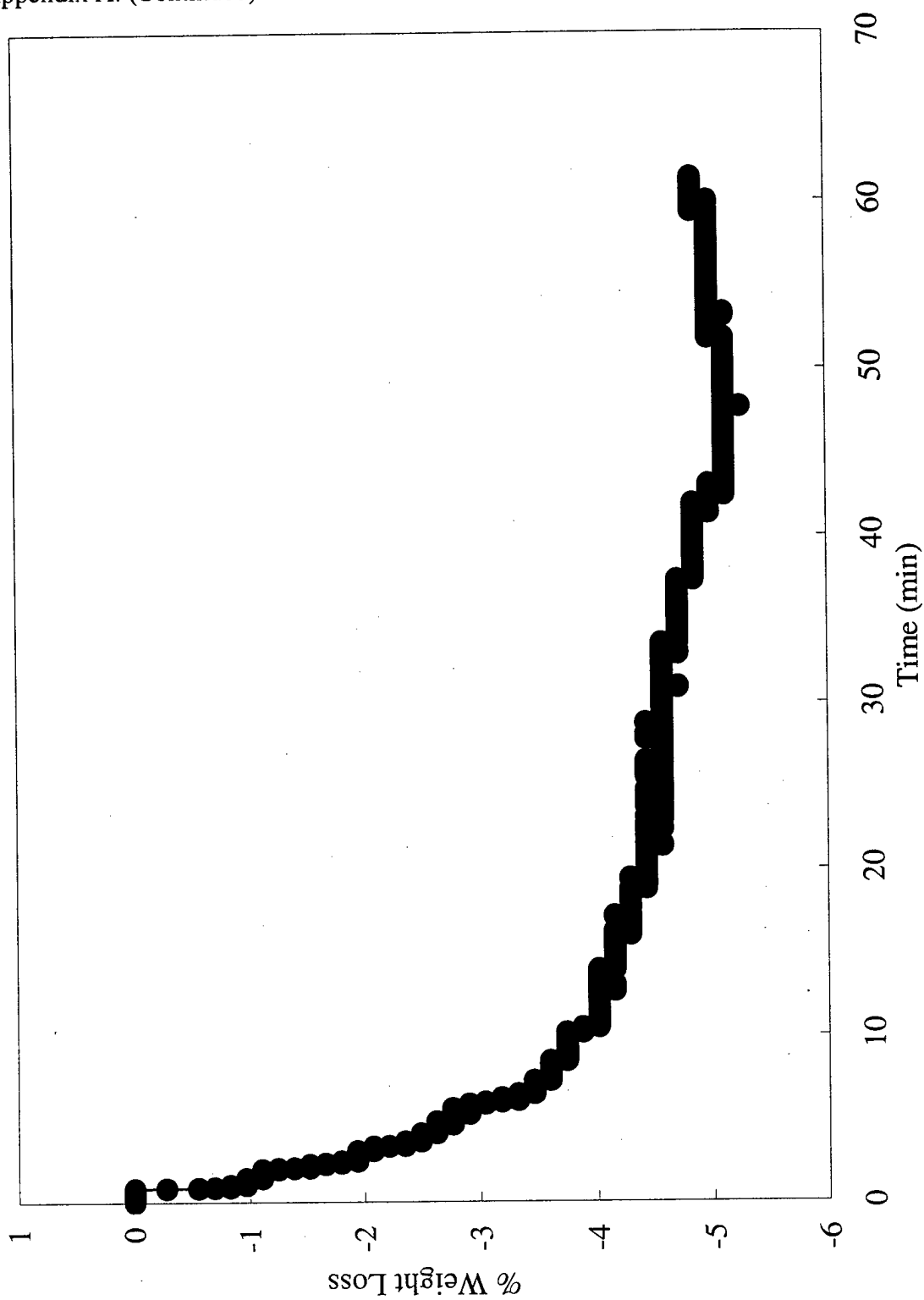


Figure A-25. Copper Octahedral 2, % Weight Loss vs Time, Profile 1

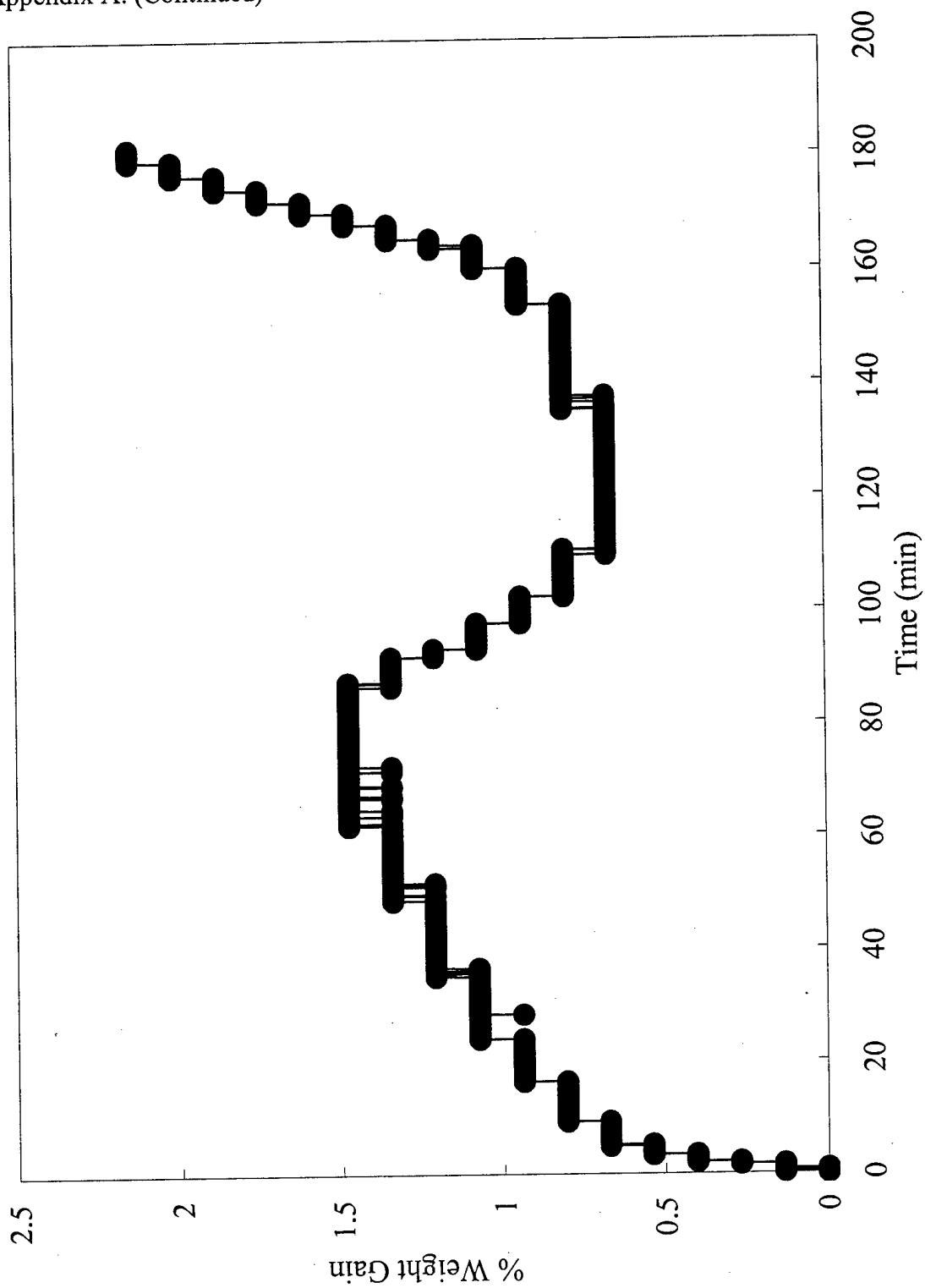


Figure A-26. Copper Octahedral 2, % Weight Gain vs Time, Profile 1

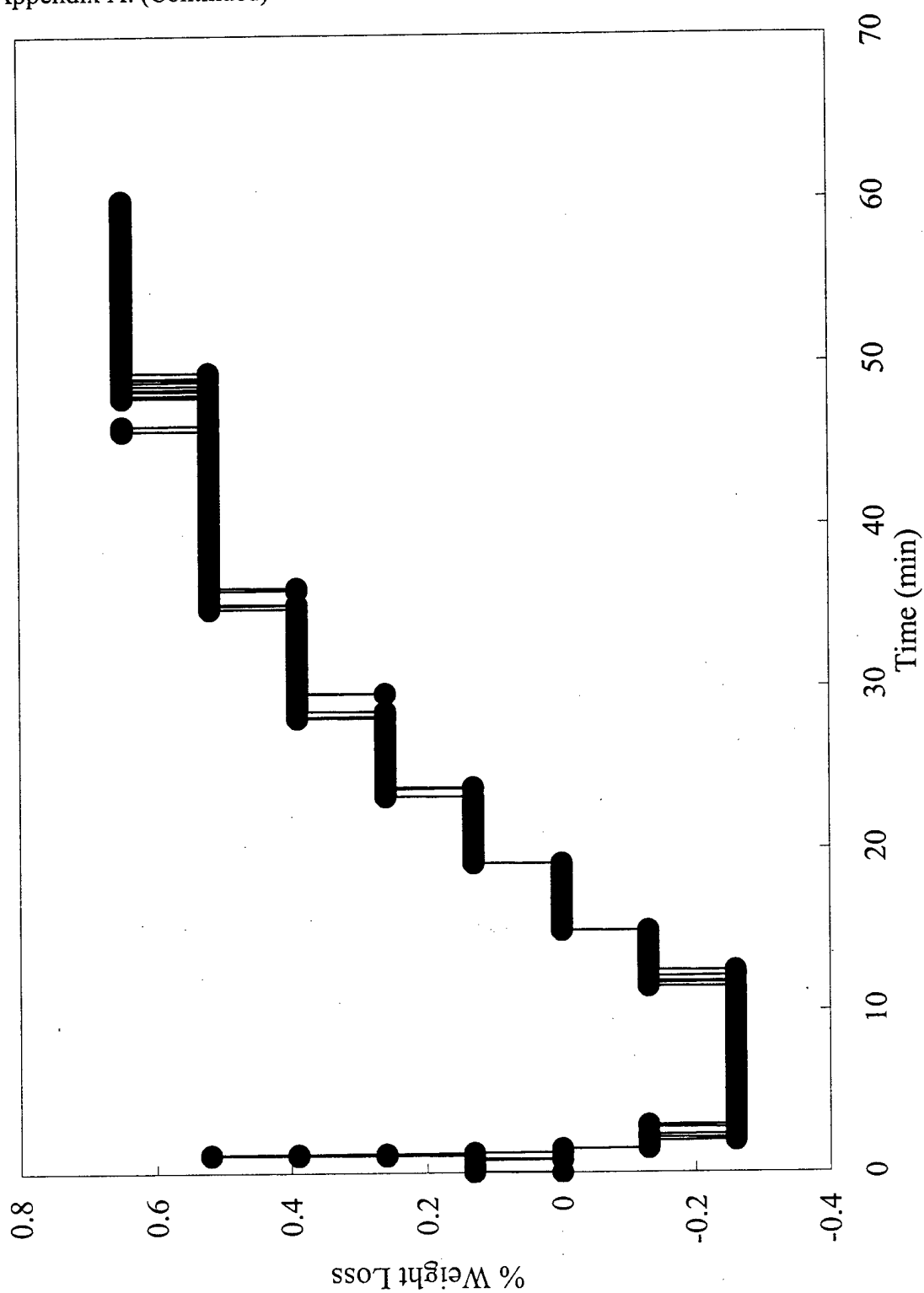


Figure A-27. Copper Octahedral 2 % Weight Loss vs Time, Profile 2

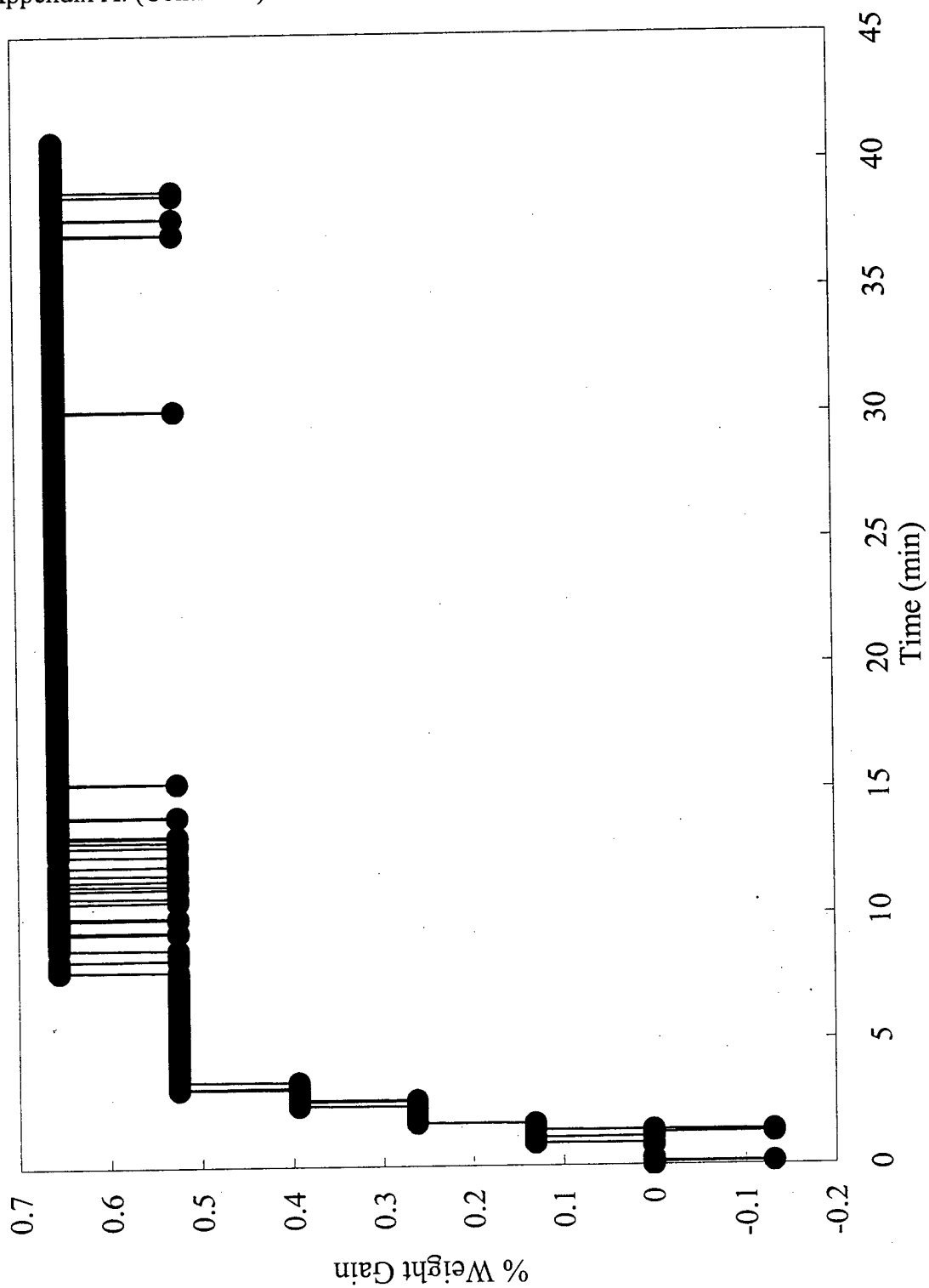


Figure A-28. Copper Octahedral 2, % Weight Gain vs Time, Profile 2

Appendix A: (Continued)

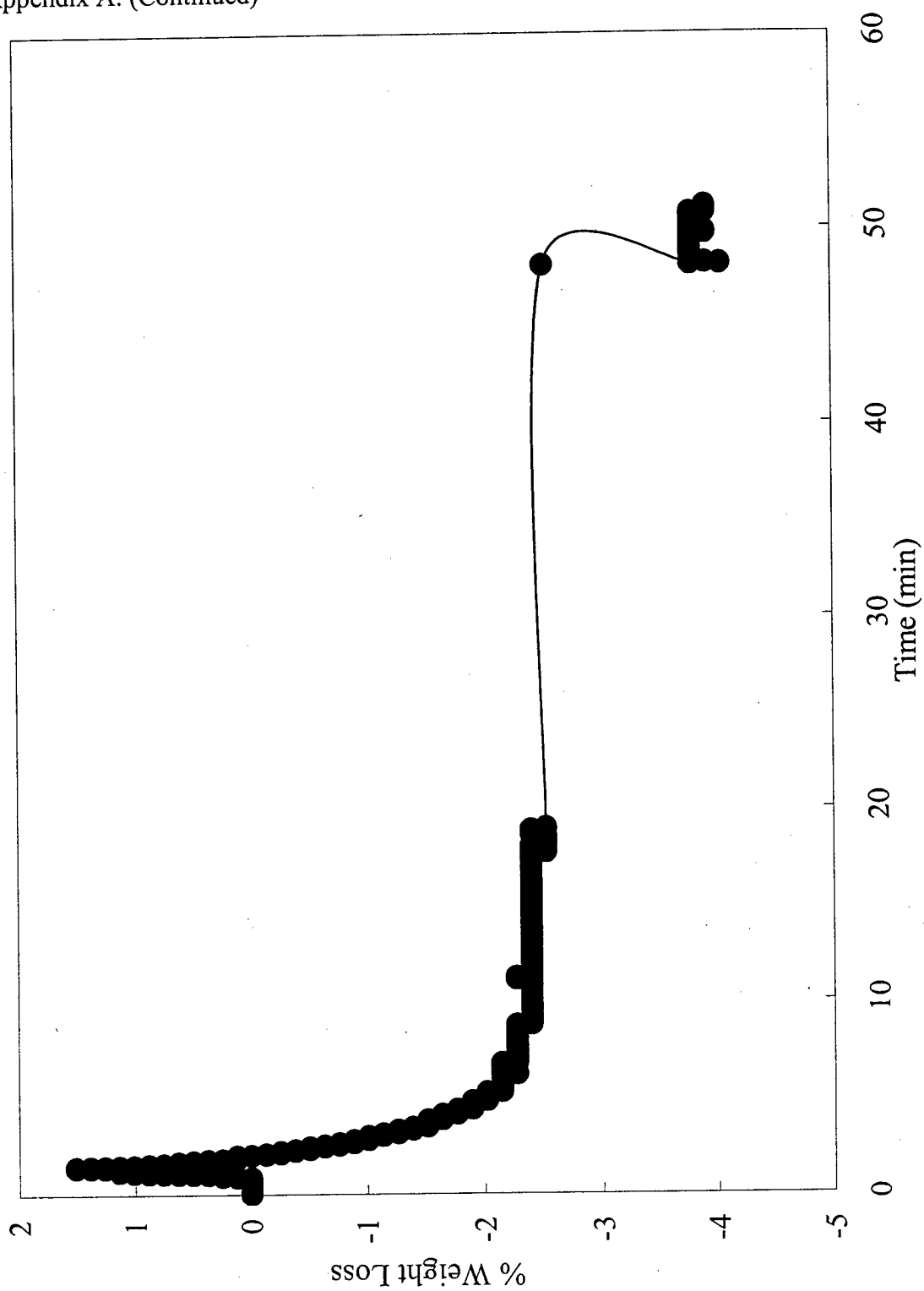


Figure A-29. Copper Octahedral 2, % Weight Loss vs Time, Profile 3

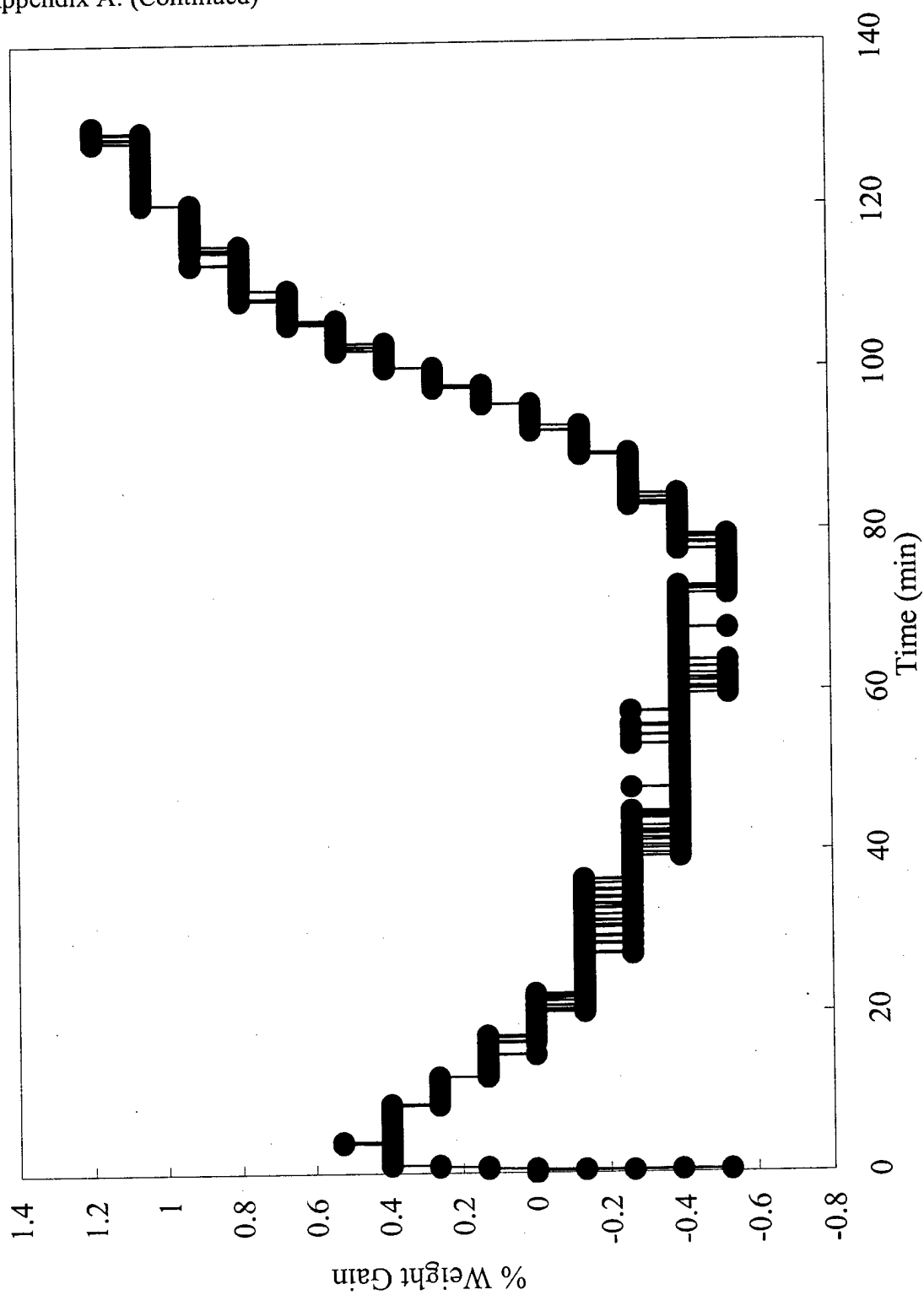


Figure A-30. Copper Octahedral 2, % Weight Gain vs Time, Profile 3

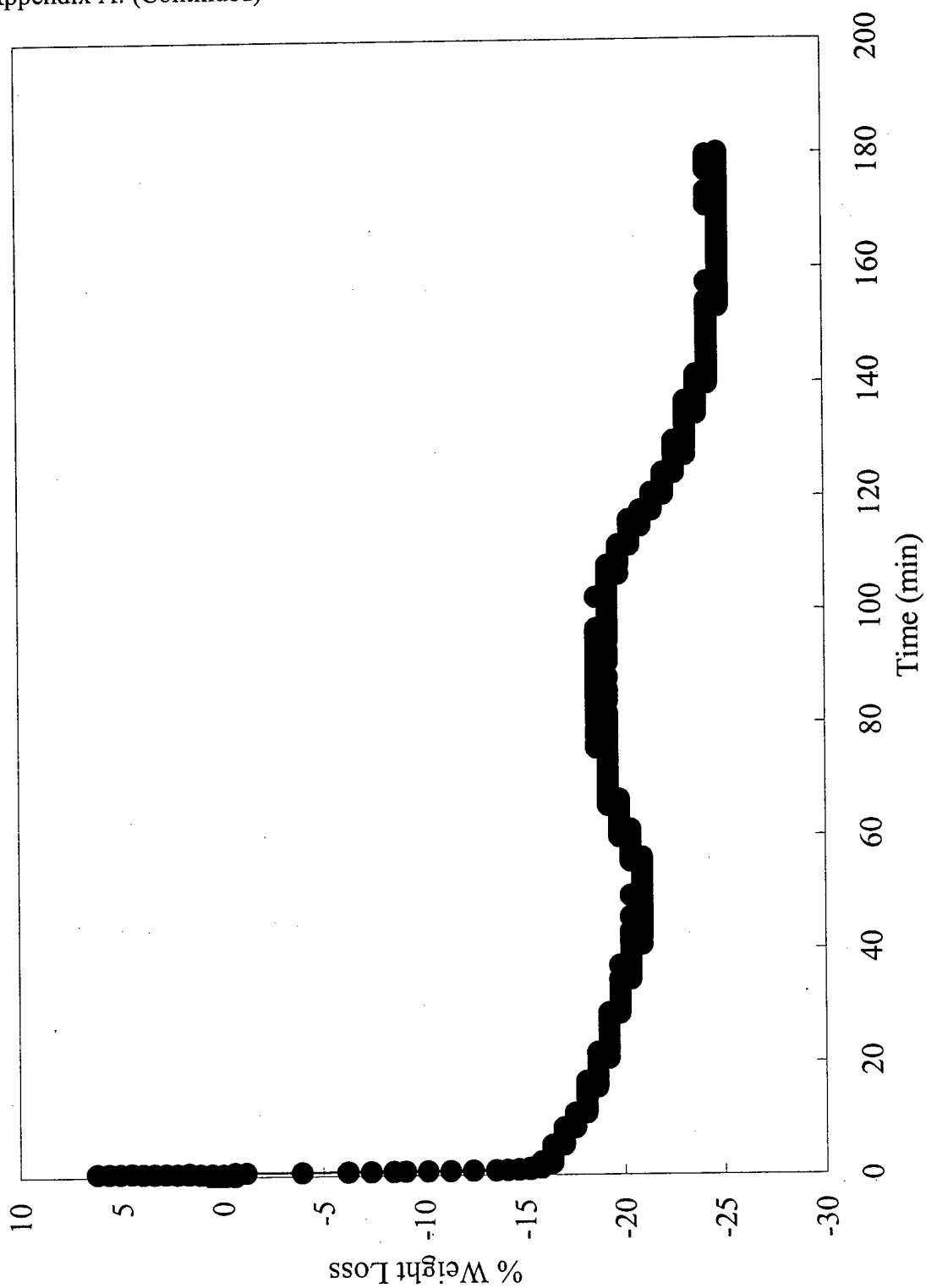


Figure A-31. Copper Octahedral 3, % Weight Loss vs Time, Profile 1

Appendix A: (Continued)

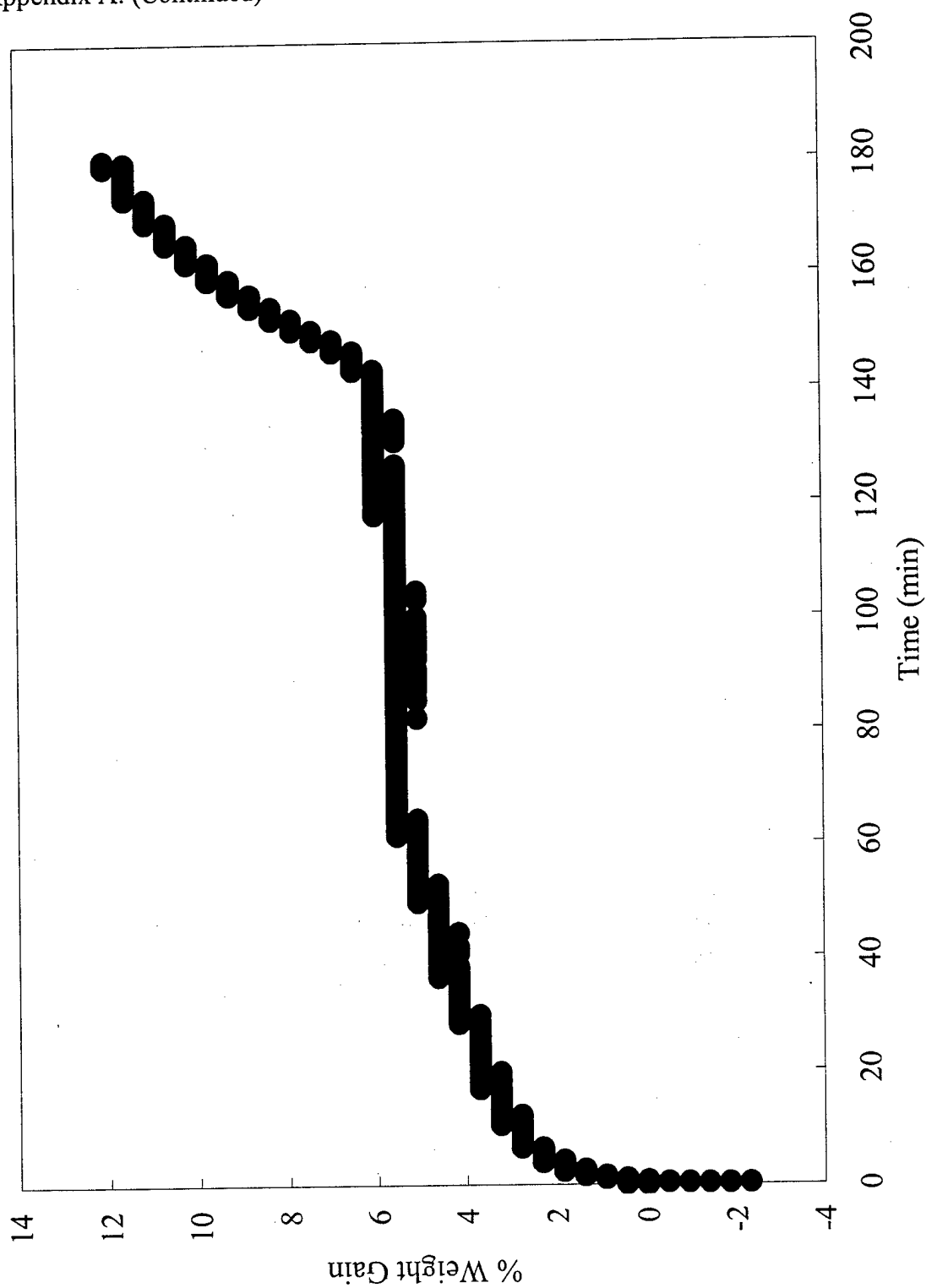


Figure A-32. Copper Octahedral 3, % Weight Gain vs Time, Profile 1

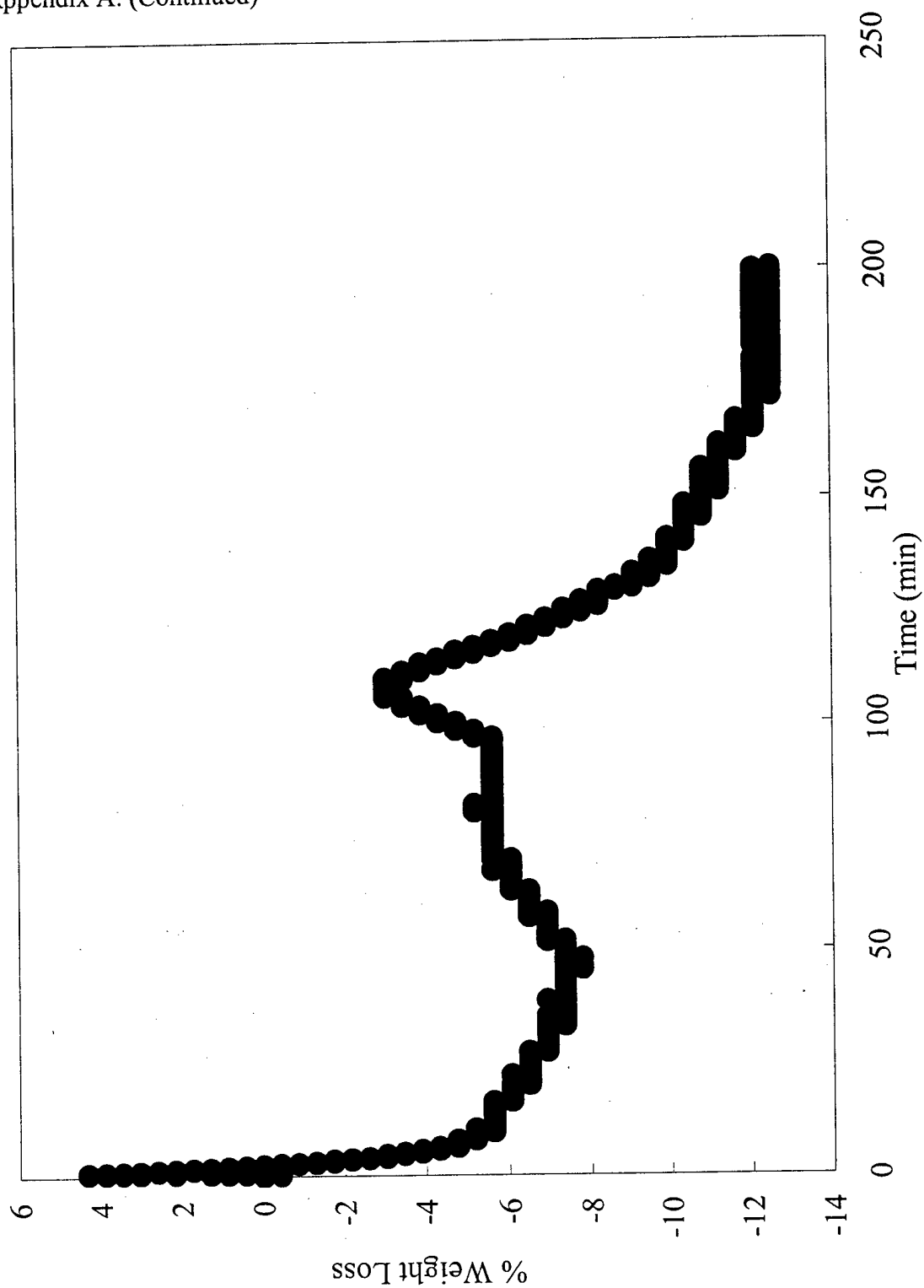


Figure A-33. Copper Octahedral 3, % Weight Loss vs Time, Profile 2

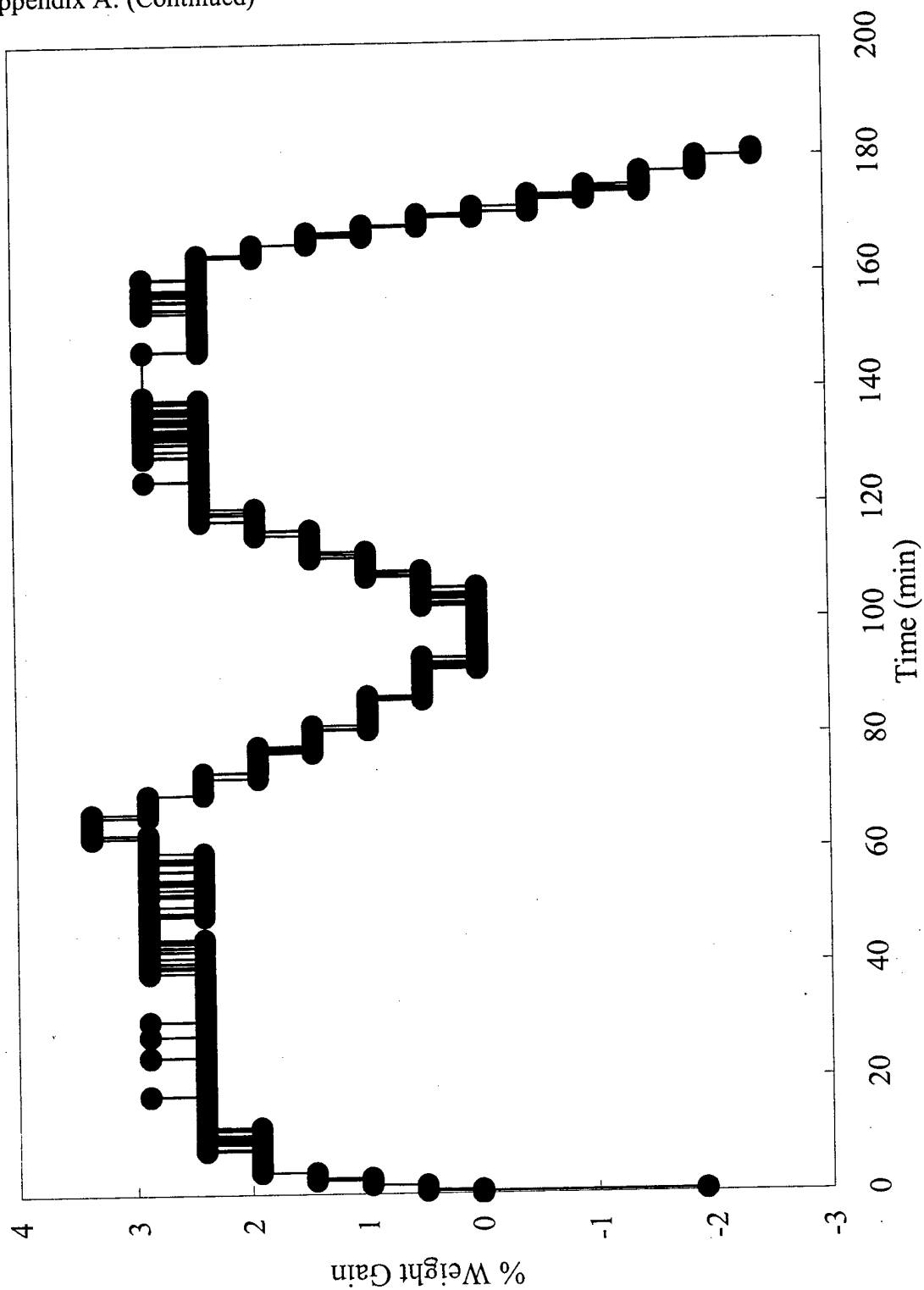


Figure A-34. Copper Octahedral 3, % Weight Gain vs Time, Profile 2

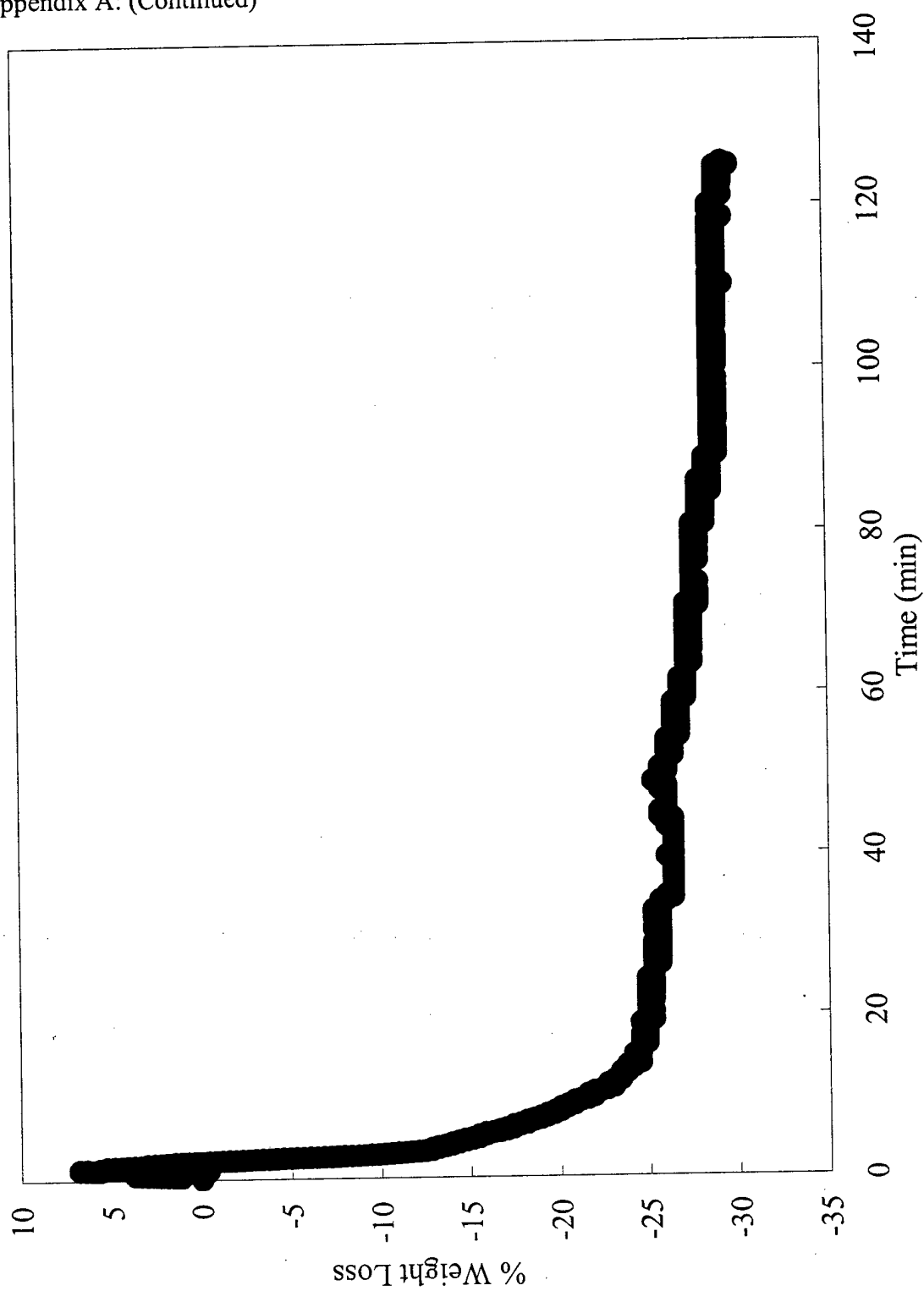


Figure A-35. Copper Octahedral 3, % Weight Loss vs Time, Profile 3

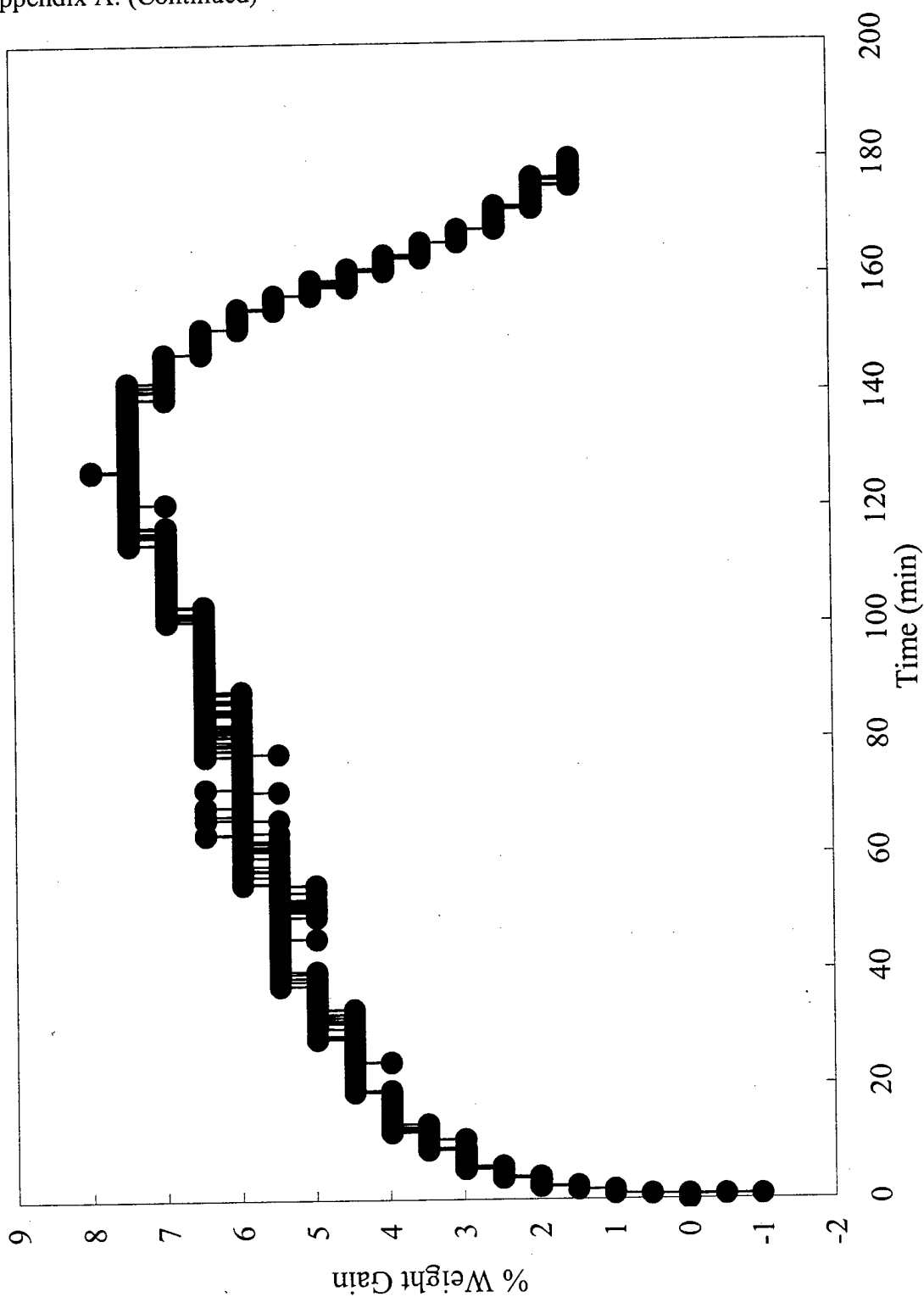


Figure A-36. Copper Octahedral 3, % Weight Gain vs Time, Profile 3

Appendix B
TGA Thermograms

Appendix B: TGA Thermograms

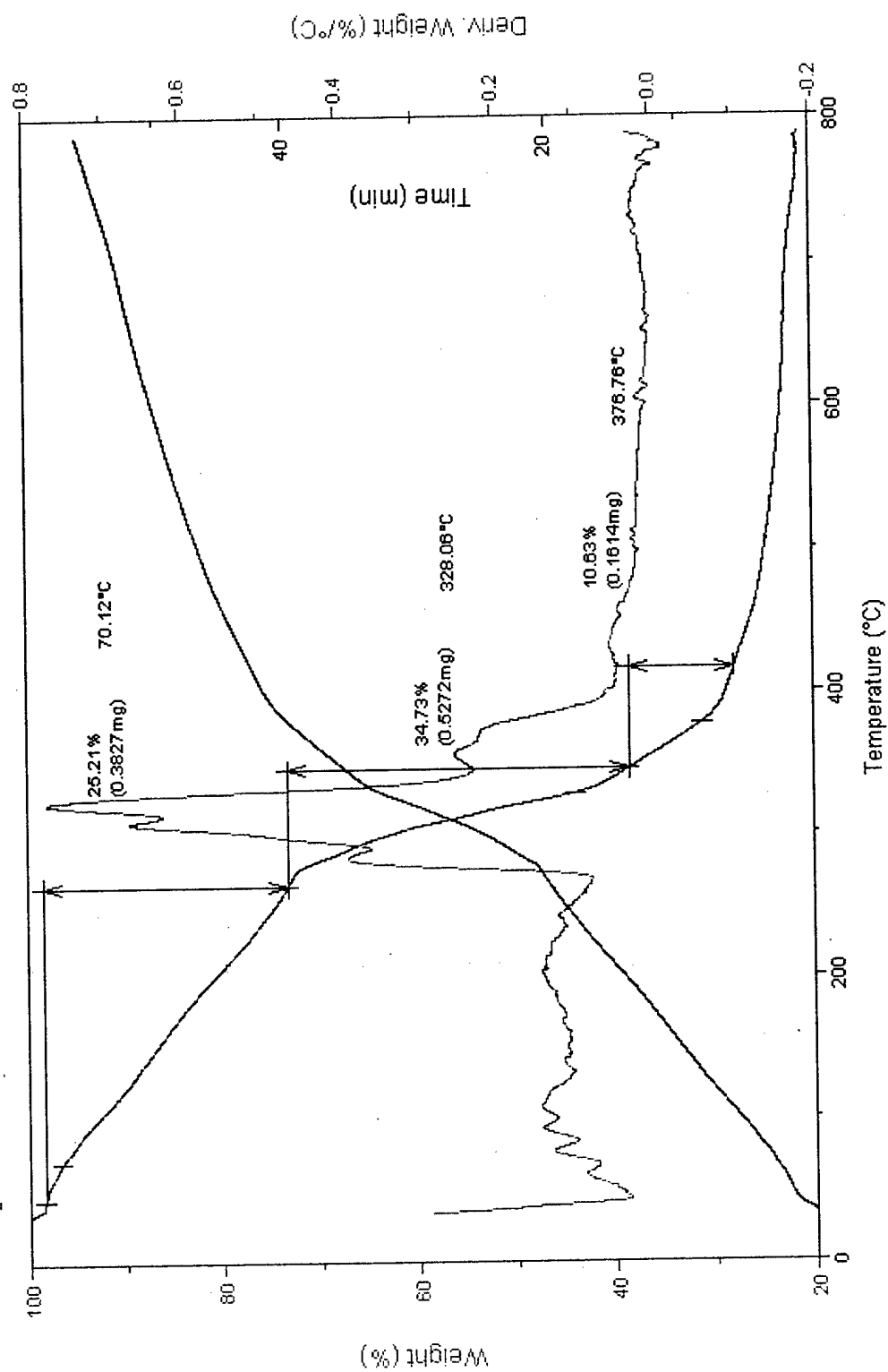


Figure B-1. Thermogram of Kagomé Material Before H-CAAAB Cycling.

Appendix B: (Continued)

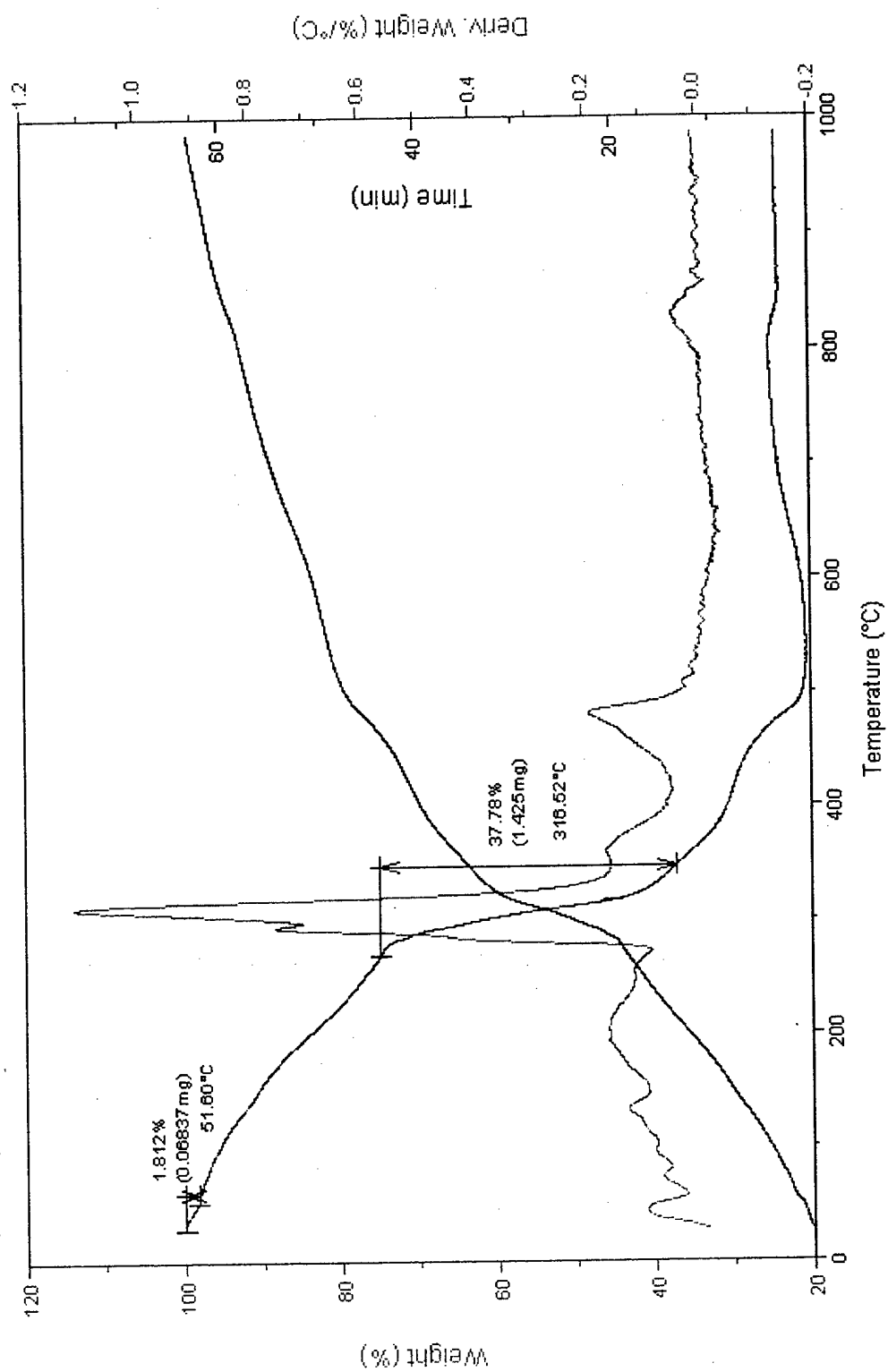


Figure B-2. Thermogram of Kagomé Material after H-CAAAB Cycling.

Appendix B: (Continued)

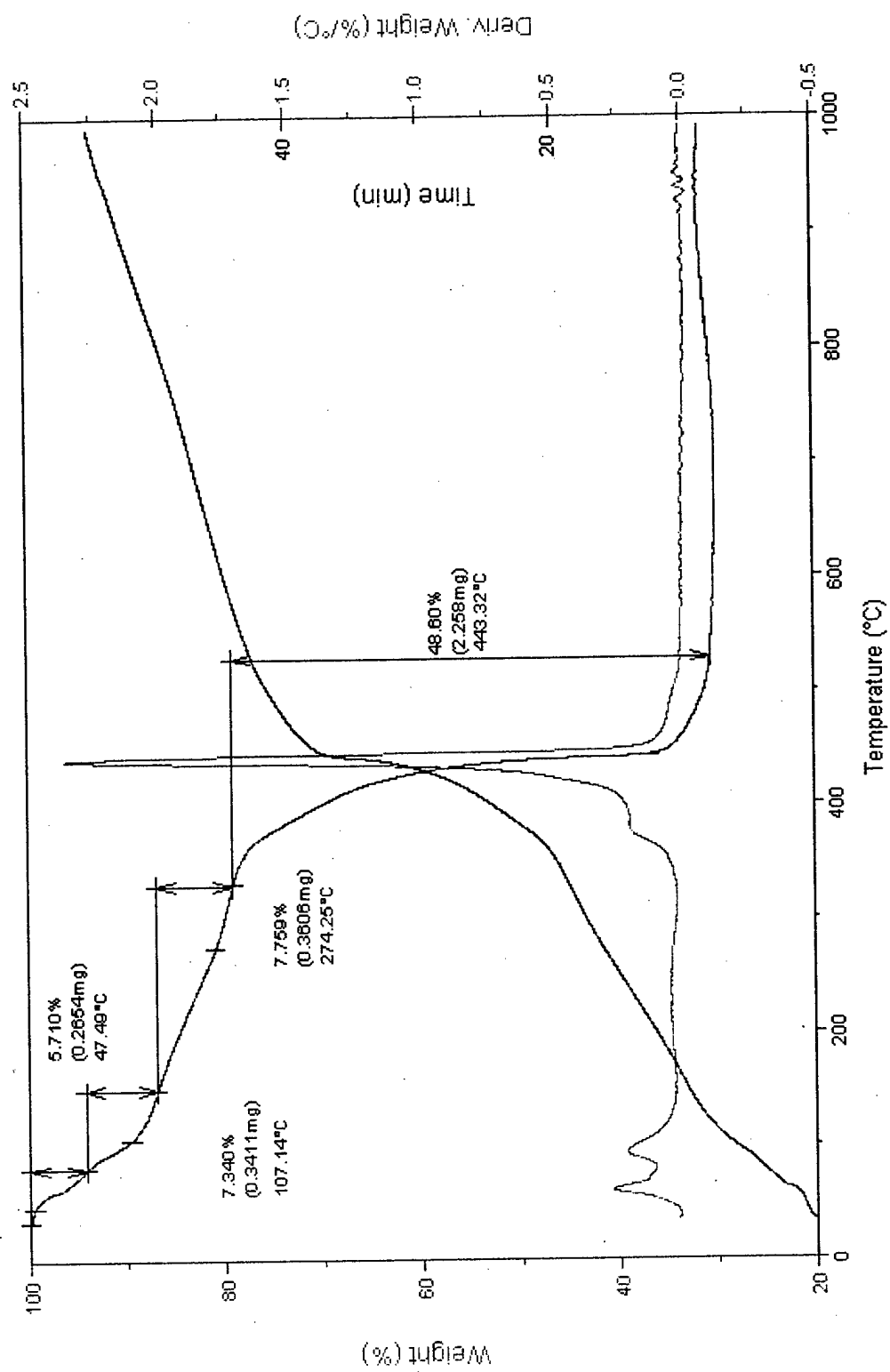


Figure B-3. Thermogram of Zinc Cubic Material Before H-CAAAB Cycling.

Appendix B: (Continued)

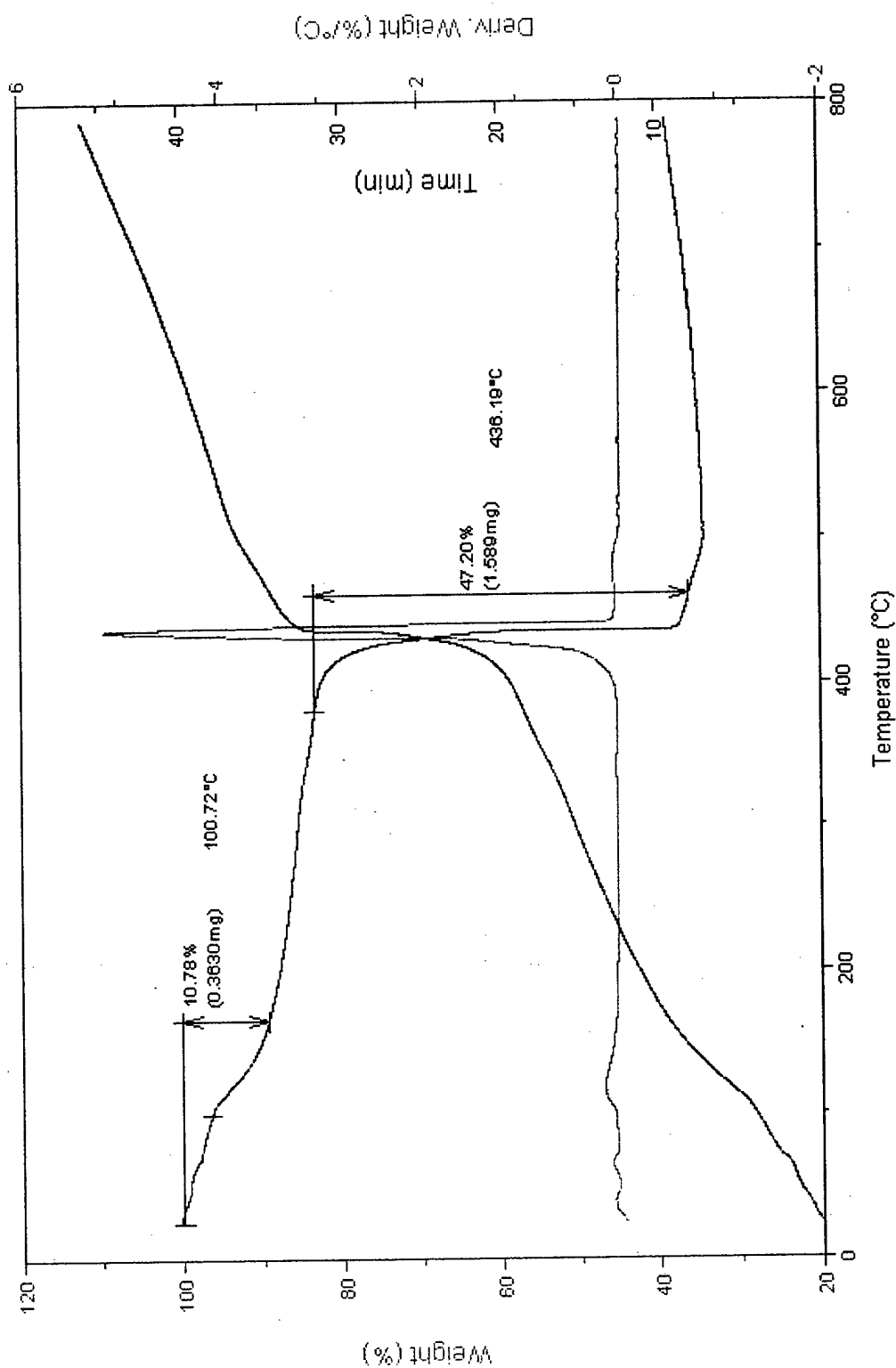


Figure B-4. Thermogram of Zinc Cubic Material After H-CAAAB Cycling.

Appendix B: (Continued)

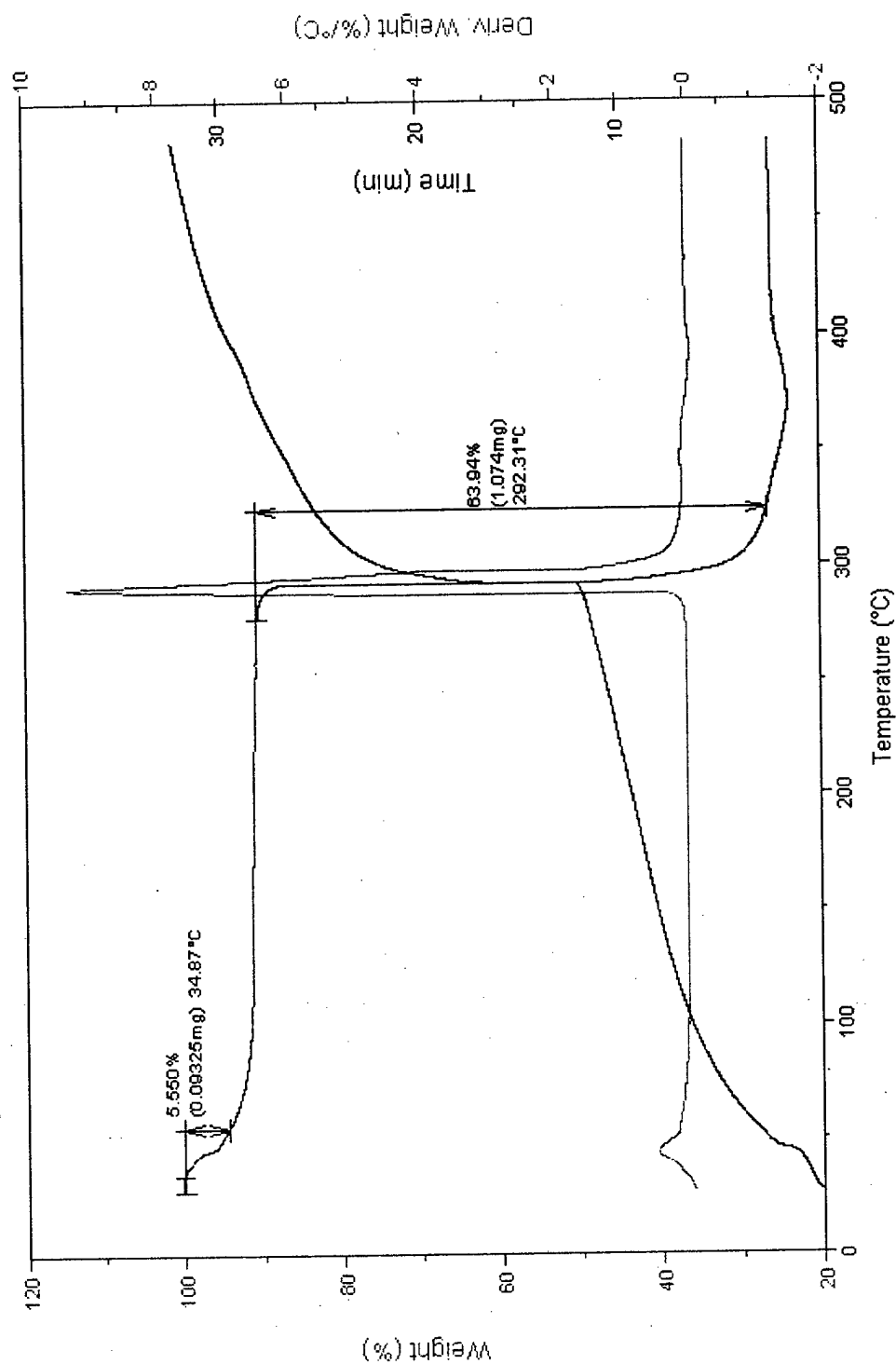


Figure B-5. Thermogram of Copper Octahedral 1 Material Before H-CAAAB cycling.

Appendix B: (Continued)

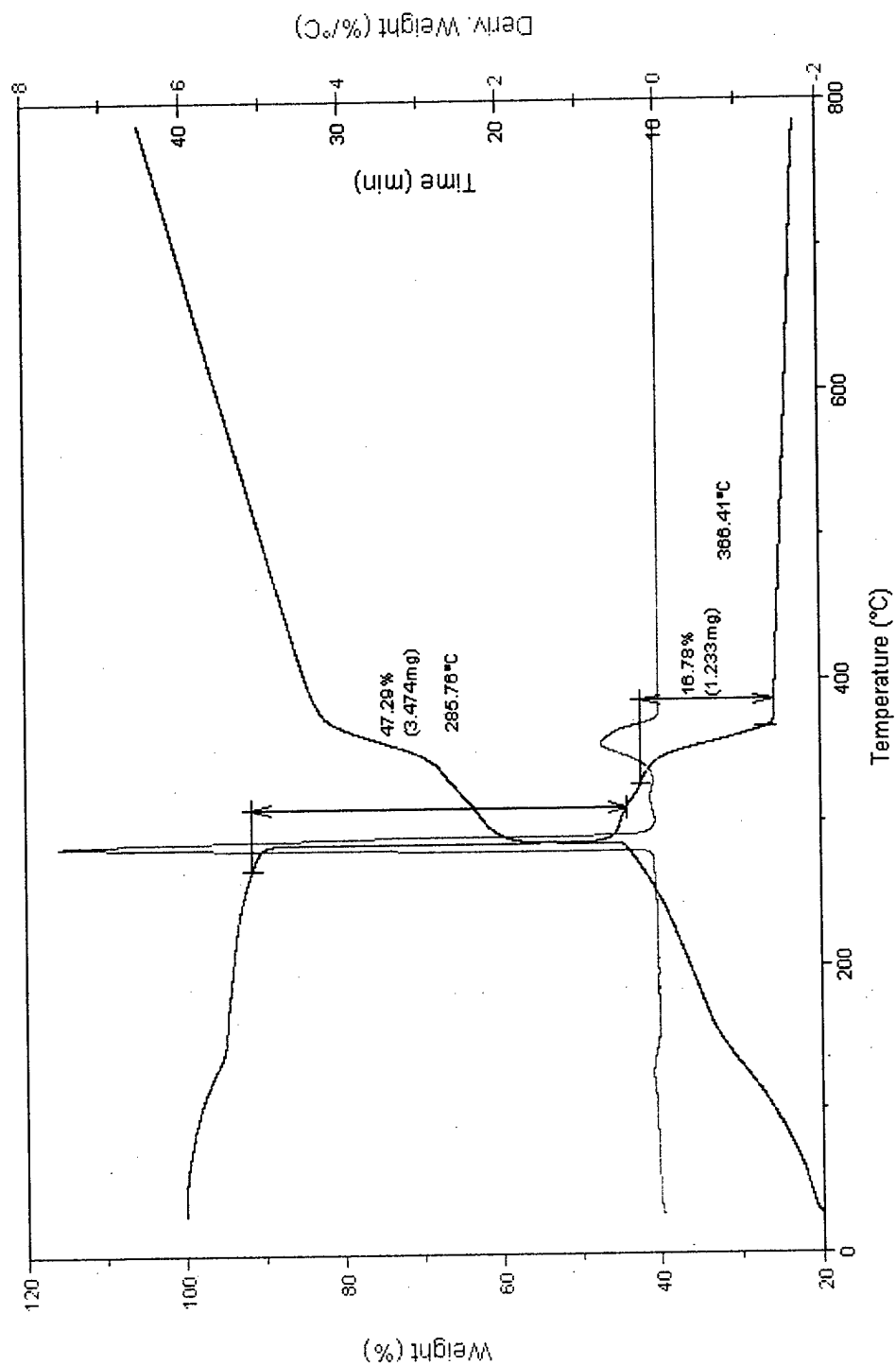


Figure B-6. Thermogram of Copper Octahedral 1 Material After H-CAAAB cycling.

Appendix B: (Continued)

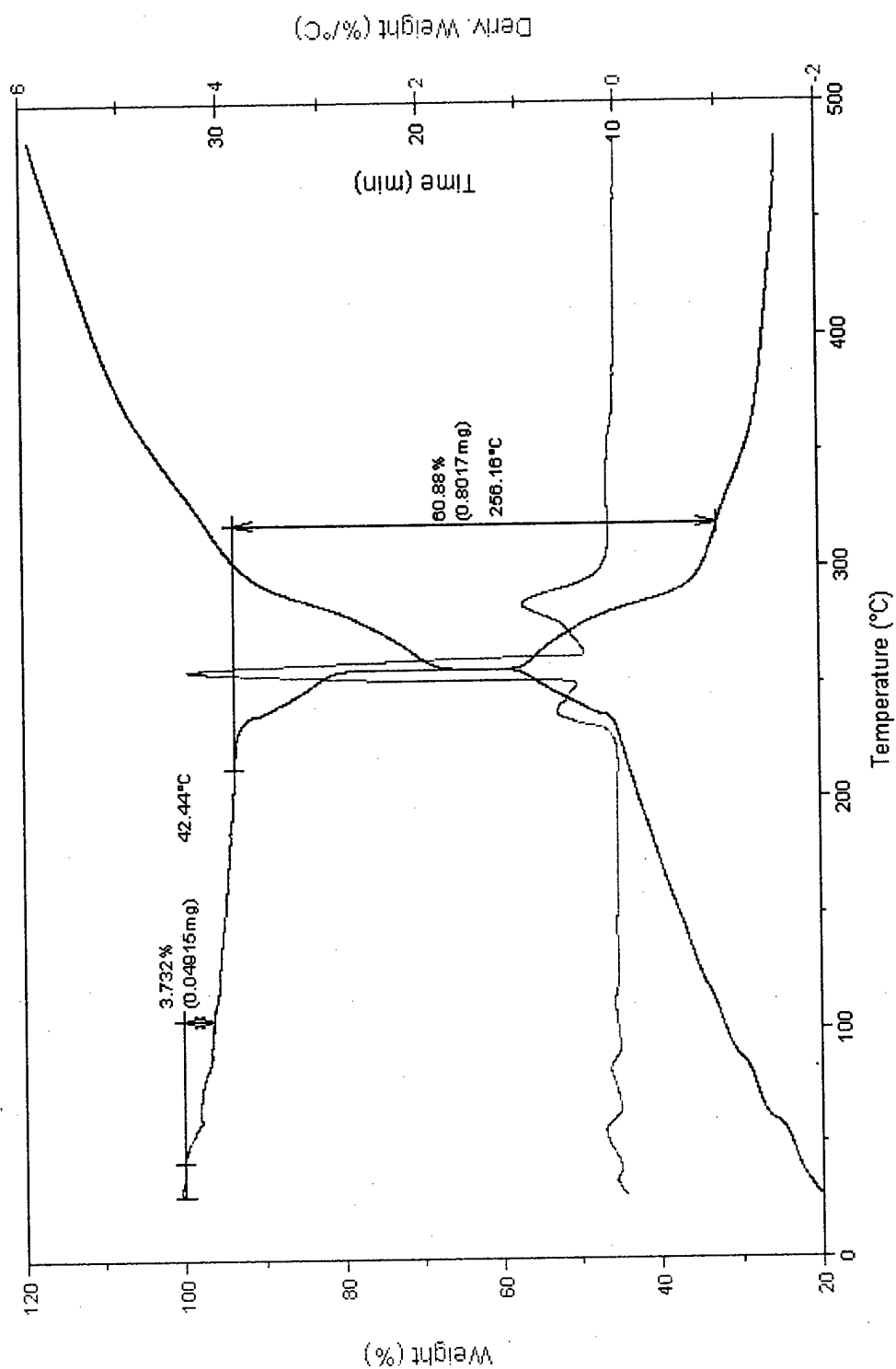


Figure B-7. Thermogram of Copper Octahedral 2 Material before H-CAAAB cycling.

Appendix B: (Continued)

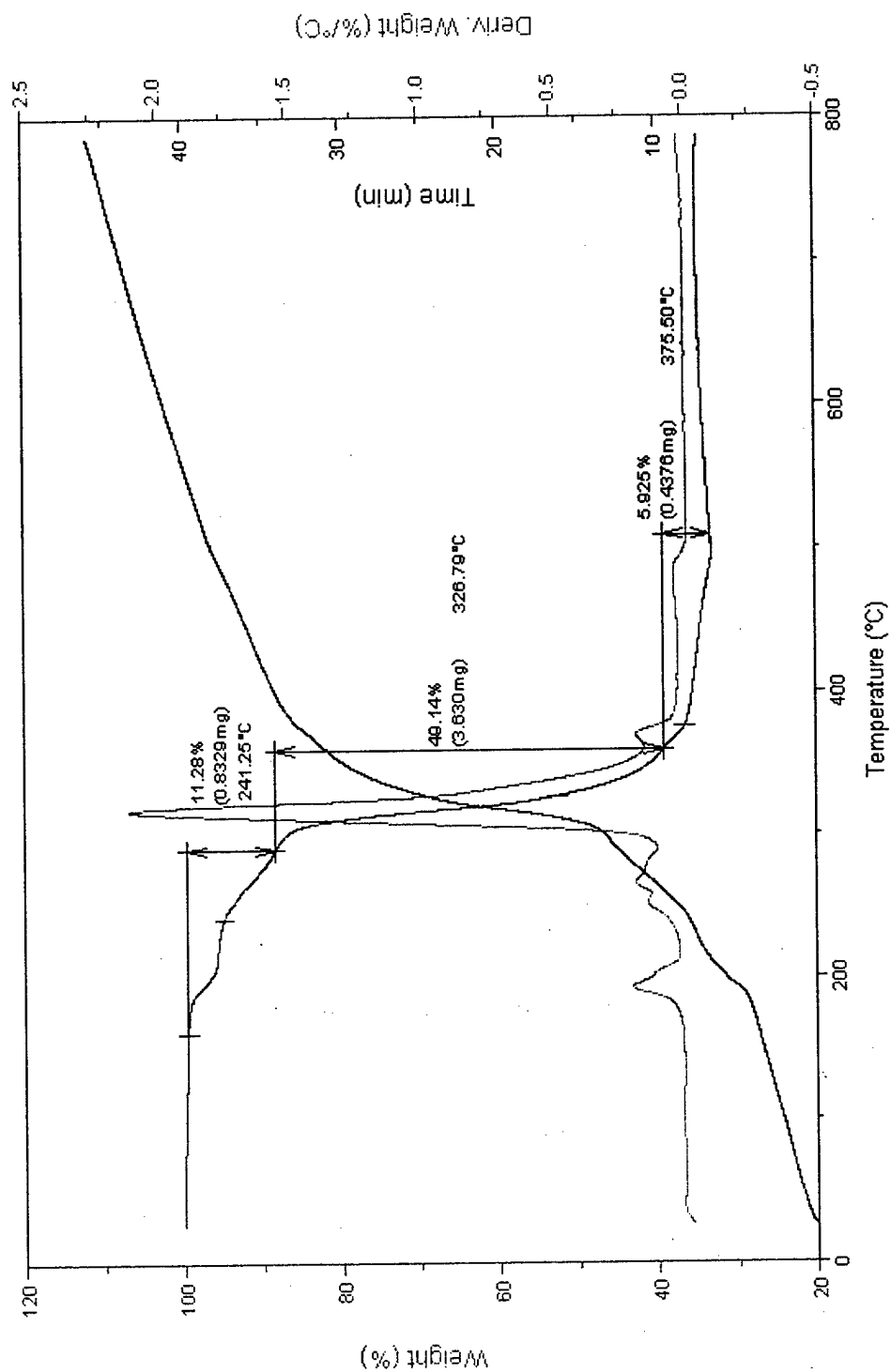


Figure B-8. Thermogram of Copper Octahedral 2 Material After Cycling in H-CAAAB.

Appendix B: (Continued)

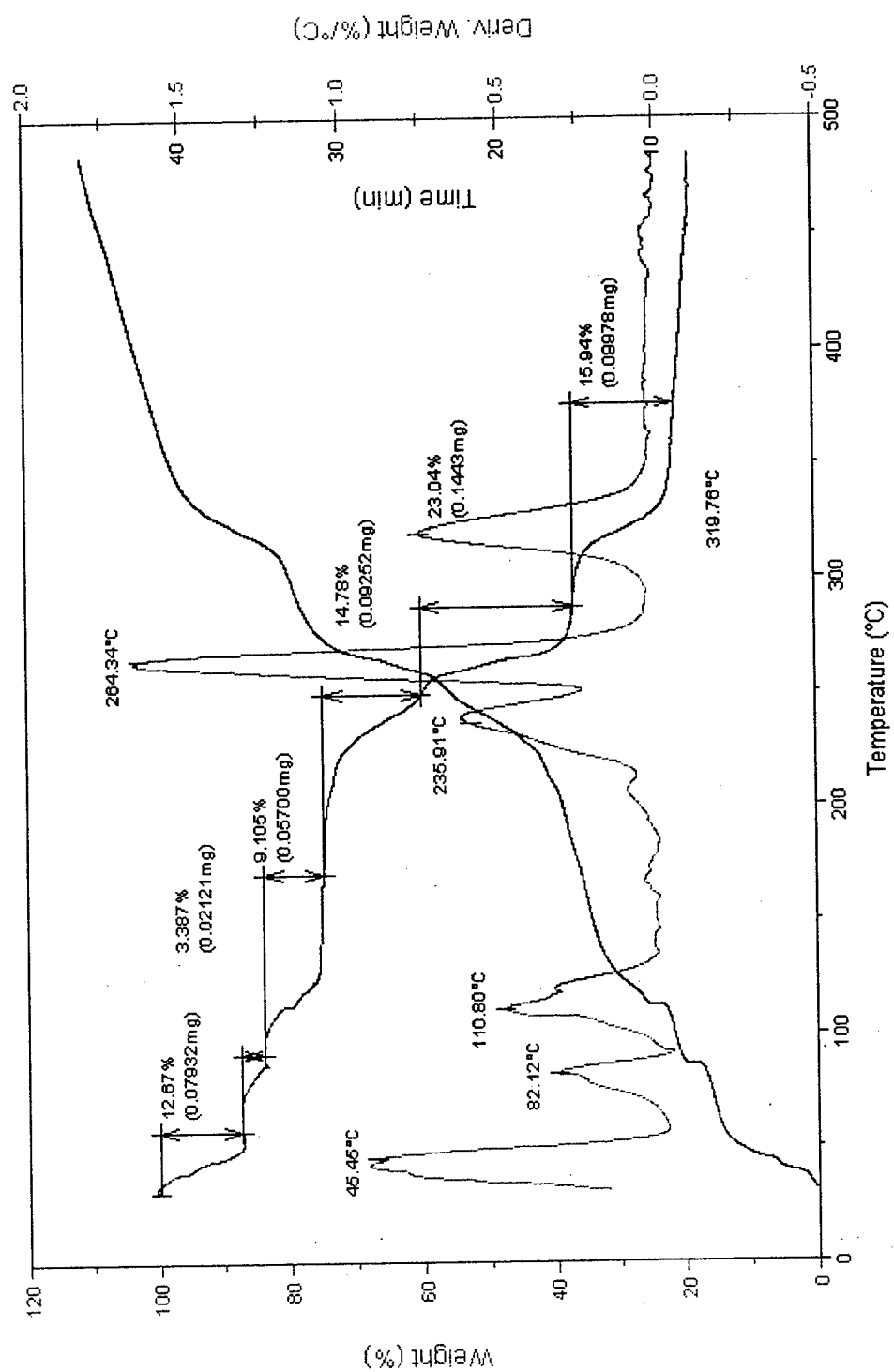


Figure B-9. Thermogram of Copper Octahedral 3 Material before Cycling in H-CAAAB.

Appendix B: (Continued)

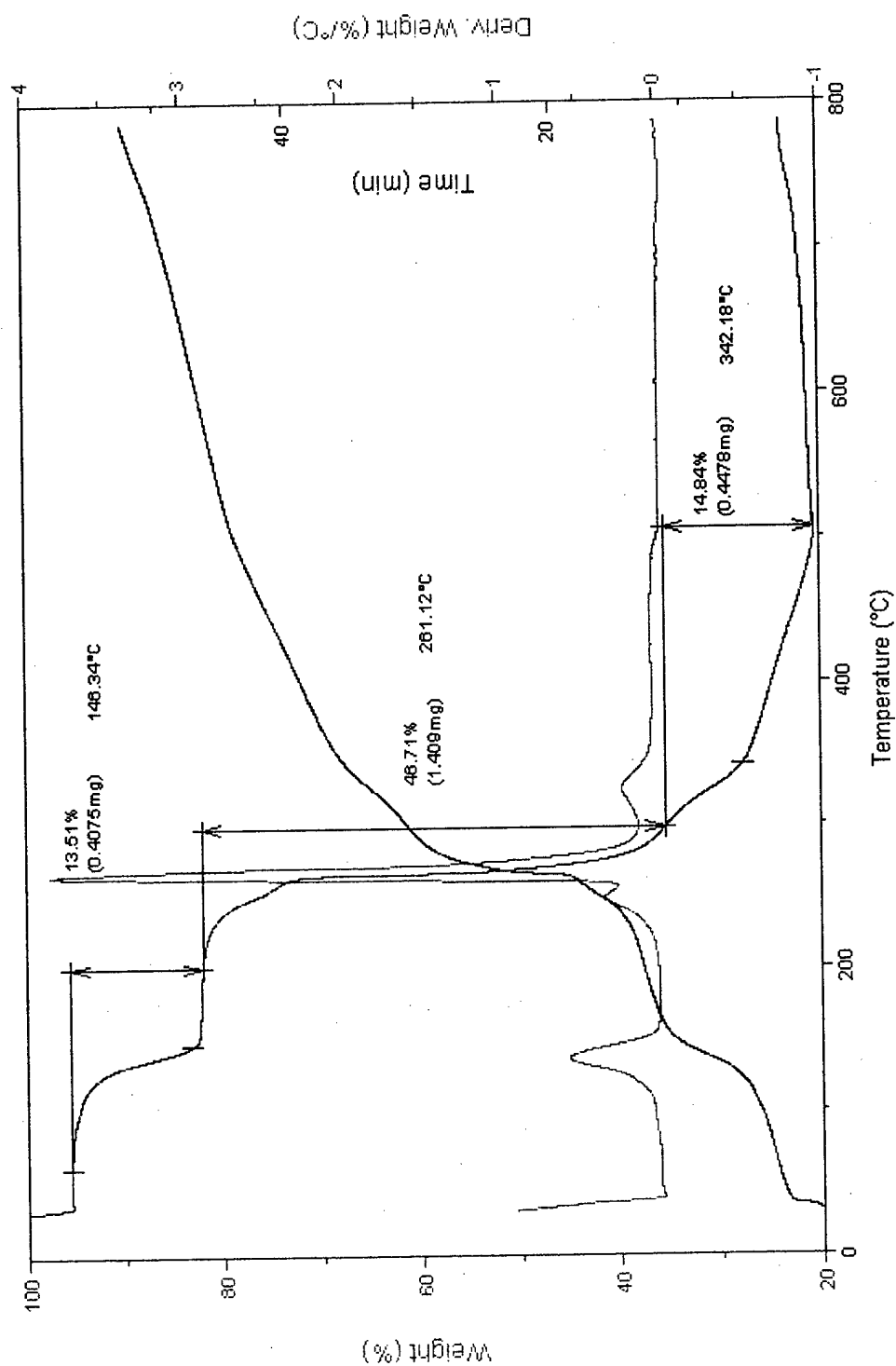


Figure B-10. Thermogram of Copper Octahedral 3 Material After Cycling in H-CAAAB.

Appendix C

X-Ray Powder Diffraction Patterns

Appendix C: X-Ray Powder Diffraction Patterns

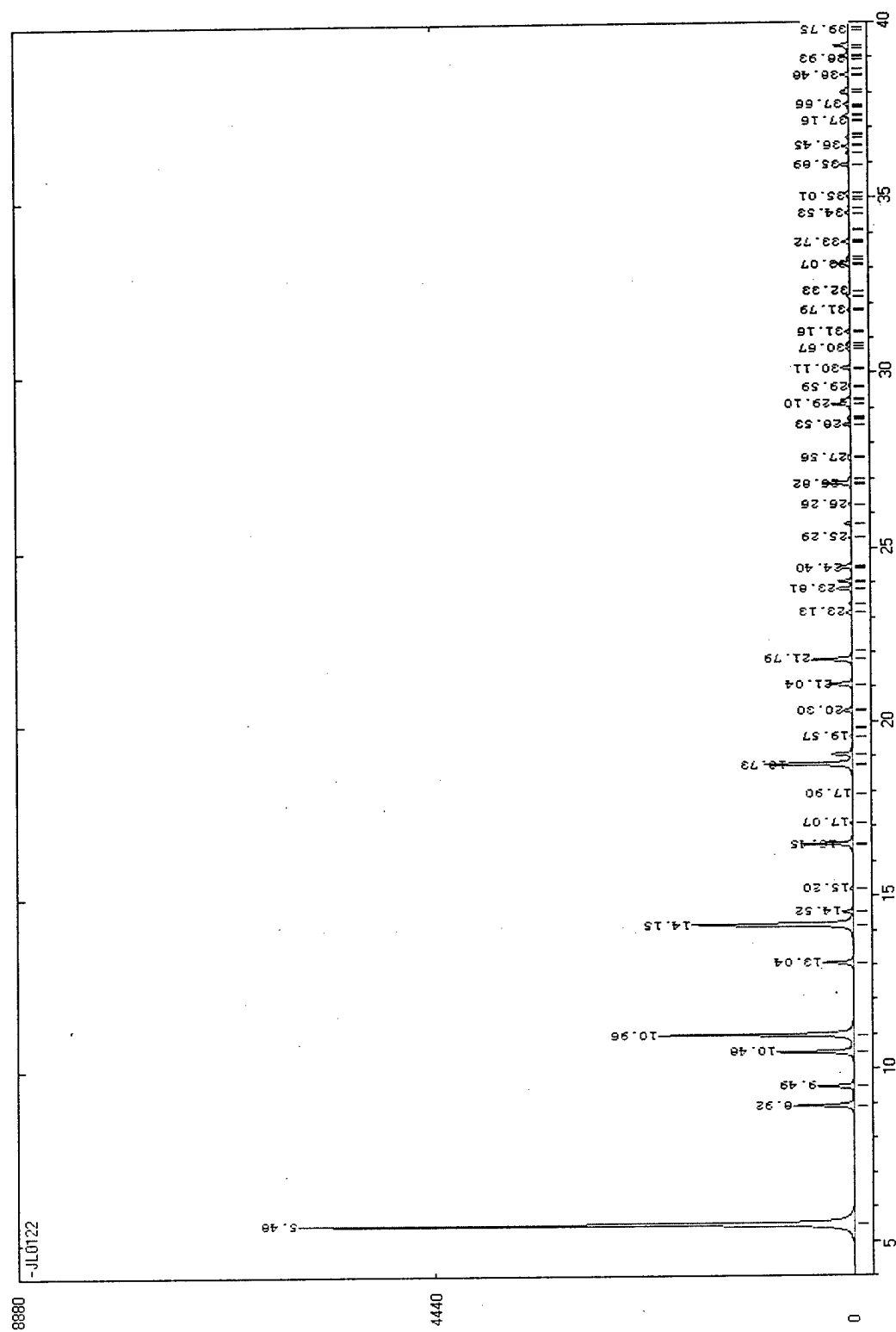


Figure C-1. Simulated XPD Pattern for the Kagomé Structure.

Appendix C: (Continued)

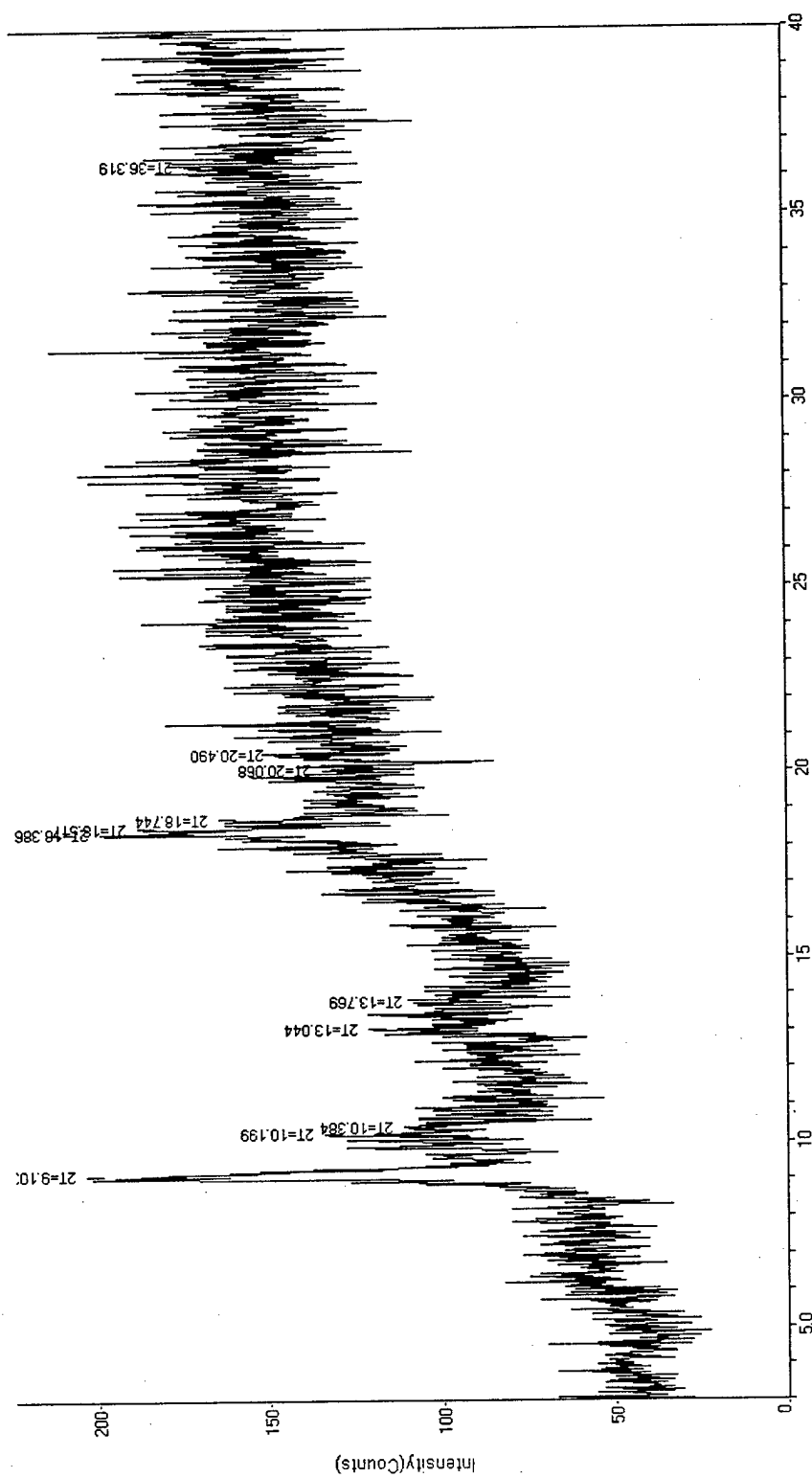


Figure C-2. XPD Pattern for the Kagomé Structure.

Appendix C: (Continued)

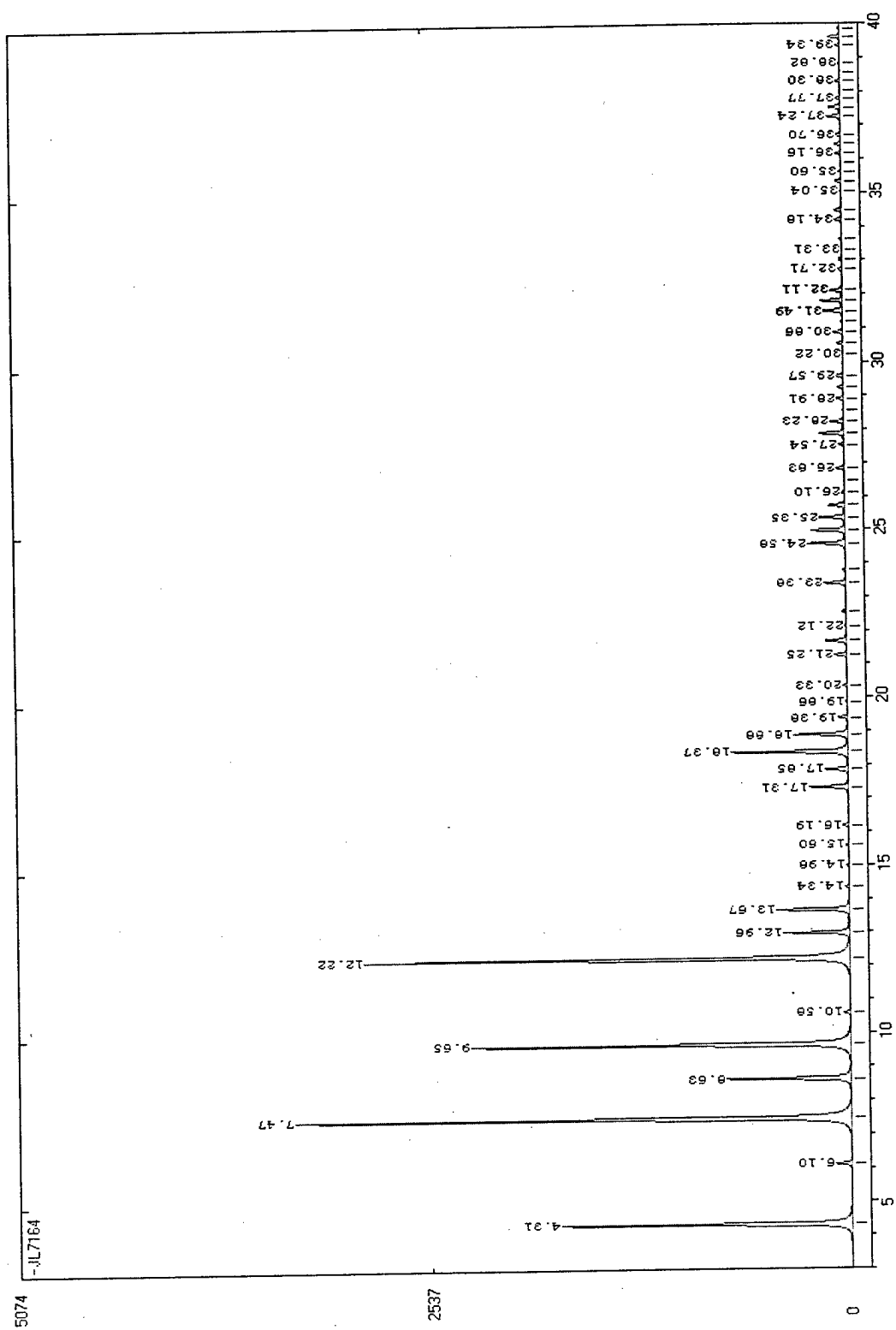


Figure C-3. Simulated XPD Pattern for the Zinc Cubic Structure.

Appendix C: (Continued)

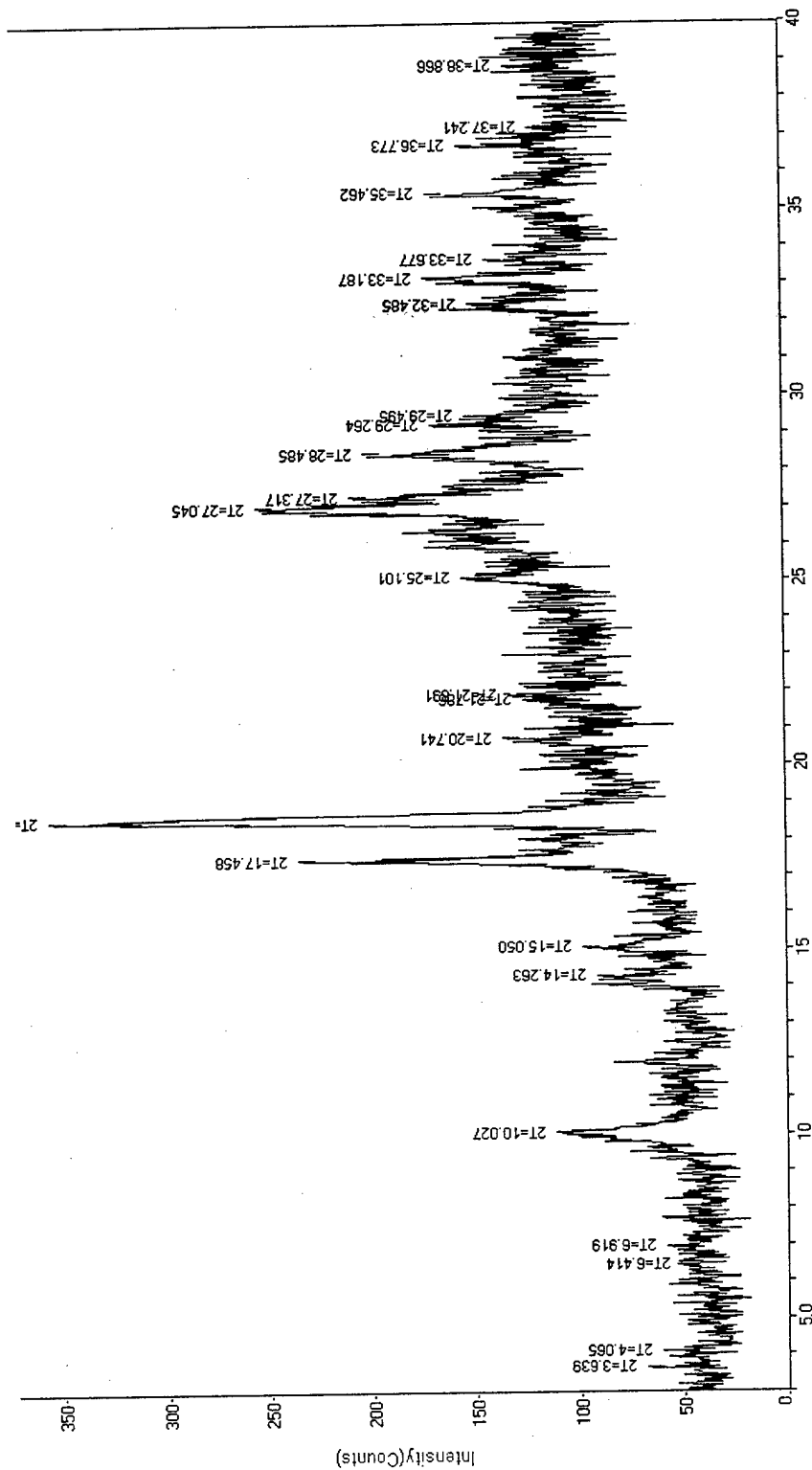


Figure C-4. XPD Pattern for the Zinc Cubic Structure.

Appendix C: (Continued)

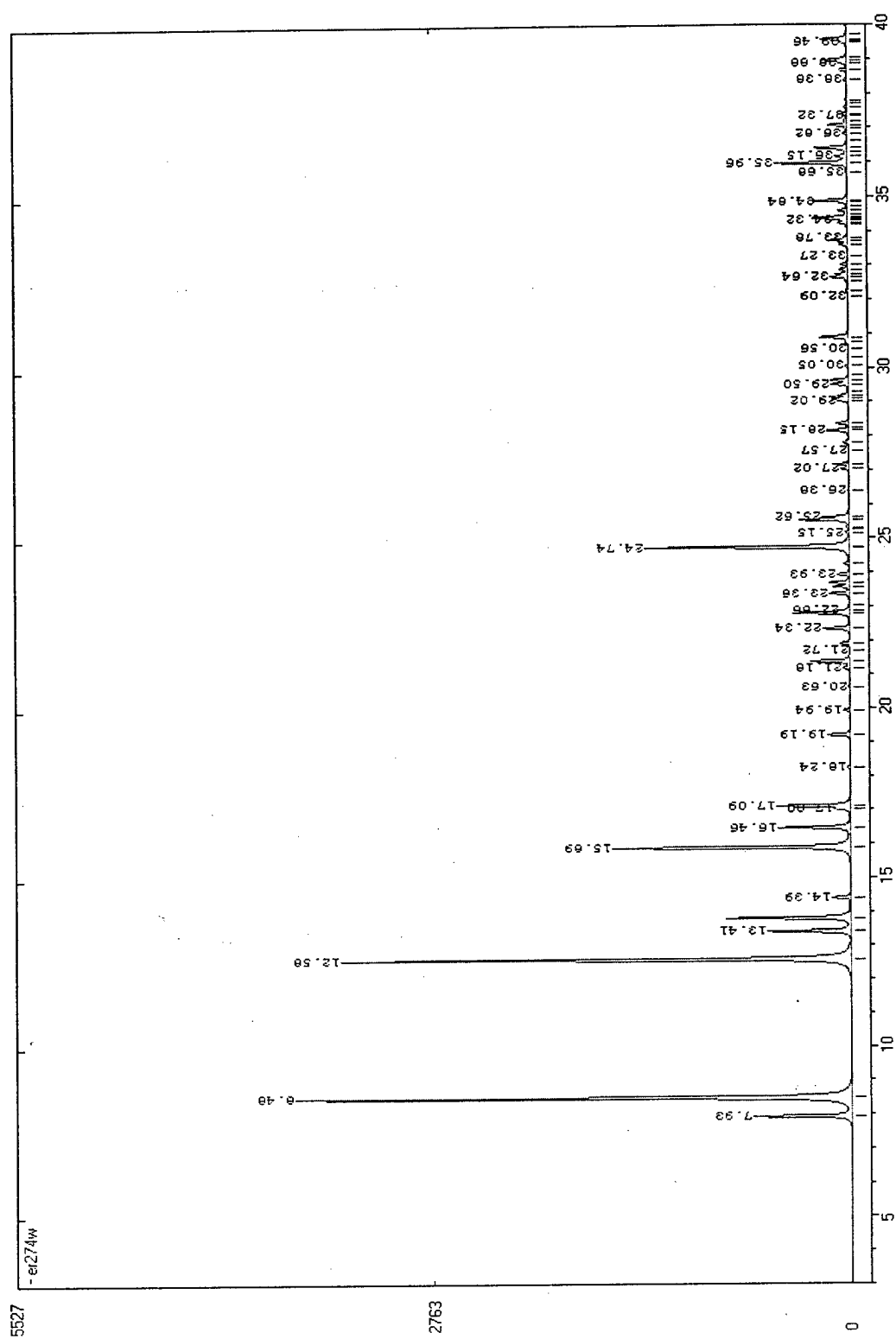


Figure C-5. Simulated XPD Pattern for the Copper Octahedral 1 Structure.

Appendix C: (Continued)

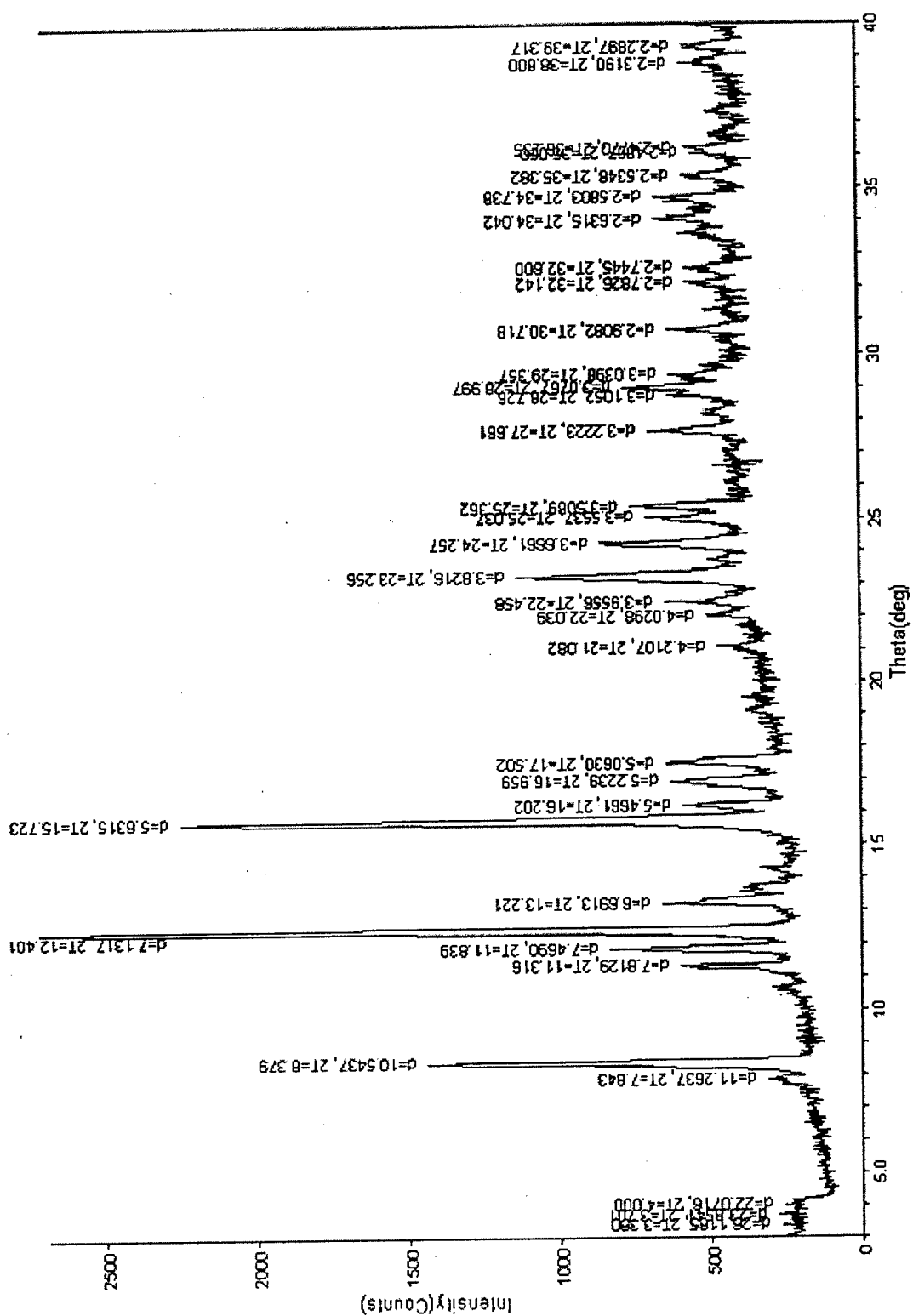


Figure C-6. XPD Pattern for the Copper Octahedral 1 Structure.

Appendix C: (Continued)

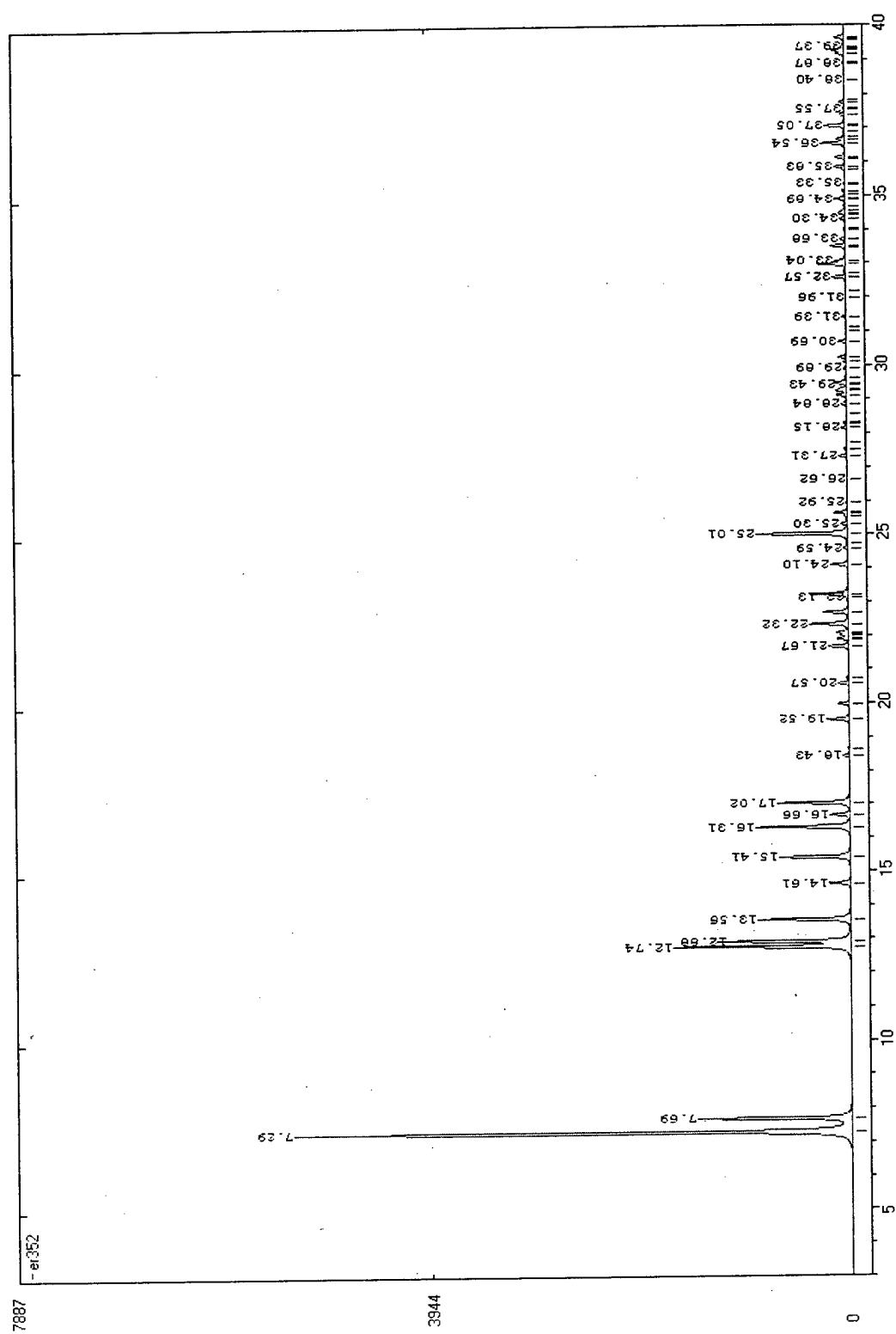


Figure C-7. Simulated XPD Pattern for the Copper Octahedral 2 Structure.

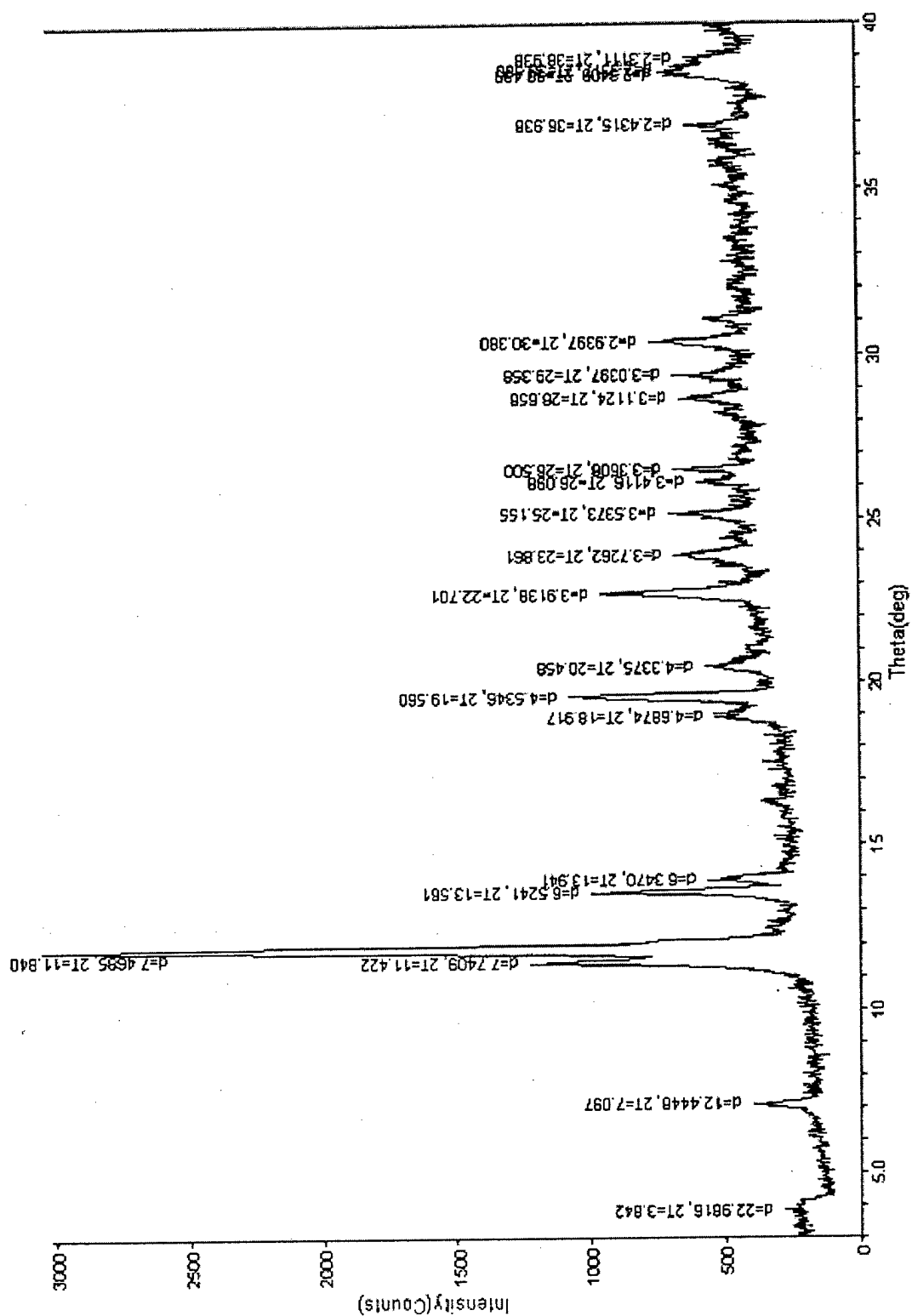


Figure C-8. XPD Pattern for the Copper Octahedral 2 Structure.

Appendix C: (Continued)

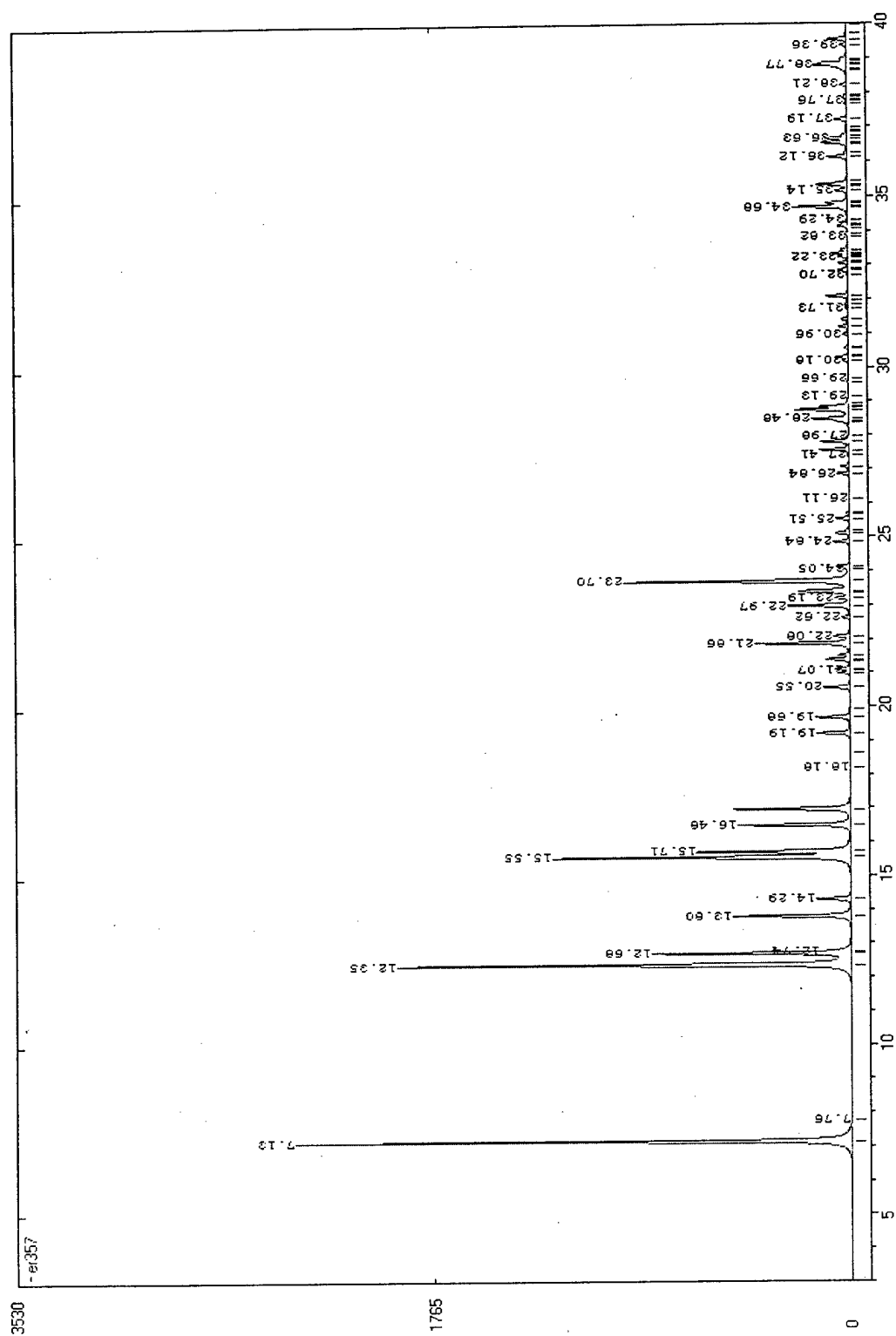


Figure C-9. Simulated XPD Pattern for the Copper Octahedral 3 Structure.

Appendix C: (Continued)

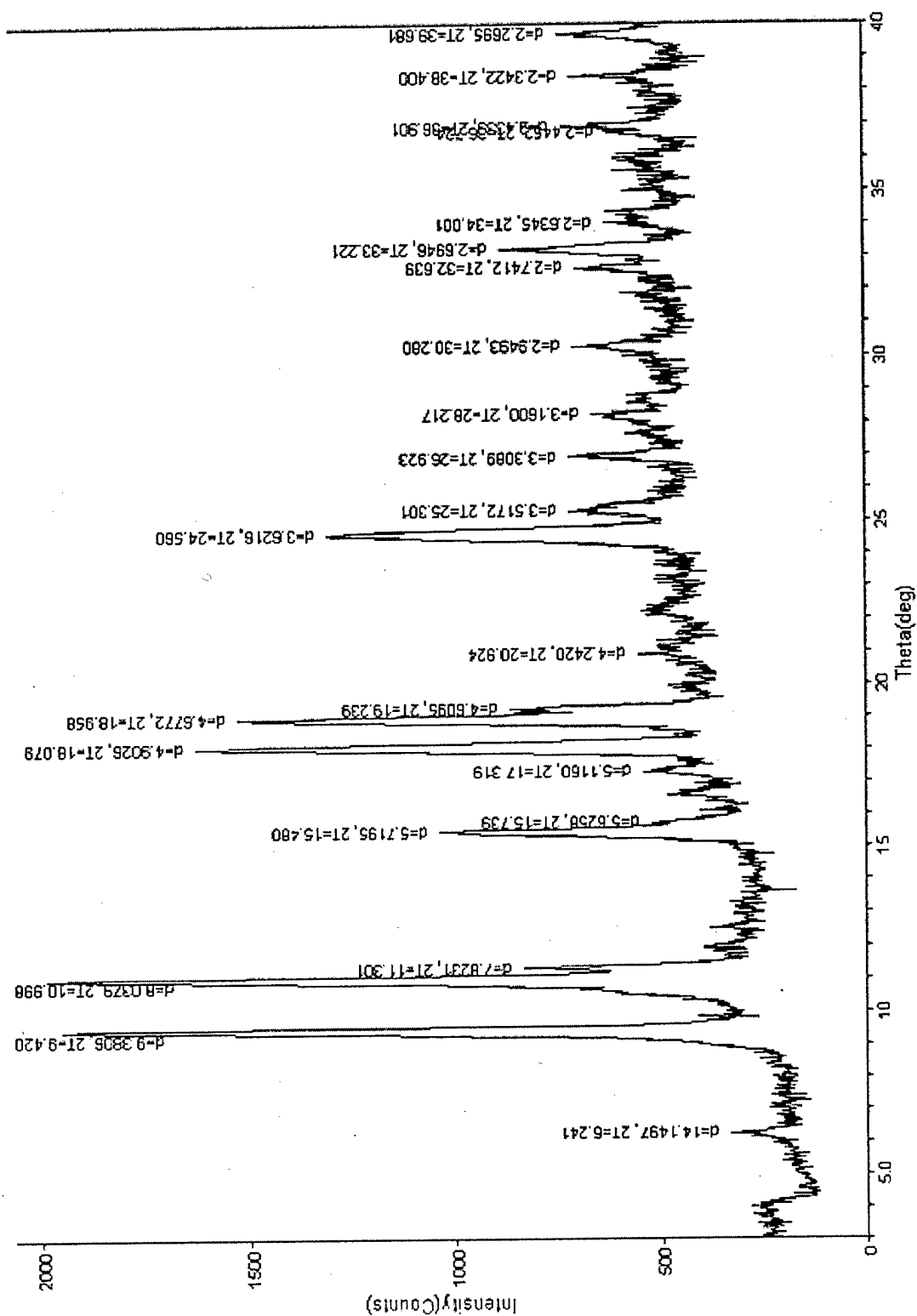


Figure C-10. XPD Pattern for the Copper Octahedral 3 Structure.